The Dissertation Committee for Chun Shen Certifies that this is the approved version of the following dissertation:

EXPERIMENTAL AND SIMULATION STUDY OF FOAM IN POROUS MEDIA

Committee:

William R. Rossen, Supervisor

Larry W. Lake

Russell T. Johns

Chun Huh

Roger T. Bonnecaze

EXPERIMENTAL AND SIMULATION STUDY OF FOAM IN POROUS MEDIA

by

Chun Shen, B.S.; M.S.

Dissertation

Presented to the Faculty of the Graduate School of

The University of Texas at Austin

in Partial Fulfillment

of the Requirements

for the Degree of

Doctor of Philosophy

The University of Texas at Austin

August, 2006

Dedication

To my husband Tao and my parents, for their support and encouragement.

Acknowledgements

I am immensely grateful to my supervisor, Dr. Rossen, for bringing me to the field of foam, for his indispensable guidance and encouragement, for his help in overcoming all kinds of problem. I will always remember his patience and kindness. It was a beneficial and enjoyable experience for me under his supervision.

I would like to acknowledge Dr. Lake for his excellent teaching and Dr. Johns for his valuable suggestions in the group seminar. Special thanks goes to Dr. Huh and Dr. Nguyen for their help on my experiments. My sincere appreciation also goes to Dr. Bonnecaze for being my committee member and take time to read my dissertation.

I would like to express my appreciation to Glen Baum, Tony Bermudez, Bob Savick, Roger Terzian, and Cheryl Kruzie. They offered me great help.

I would like to thank current and previous members of foam research group I had the pleasure to work with: Qiang Xu, Jianguo Rong, Qichong Li, and Zhen Li. Thank them for creating a cooperative and friendly atmosphere in the group.

Finally, by the fact of completing this thesis, I am immensely indebted to my husband, my parents and my sisters for their persistent love and understanding during my long education.

EXPERIMENTAL AND SIMULATION STUDY OF FOAM IN POROUS MEDIA

Publication No._____

Chun Shen, Ph.D.

The University of Texas at Austin, 2006

Supervisor: William R. Rossen

This dissertation comprises two studies of foam in porous media. The first part is an experimental study of the effect of polymer on the properties of foam in porous media. Addition of polymer has been proposed as a way to stabilize foam, especially in the presence of oil. This study probes the possible stabilizing effect of polymer on foam in terms of steady-state properties. Specifically, we tested the effect of polymer addition on the two steady-state foam regimes identified by Alvarez *et al.* (2001).

For the two polymers (Xanthan and partially hydrolyzed polyacrylamide), two oils (decane and 37.5°API crude oil), and surfactant (an alpha-olefin sulfonate surfactant (AOS)) tested, it appears from coreflood pressure gradient that polymer destabilizes foam modestly. The increased viscosity of the aqueous phase with polymer mitigates the effects of destabilization of foam. For the same polymers and surfactant, polymer does

not stabilize foam in the presence of decane or 37.5°API crude oil relative to foam without polymer. Surface-tension measurements with these polymers and surfactant likewise showed no evidence of presence of polymer at the air-water interface that might stabilize foam lamellae between bubbles. This suggests that, for similar polymers and surfactants, addition of polymer would not give stronger foams in field application or stabilize foam against the presence of crude oil.

Complex behavior, some of it in contradiction to the expected two steady-state foam regimes, was observed. At the limit of, or in the place of, the high-quality regime, there was sometimes an abrupt jump upwards in pressure gradient as though from hysteresis and a change of state. In the low-quality regime, the pressure gradient was not independent of liquid superficial velocity, but decreased with increasing liquid superficial velocity, as previously reported and explained by Kim *et al.* (2004).

The second part of this dissertation is a simulation study of gravity segregation during injection of shear-thinning foam in a homogenous reservoir. A useful model for gravity override with Newtonian flow is Stone's model (1982), which describes gravity override during simultaneous water-gas flow. Shi and Rossen (1998) extend the model to foam processes with Newtonian rheology. However, foams are non-Newtonian, often in the high-quality regime, and always in the low-quality regime. In this study we examined the ability of shear-thinning foam to overcome gravity segregation in homogeneous reservoirs with different foam properties. In the limited range of conditions tested, we extended Stone's model to non-Newtonian flow using the estimated mobility at a representative "average" location which depended on the degree of shear-thinning behavior. We then developed a method to estimate the segregation distance for non-Newtonian foams that required iterative calculation but not computer simulation. The estimates were qualitatively, but not quantitatively, correct.

Table of Contents

List of Tables

List of Figures

Chapter 1: Introduction

1.1 FOAM APPLICATION IN PETROLEUM ENGINEERING

Foam is a dispersion of gas in liquid with surfactant present. Foam is a promising tool in various processes in oil and gas production, including mobility control in enhanced oil recovery (EOR), acid diversion in well stimulation, and recovery of wastes in environmental remediation.

1.1.1 Foam in EOR

Primary and secondary recovery typically recover less than half of the original oil in place (Lake, 1989). To recover more oil from a reservoir, it is necessary to apply EOR techniques. The three major EOR processes are thermal, miscible and chemical. Each method is subdivided further into different processes, such as steam, nitrogen, and CO_2 (Lake, 1989). Steam is more mobile than oil, overriding the oil and channeling through thief zones. Gas flooding also suffers from low density of gas and adverse mobility ratio due to the low viscosity of gas compared to oil (Lake *et al.*, 1992). High gas mobility directly causes fingering, and makes the effects of heterogeneity and gravity segregation worse. Gravity override and channeling from heterogeneity result in early breakthrough of injected fluid, and thus reduce oil production.

Gas in foam has a lower mobility than the displaced fluids, so it can be used to counteract these kinds of sweep problems. This effect can prevent fingering and increase the role of pressure gradient in competition with gravity, thereby reducing gravity

override, and slowing the breakthrough of injected gas. In addition, foam reduces gas mobility more in higher-permeability layers than in lower-permeability layers, so it can directly mitigate reservoir heterogeneity to improve both horizontal and vertical sweep efficiency.

1.1.2 Foam in acid diversion

Matrix acidizing is a treatment for damaged sandstone or carbonate formations. The proper placement of acid into low-permeability or damaged layers is a crucial factor in a matrix acidizing treatments (Hill and Rossen, 1994). The success of stimulation treatment is less than ideal because acid tends to flow into the high-permeability or less-damaged layers much more than to the low-permeability or more-damaged layers. Increasing the success of acid treatments by a properly designed diversion treatment would increase acid penetration into low-permeability or damaged layers. Foam diversion is an attractive technology for diverting acid to desired layers in matrix acidization. It has been used successfully in the field (Smith *et al.*, 1969; Kennedy *et al.*, 1992; Gdanski, 1993; Zerhboub *et al.*, 1994; Robert and Rossen, 1997; Thomas *et al.*, 1998).

In acid diversion, foam reduces the injectivity of acid into layers where less is needed and thereby diverts acid into layers in need of stimulation. Good diversion is expected for permeability ratios less than 10:1, according to Burman and Hall (1987). To divert acid, foams of 70% or 80% gas are the most effective, according to Thompson and Gdanski (1993). The key to foam effectiveness in acid diversion is to reduce liquid saturation and relative permeability of liquid by placing as much gas as possible into

high-permeability or undamaged layers, and then trapping all the gas in the foam in place during acid injection (Kibodeaux *et al*., 1994).

1.1.3 Foam in environmental remediation

In environmental remediation, contaminant can be of light non-aqueous phase liquids ("LNAPL"), such as gasoline, which are less dense than water, and dense non-aqueous phase liquid ("DNAPL"), such as chlorinated solvents, which are more dense than water (GeoTrans, 2001; Hirasaki *et al.*, 1997). One of the challenges for remediation technologies is to remove these contaminants from low-permeability layers in the presence of higher-permeability layers (Keely, 1989; Mackay and Cherry, 1989; Hirasaki *et al.*, 1997). One approach to reduce the effects of heterogeneity is to use mobility control to prevent the channeling of injected fluids through high-permeability zones. Foam is a promising solution as a blocking agent to divert flow, by reducing fluid flow in high-permeability zones (Mamun *et al.*, 2002). In addition, foam is not toxic, depending on the choice of surfactant.

The key for foam to improve sweep efficiency is to redirect the flow of injected gas or liquid toward wastes, which is similar to the goals of acid diversion. However, since foam-remediation processes are performed in relatively shallow formations, weak foams, causing small pressure drops, are preferred to strong foams, which may increase pressure so much that it lifts the overburden.

1.2 FOAM PROPERTIES

Foam is a dispersion of a gas in a liquid phase. Foams can be characterized as bulk foam or foam in porous media.

1.2.1 Bulk foam

Bulk foam is foam which is in a container or conduit much larger than bubbles. This sort of foam can be treated as a single homogeneous phase, with almost the same velocities of liquid and gas (Calvert, 1989). Bikerman (1973) defined bulk foam as an agglomeration of gas bubbles separated from each other by thin liquid films. The thin liquid film is called a *lamella* (plural *lamellae*), which can be stabilized by the presence of surfactant molecules. Lamellae touch each other or the solid wall at a region called a Plateau border (Figure 1.1). Foams are not thermodynamically stable and finally break. Foam disappears when lamellae break from high capillary pressure or when gas diffuses through the lamellae, causing smaller bubbles to shrink until they disappear.

The thickness of a lamella at rest and at equilibrium is governed by capillary pressure through the disjoining pressure (Jimenez and Radke, 1989), which is the repulsion between the opposite surfaces of the lamella, caused by the presence of surfactant (Figure 1.2). At equilibrium, the disjoining pressure equals capillary pressure. Higher capillary pressure causes a lamella to thin. When the lamella reaches a critical thickness h_{cr}, it ruptures. Film stability can be increased by increasing π_{max} (Figure 1.2), also called the critical capillary pressure (Khatib *et al.*, 1988); by slowing down the drainage rate; or by stabilizing foam to small mechanical disturbances. The critical capillary pressure can be changed through adjusting the type and concentration of

surfactant, salinity, temperature, etc. However, in bulk foam, beyond the critical micelle concentration, increasing surfactant concentration does not improve foam stability much.

Bulk foam is widely used in the oil industry in drilling, fracturing, and cementing. The half-life of bulk foam is also sometimes used in screening surfactants for foam in porous media.

1.2.2 Foam in porous media

Rossen (1996) defined foam in porous media as a dispersion of gas in liquid such that the liquid phase is connected and at least some part of the gas is made discontinuous by liquid films. Therefore, foam in porous media is divided into continuous-gas foam, in which there is at least one continuous gas flow path, and discontinuous-gas foam, in which there is no gas flow path not blocked by liquid or lamellae, as shown in Figure 1.3 (Falls *et al.*, 1988; Rossen, 1996). For continuous-gas foams at low pressure gradient, gas mobility is reduced because gas relative permeability is reduced by a fixed amount. At higher pressure gradient lamellae are mobilized and either break, thereby increasing gas mobility, or divide and reproduce, which leads to a discontinuous-gas foam of very low mobility. There is no flow of gas at all at low pressure gradient for discontinuous-gas foams. However, at high pressure gradient, gas may flow through some or all pores, as all or part of trapped gas is mobilized. Thus the velocity of gas is not proportional to pressure gradient in a discontinuous-gas foam. The strongest and most stable foam is thought to be a discontinuous-gas foam, and weak foam is associated with continuous-gas foam (Friedmann *et al.*, 1991).

In porous media, foam splits into liquid, flowing gas and trapped gas (Figure 1.4). Flowing gas flows through the large pores, taking a small fraction of the liquid along as lamellae and plateau borders; trapped gas bubbles reside in the intermediate-size pores; and the majority of the liquid separates from the gas and flows in the same small pores and pore corners as in conventional gas liquid flow. Only a small amount of liquid is transported with gas as lamellae and Plateau borders.

1.2.3 Foam mobility

There is no such thing as a foam "phase." Foam mobility means the separate mobilities of liquid and gas in the presence of foam.

As noted, almost all water injected with the foam separates from the foam and flows through the same network of small pores and pore corners that water would occupy at the same water saturation with or without foam. Therefore the viscosity and relative permeability of the liquid phase are not affected by foam (Bernard *et al.*, 1965; Friedmann and Jensen, 1986; Huh and Handy, 1989; Sanchez and Schechter, 1989; de Vries and Wit, 1990; Friedmann *et al.*, 1991). However, foam does change the relative permeability of the liquid phase by changing the water saturation. The relative permeability of the liquid phase can be calculated from pressure gradient and flow rate using Darcy's law as follows:

$$k_{rw}\left(S_w\right)=\left(\frac{Q_w}{A}\right)\frac{\mu_w}{\left(\nabla P\ k\right)} \tag{1.1}$$

where k_{rw} is relative permeability of the liquid phase, Q_w is volumetric flow rate of the liquid phase, A is cross-sectional area, μ_w is liquid viscosity, ∇P is pressure gradient (assumed to be the same for water and gas phases), and k is absolute permeability.

Gas mobility in the presence of foam is more complicated. It is dominated by bubble size, and also depends on gas fraction, pressure gradient, flow rate, and other factors (Falls *et al.*, 1988; Falls *et al.*, 1989; Friedmann *et al.*, 1991; Kovscek and Radke, 1994). Small bubbles reduce gas mobility more than large bubbles. Bubble size can change drastically in porous media with slight changes in conditions, and, sometimes, even with no deliberate change at all (Rossen, 1996). At fixed bubble size, gas in foam may exhibit a minimum pressure gradient for flow, as though the gas were a fluid with a yield stress, like a Bingham plastic (Rossen and Wang, 1999). When pressure gradient is above the minimum pressure gradient, foams are usually shear-thinning at fixed bubble size. Darcy's law can be applied to the gas phase in foam. However, the viscosity and relative permeability of gas depend on the number of lamellae and other factors in complex ways.

Foam reduces gas mobility in two ways. First, foam traps some gas, reducing the number of flow paths for foam (Figure 1.4). Some experiments (Friedmann, *et al.*, 1991; Gillis, *et al.*, 1990) showed that the fraction of trapped gas can be in the range of 80% to 99%. Second, foam increases gas viscosity, because of the effect of drag on flowing bubbles and of a yield stress. Falls *et al.* (1989) split apparent viscosity of gas in the presence of foam into two parts:

$$\mu_{g,app} = \mu_{con} + \mu_s \tag{1.2}$$

where μ_{con} describes the effect of pore constrictions, and μ_s reflects the effect of gas velocity. μ_{con} scales inversely with gas velocity, which implies a fixed yield stress or minimum pressure gradient. This is then implies:

$$\nabla P = (\nabla P)_{\min} + (\nabla P)_{flowing} \tag{1.3}$$

where $(\nabla P)_{min}$ reflects μ_{con} and $(\nabla P)_{flowing}$ reflects μ_s. At low gas velocity, μ_{con} dominates, and pressure gradient reflects a minimum pressure gradient; at high gas velocity, μ_s dominates and, according to Falls *et al.* (1989), pressure gradient is proportional to the (2/3) power of gas flow rate.

To summarize, the viscosity and relative-permeability functions for the liquid phase are unaffected by foam. The mobility of gas is dominated by gas bubble size. Small bubbles reduce gas mobility more, because of larger resistance caused by increasing the number of lamellae in per unit length along the flowing path of gas. At fixed bubble size, foam has a yield stress and shear-thinning rheology.

1.2.4 Foam stability

Foam stability in porous media is controlled by the stability of flowing lamellae. A lamella stretches and contracts as it moves through pores. As the lamella stretches and contracts in response to the pore cross section, wetting liquid from the surrounding pores fills or drains from the moving lamella, partially mitigating the effects of the stretching and shrinking (depending on how fast the lamella is moving). Therefore, film stability depends on the capillary pressure of surrounding rock and on gas velocity (Jimenez and Radke, 1989). Drier foams are less stable, due to higher capillary pressure (Figure 1.2).

Foam is less stable in lower-permeability layers also because of higher capillary pressure there.

1.3 RESEARCH OBJECTIVES

This dissertation describes two projects: an experimental study of the effect of polymer on the properties of foam in porous media, and a simulation study of gravity segregation during injection of a shear-thinning foam into a homogenous reservoir.

It is a familiar observation that polymer increases liquid viscosity and slows the rate of liquid drainage from bulk foam. Whether polymer stabilizes foam in porous media is not clear. In the first part of this dissertation, we investigated the effect of polymer additives on the stability of foams made from surfactant alpha-olefin sulfonate (AOS) in sandpacks and Boise sandstone cores. We also examined the effect of polymer on foam stability in the presence of oil.

The second project concerned gravity override. As discussed above, gas can be used as driving agent in EOR. However, because gas is less dense than oil, gas tends to migrate the top of the reservoir, overriding oil-rich zones. Foam is predicted to control gas override by reducing gas mobility. A useful model describing gas override is that of Stone (1982). This model was originally derived for gas and water flow in a homogeneous reservoir. Shi and Rossen (1998) and Cheng *et al.* (2000) extended the model to foam flow with Newtonian rheology. In the second project, we used the STARS™ simulator (Computer Modeling Group, Calgary, Alberta, Canada) to examine the ability of shear-thinning foam to overcome gravity override in a homogenous reservoir, and explored the application of Stone's model to shear-thinning foam.

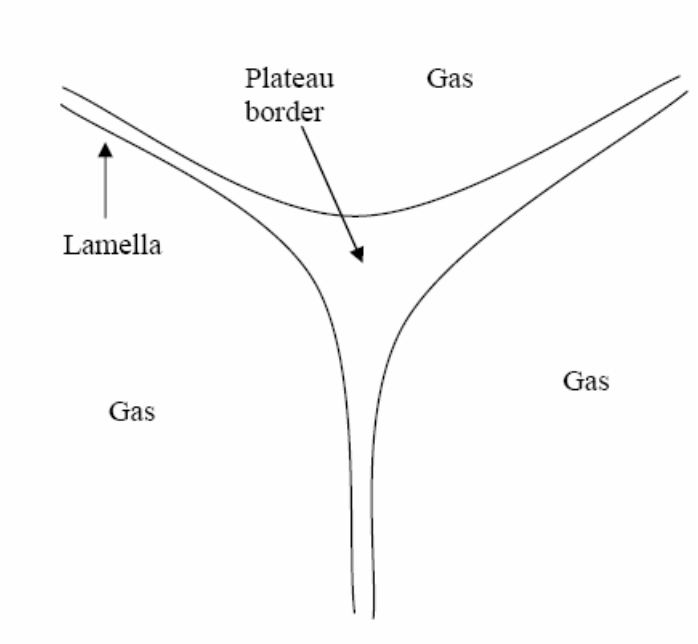

Figure 1.1: A schematic of three bubbles meeting at a Plateau border. The thickness of the lamella is greatly exaggerated in this figure.

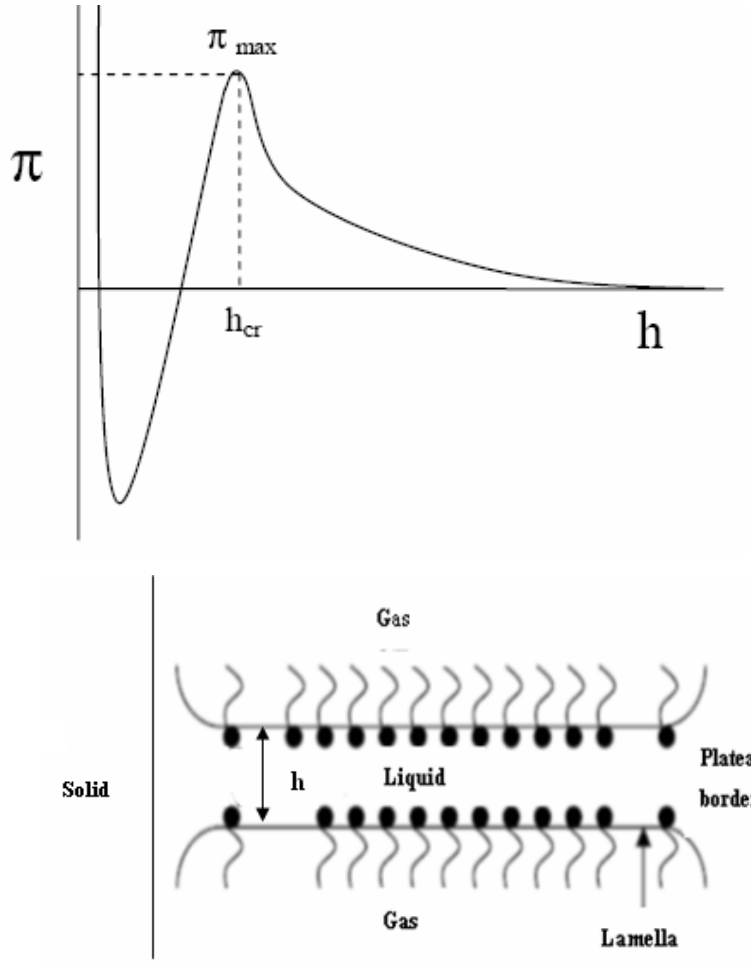

Figure 1.2: The lamella develops a repulsion (disjoining pressure), $\pi(h)$, between the surfaces when surfactant molecules are adsorbed on the surfaces. π_{max} is the maximum disjoining pressure and sets the maximum capillary pressure the film can resist.

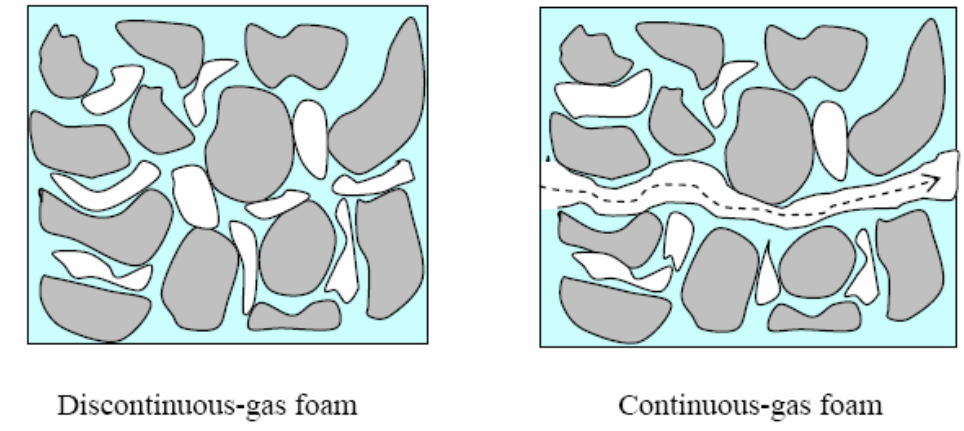

Figure 1.3: A schematic of foam in porous media. The gray is solid, the white is gas, and the light blue is liquid. The left figure represents discontinuous-gas foam: bubbles that are trapped and block gas flow. The right side represents continuous-gas foam, in which the dotted line is the continuous gas flow path.

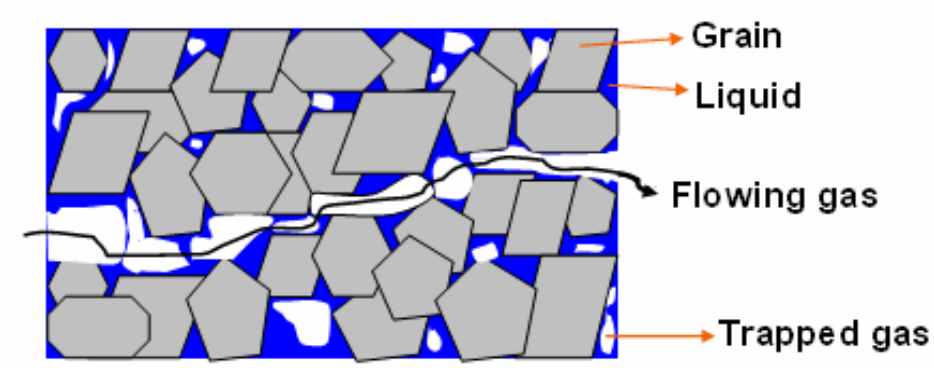

Figure 1.4: Schematic of discontinuous-gas foam in porous media with some bubbles flowing. Gray angular objects represent solids, the light blue is liquid and the white is gas.

Chapter 2: Steady-State Foam Behavior: Two Foam-Flow Regimes

2.1 INTRODUCTION

At the same injection rates of gas and liquid, foam can exist in as many as three distinct states (Gauglitz *et al.*, 2002). First there is a state of high gas mobility, "coarse foam" (or no foam). Second is a state of lower mobility, "strong foam," and, in between, an unstable intermediate state. For a given surfactant formulation and porous medium, there is one continuous surface of pressure gradient as a function of flow rates of liquid and gas. Figure 2.1 illustrates a slice through this surface at fixed liquid interstitial velocity, giving a continuous curve for pressure gradient as a function of gas interstitial velocity. There is low pressure gradient for coarse foam. At the onset of foam generation this surface folds over to form an intermediate regime that is unstable, folding back to form the steady-state strong-foam regime at higher pressure gradient. Steady-state strong foam exists on the upper branch of this surface; imagine the upper branch of the curve in Figure 2.1 extended in a third dimension representing water superficial velocity.

This dissertation concerns steady-state strong foam. In 1992, Osterloh and Jante found that the strong-foam state in turn exhibits two distinct flow regimes, depending on foam quality (gas fractional flow f_g, or ratio of gas superficial velocity to total superficial velocity, often expressed in %) and other factors: a high-quality regime and a low-quality regime, as shown in Figure 2.2. There is a transition zone between the two regimes characterized by a critical value of fractional flow of gas, f_g^*. In Figure 2.2, f_g^* is 0.94, illustrated by the straight line through the origin. Rossen and Wang (1999), Alvarez *et al.*

(2001) (Figure 2.3) and Rong (2002) observed the two foam-flow regimes with a variety of porous media and surfactants in a series of foam coreflooding experiments. The rest of the dissertation discuses steady-state strong-foam behavior based on the two foam-flow regimes. The coarse-foam state and intermediate state in Figure 2.1, which is important to foam generation, will not be discussed further.

2.2 THE FIXED-P_C* MODEL FOR THE HIGH-QUALITY REGIME

Khatib *et al.* (1988) found that foam stability in porous media is limited by capillary pressure. One expects all foams to collapse at sufficiently high capillary pressure, since lamellae thin and finally break at $P_c^{cr} = \pi_{max}$ (Figure 1.2) (Jimenez and Radke, 1989). However, experiments show that for strong foams there is a narrow range in capillary pressure at which foam collapses abruptly. This range is so narrow that it can be identified with a single value, the "limiting capillary pressure," called P_c* (Khatib *et al.*, 1988). The value of P_c* depends on the type and concentration of surfactant, rock properties and other variables.

Water saturation S_w is related to P_c through the capillary-pressure function for the porous medium (Figure 2.4) (Lake, 1989). This implies that foam remains at a given fixed water saturation $S_w^* = S_w(P_c^*)$ over a wide range of flow rates and foam qualities. Since S_w is fixed and does not change, $k_{rw}(S_w)$ is also nearly constant over the same wide range of flow rates, and pressure gradient is simply proportional to the viscosity and superficial velocity of water (Rossen and Wang, 1999; Vassenden and Holt, 1998):

$$\nabla P = \frac{U_w \mu_w}{k k_{rw}\left(S_w^*\right)} \tag{2.1}$$

Foam bubble size adjusts itself as needed to keep water saturation at S_w* and capillary pressure at P_c*. For example, if P_c increases above P_c*, bubbles collapse and gas mobility increases, which raises S_w, and therefore P_c falls back to P_c*.

In the high-quality regime, P_c* controls gas mobility in foam (Khatib *et al.*, 1988; Rossen, *et al.*, 1991; Zhou and Rossen, 1994). Without cross-flow between layers, foam diverts injection into lower-permeability layers because foam is weaker at the higher P_c in these layers. However, P_c* may increase gradually as k decreases (Khatib *et al.*, 1988; Rossen *et al.*, 1995; Zhou, 1994). If so, at capillary equilibrium, where P_c is the same in both layers but P_c* is higher in the lower-permeability layer, foam is stronger in the low-permeability layer than that in the high permeability layer, because P_c in that layer is lower, relative to P_c*.

Supporting experimental evidence for the fixed-P_c* model includes the studies of Khatib *et al.* (1988), Ettinger and Radke (1992), de Vries and Wit (1990), and Persoff *et al.* (1991). Khatib *et al*. found that foam stability in a sandpack or beadpack was limited to a capillary pressure below the limiting capillary pressure. Ettinger and Radke found in their experiments with fired Berea sandstone that pressure gradient was constant when liquid flow rate was kept constant while varying gas flow rate. Also, water saturation determined from microwave attenuation was found to be nearly constant and independent of gas flow rate. de Vries and Wit (1990) observed that, at a fixed liquid flow rate, pressure gradient and water saturation were virtually unchanged as gas flow rated increased. A similar result was observed by Persoff *et al.* (1991). They measured water saturation using gamma-ray densitometry, and found that S_w was independent of flow rates of both gas and liquid.

2.3 THE FIXED-BUBBLE-SIZE MODEL FOR THE LOW-QUALITY REGIME

As Osterloh and Jante (1992) observed, at high liquid superficial velocity and lower gas superficial velocity (lower-right portion of Figure 2.2), that pressure gradient was independent of the liquid flow rate, but depended on gas flow rate. Alvarez *et al.* (2001) called this the "low-quality regime" (Figure 2.3). The P_c^* model does not apply here; rather, P_c is thought to be less than P_c^*. Supporting evidence has been cited by Rossen and Wang (1999), Vassenden and Holt (1998), Alvarez *et al.* (2001) and Rong (2002).

To explain the observed behavior in the low-quality regime, Rossen and Wang (1999) proposed a fixed-bubble-size model. They contended that if P_c were below P_c^*, bubble size might be fixed at roughly bubble size. For $P_c < P_c^*$, lamellae would not break by capillary suction, and, with lamellae being created but not breaking, bubble size would shrink. Once bubble size reached roughly pore size, lamella creation by its two most important mechanisms, lamella division and snap-off, would be inhibited (Rossen and Wang, 1999). If bubbles did shrink further, diffusion between bubbles would rapidly cause bubbles smaller than the pore size to disappear or grow to rough pore size (Rossen and Wang, 1999). Thus it is at least plausible that for $P_c < P_c^*$ bubble size might be fixed at roughly pore size. In this case, foam can be modeled as a Bingham plastic with fixed yield stress and plastic viscosity. So, in this model, Rossen and Wang postulated the following assumptions: (1) the porous medium consists of a bundle of parallel, cylindrical tubes with a variety of tube radii; (2) water is a Newtonian fluid that occupies the narrower tubes, and gas occupies the wider tubes; (3) in foam, gas behaves as a Bingham plastic with fixed yield stress and plastic viscosity; (4) gas can flow in a given

tube it occupies if the pressure gradient exceeds the threshold value for flow for the given tube radius. Based on these assumptions, they presented a plausible explanation for observed behavior in the low-quality regime, as follows:

At steady-state, for a given foam quality and an injection rate, small pores are filled with water, large pores are filled with flowing gas, and most gas is trapped in the intermediate-size pores, as in Figure 2.5 (a).

If, at constant gas superficial velocity, water superficial velocity is increased (a movement to the right in the low-quality regime of Figure 2.2), capillary pressure is reduced. Reduced capillary pressure drives water into wider pores. Therefore, some trapped gas is displaced by invading liquid phase, and liquid relative permeability increases proportionately to liquid superficial velocity. However, gas continues to flow in the same fraction of larger pores as before, keeping the same pressure gradient (Figure 2.5 (b)).

However, if liquid superficial velocity is held constant and gas superficial velocity increases (a movement upward in the low-quality regime of Figure 2.2), pressure gradient increases. Since liquid flow rate is held constant at increasing pressure gradient, liquid relative permeability must decrease to correspond the increase in pressure gradient. That is, liquid phase has to concede some pores to trapped gas, as shown in Figure 2.5 (c). In addition, because increased pressure gradient allows more gas to flow both in pores already opened to flow and in ones newly opened by the higher pressure gradient, foam shows shear-thinning rheology with respect to gas flow rate.

This fixed-bubble-size model implies that pressure gradient is set by bubble trapping and depends mainly on pore geometry and surface tension. However, surface

tension in foam does not vary greatly among surfactant formulations. Therefore, rock properties should be the key factor affecting pressure gradient in the low-quality regime, while surfactant formulation is the key parameter, through its effect on foam coalescence, in the high-quality regime.

Various factors influence behavior in the two flow regimes differently, as illustrated in the following sections.

2.4 EFFECT OF SURFACTANT ON THE TWO FOAM-FLOW REGIMES

Khatib *et al.* (1988) found that the limiting capillary pressure in porous media depended on surfactant concentration. Apaydin and Kovscek (2002) also reported that the foam stability increased with increasing surfactant concentration. Presumably higher surfactant concentration increases the disjoining pressure and therefore stabilizes foam (Figure 1.2). Lee *et al.* (1991) also found that CO_2 foam was more stable at higher surfactant concentrations. Alvarez *et al.* (2001) contended that surfactant properties played an important role in stabilizing foam against high capillary pressure in the high-quality regime, while surfactant properties had little effect in the low-quality regime. Rong (2002) also reported that surfactant concentration played a key role in the high-quality regime, while the low-quality regime was insensitive to the effects of surfactant concentration.

If surfactant concentration is reduced, destabilizing foam in the high-quality regime, a higher flow rate is required to obtain the same pressure gradient in that regime. This means that the vertical contour for a given pressure gradient in a plot like Figure 2.2 shifts to the right. In the meantime, in the low-quality regime, the horizontal contour for

the same pressure gradient is unaffected. As a result, f_g* shifts to a lower value. Figure 2.6 illustrates this effect for a plot with two pressure-gradient contours. In each case the contour in the high-quality regime shifts to the right as surfactant concentration decreases, while the low-quality regime is unaffected. The result is a decrease in f_g*.

2.5 EFFECT OF PERMEABILITY ON THE TWO FOAM-FLOW REGIMES

Khatib *et al.* (1988) measured P_c* over a range of permeabilities and showed a trend of P_c* decreasing as permeability increases, as shown in Figure 2.7. Alvarez *et al.* (2001) showed that the pressure-gradient contours in the high-permeability regime did not shift significantly with permeability change. Rong (2002) found that permeability dominated foam behavior in the low-quality regime, while it had only a small effect in the high-quality regime. Specifically, the horizontal pressure-gradient contours in the low-quality regime moved upward as permeability increased (higher gas superficial velocity required to obtain the same pressure gradient). The vertical pressure-gradient contours in the high-quality regime shifted in general somewhat to the right or remained unchanged. Thus, the net result was an increase in f_g* with increasing permeability, as illustrated in Figure 2.8.

2.6 EFFECT OF OIL ON THE TWO FOAM-FLOW REGIMES

It is commonly accepted that oil is detrimental to foam stability. Several studies pointed out that the influence of oil on foam stability depends on surfactant concentration and type (Jensen and Friedmann, 1987; Mannhardt *et al.*, 2000), foam

quality (Mannhardt *et al.*, 2000), and oil saturation and type (Lau and O'Brien, 1988; Mannhardt, 1999).

As discussed before, in the high-quality regime foam is controlled by capillary pressure, which suggests foam stability is the key issue in this regime. Therefore, in the high-quality regime foam one would expect foam to be sensitive to the presence of oil, since oil affects foam stability. On the other hand, in the low-quality regime, foam behavior is dominated by trapping and mobilization of gas, not foam stability. Therefore, one would not expect foam behavior to be sensitive to the presence of even a destabilizing oil in the low-quality regime. As a result, one would expect f_g* to decrease in the presence of oil as shown in Figure 2.6, and the high-quality regime to extend to lower foam qualities in the presence of oil.

Rong (2002) investigated the effect of oil on the two foam-flow regimes with two anionic surfactants and three oils in porous media with permeabilities of 5 to 200 darcy. The experimental results indicated that oil had a drastic effect in the high-quality regime but less effect in the low-quality regime. However, the degree of the effect depended on the oil type. Specifically, the effect of fluorinated oils on foam stability was smaller than that of decane. In addition, the degree of the effect of oil on the high-quality regime also depended on oil fractional flow. In general, foam stability decreases with increasing fractional flow of oil. However, Rong did not attempt to quantify the minimum fractional flow of oil which would affect foam stability.

2.7 FOAM RHEOLOGY IN THE TWO FOAM-FLOW REGIMES

Foam rheology appears to depend on flow regime. In experiments in a sandpack or Berea core, Alvarez *et al.* (2001) found shear thinning rheology in the low-quality regime, which was consistent with the fixed-bubble-size model (Rossen and Wang, 1999), and shear-thickening behavior in the high-quality regime. Rong (2002) conducted coreflooding experiments in a variety of high-permeability sandpacks. The experimental results showed Newtonian, shear-thickening and shear-thinning behavior in the high-quality regime, and consistently shear-thinning behavior in the low-quality regime (Figures 2.9, 2.10 and 2.11).

2.8 EFFECT OF AQUEOUS-PHASE VISCOSITY ON THE TWO FOAM-FLOW REGIMES

According to Eq. 2.1, if addition of polymer leaves the stability of foam unchanged, i.e. if it leaves S_w^* and $k_{rw}(S_w^*)$ unchanged, but polymer increases μ_w, then ∇P increases for the same value of U_w, or U_w decreases for a given value of ∇P. In other words, a given contour of ∇P in the high-quality regime in Figure 2.2 would shift to the left. The effect of μ_w on the low-quality regime is less clear, but since that regime depends primarily on gas trapping and mobilization, it would be expected to be less sensitive to μ_w. Therefore, if polymer has no effect on foam stability, one would expect that f_g^* would increase upon the addition of polymer (the opposite effect to Figure 2.6, where ∇P contours shift to the right), and the low-quality regime would extend over a wider range of foam qualities. The low-quality regime is less sensitive than the high-quality regime to foam stability, and therefore might be expected to be less sensitive to

the presence of oil. Therefore, *if* polymer stabilizes foam to the presence of oil, it is possible that this results from the effect of polymer on the two flow regimes through its effect on viscosity, and not to any intrinsic stabilization of the foam lamellae. This hypothesis forms the basis for our study of the effect of polymer and oil on foam in chapters 4 to 5.

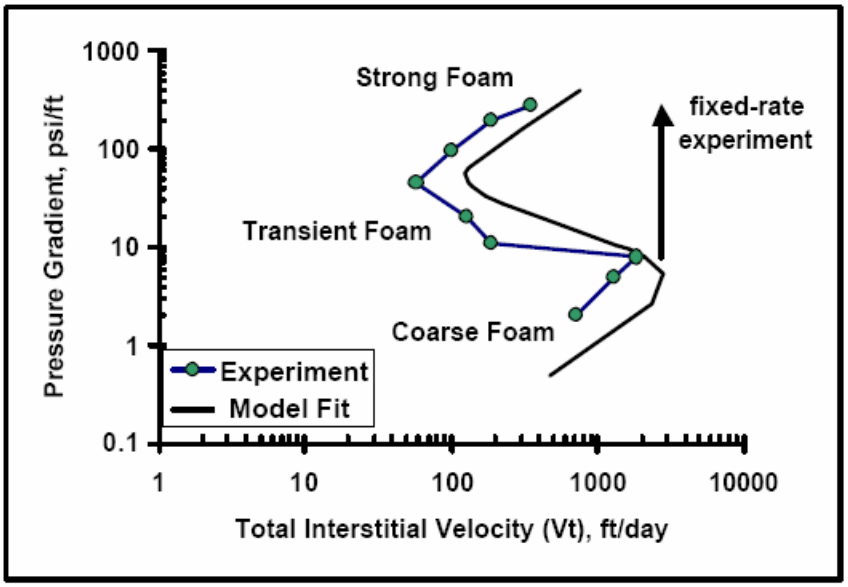

Figure 2.1: Foam-generation experiment in Berea core, from Gauglitz *et al.* (2002) (open symbols), with model fit (solid curve) from Kam and Rossen (2003). At low pressure gradient (coarse foam regime), gas mobility is high. At high pressure gradient (strong foam regime), gas mobility is much lower. In between these is an unstable transient regime.

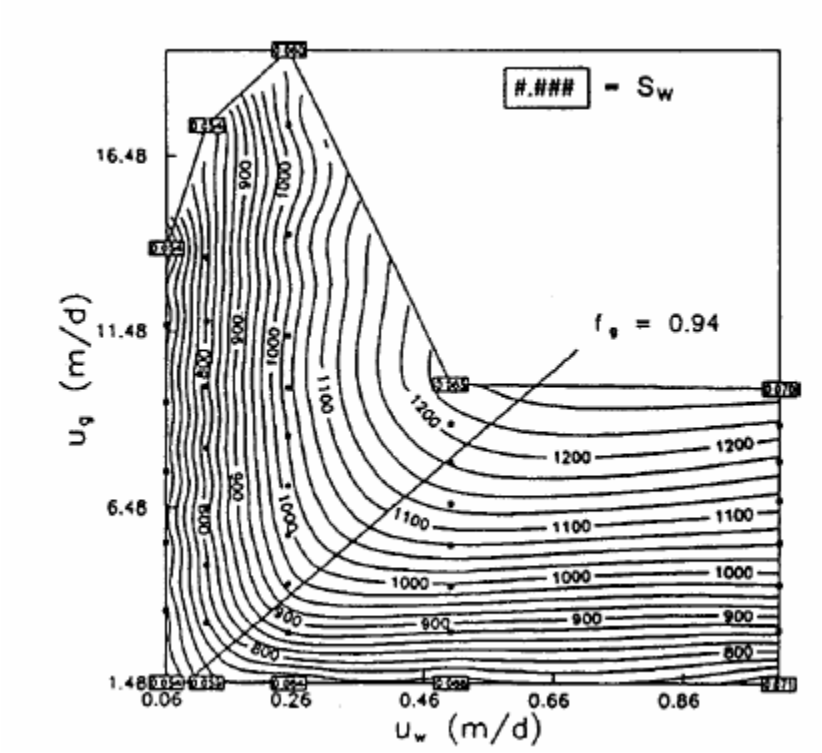

Figure 2.2: Contour drop of pressure drop as function of superficial velocities of gas (U_g) and water (U_w) in steady-state foam injection across a 2-ft sandpack, from Osterloh and Jante (1992). The upper-left region is the high-quality regime, and the lower-right region is the low-quality regime. In this case, the transition occurs at a foam quality f_g of about 0.94.

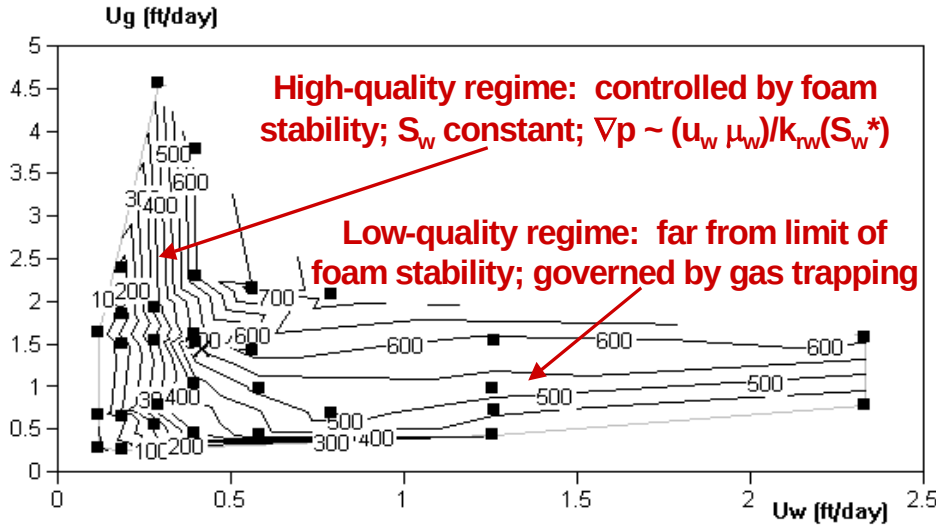

Figure 2.3: Steady-state pressure gradient as a function of superficial velocities of gas (U_g) and water (U_w) for one N_2 foam formulation in a Berea core, from Alvarez *et al*. (2001), illustrating the two conventional steady-state strong-foam regimes. Dark dots represent individual steady-state data.

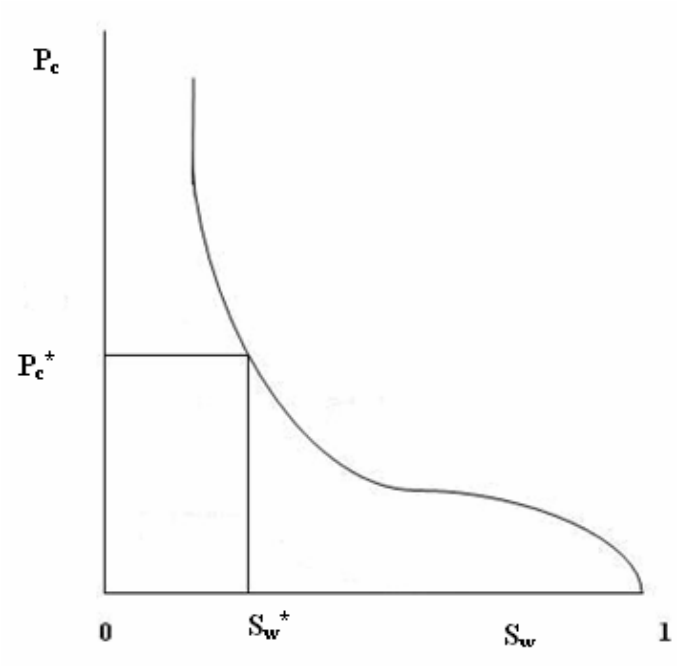

Figure 2.4: Schematic of capillary pressure P_c as a function of wetting-phase saturation S_w in a water-wet porous medium. S_w^* is water saturation at P_c^*)

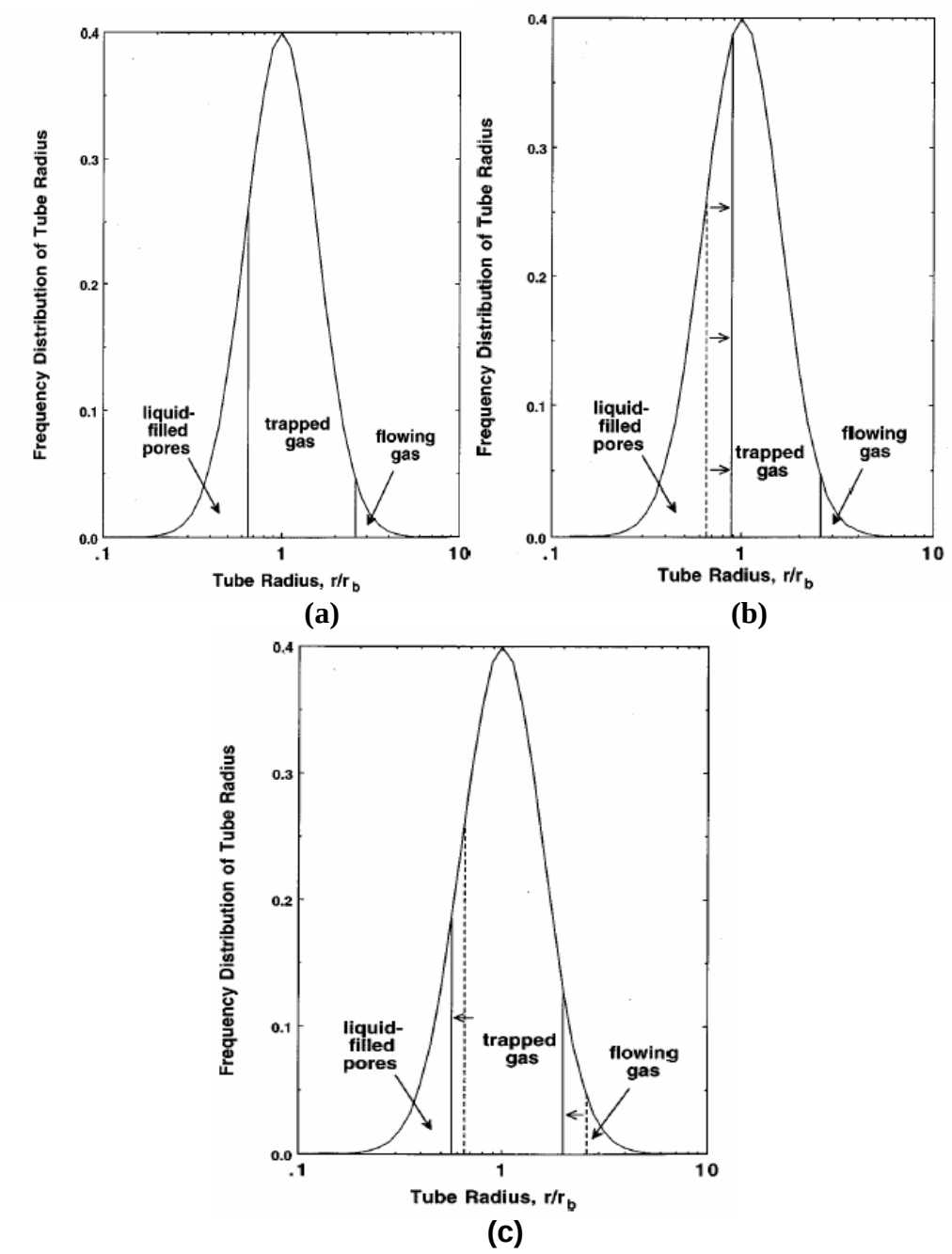

Figure 2.5: (a) Schematic of distribution of phases in foam flow in the low-quality regime. (b) Effect of increasing liquid flow rate in low-quality regime. (c) Effect of increasing gas flow rate in low-quality regime (From Rossen and Wang, 1999).

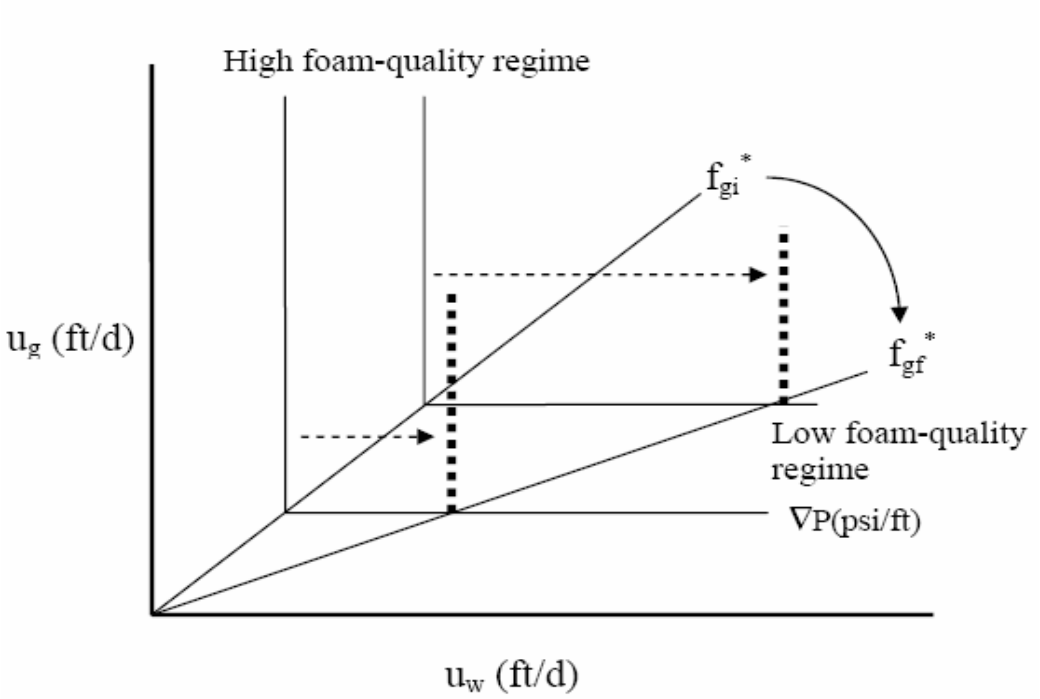

Figure 2.6: A schematic of the expected effect of reducing surfactant concentration on the two foam-flow regimes. The thin lines are two pressure-gradient contours. The thick dotted lines represent the shift in the contours when surfactant concentration decreases or oil is present, destabilizing the high-quality regime but leaving the low-quality regime unchanged. f_{gi}^* is the original value of f_g^*, and f_{gf}^* is the value after reducing surfactant concentration (Rong, 2002).

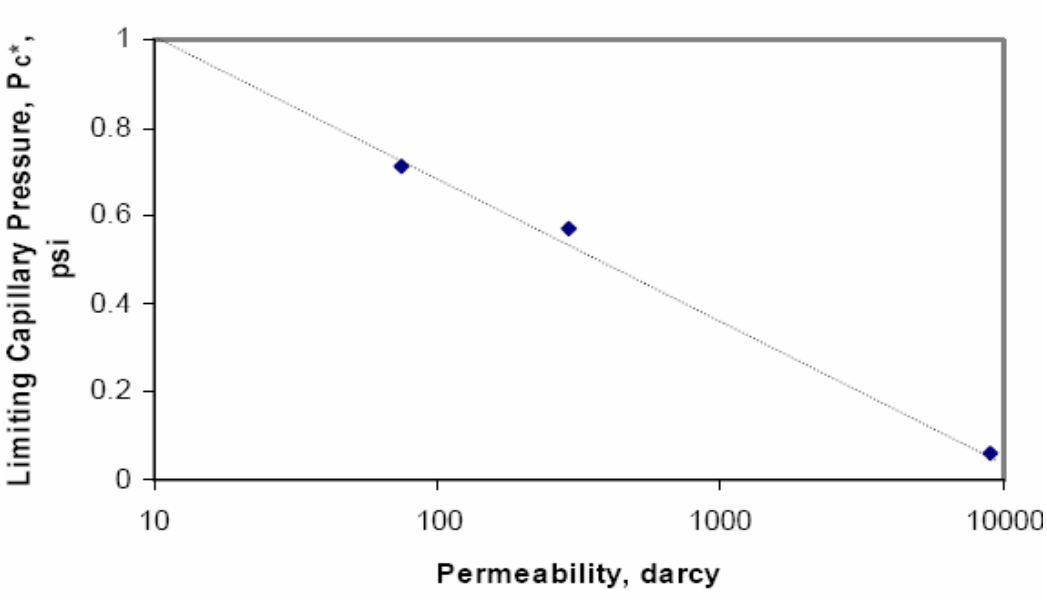

Figure 2.7: Effect of permeability on limiting capillary pressure (foam made with Siponate DS-10 surfactant at Q_g = 0.06 cm/min) (Khatib *et al.*, 1988).

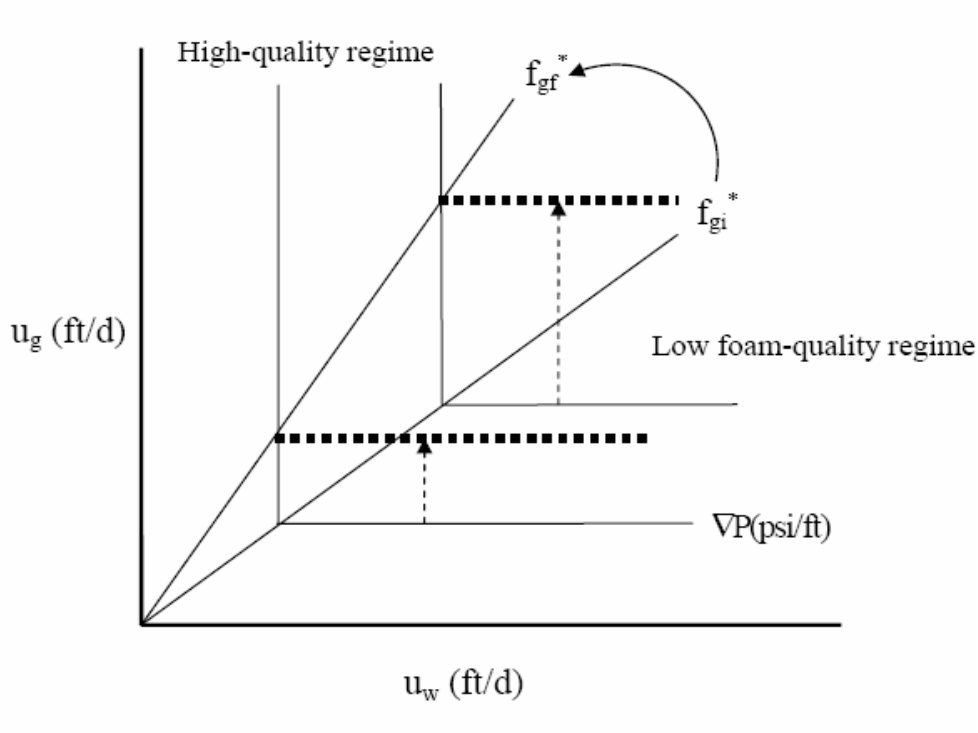

Figure 2.8: A schematic of the expected effect of increasing permeability on the two foam-flow regimes. The thin lines are two pressure-gradient contours. The thick dotted lines represent the shift in the contours when permeability increases. f_{gi}^* is the original value of f_g^*, and f_{gf}^* is the value at higher permeability (from Rong, 2002).

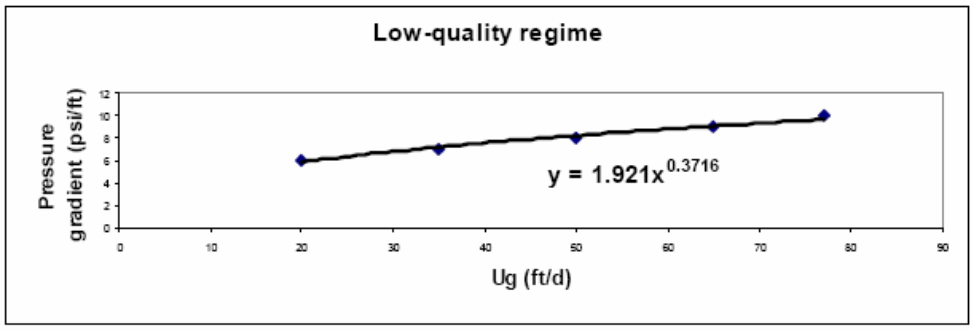

Confidence Interval = 0.104; $\rho = 0.377 \pm 0.105$
Foam rheology: Shear-thinning

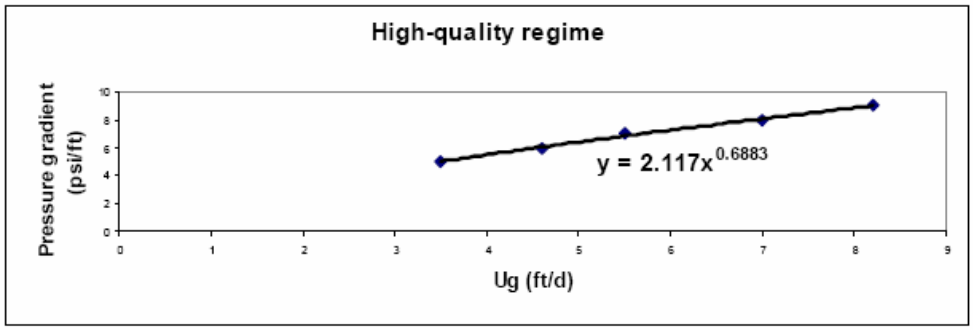

Confidence Interval = 0.072; $\rho = 0.688 \pm 0.072$
Foam rheology: Shear-thinning

Low-quality regime		High-quality regime	
U_w = 20 ft/d		U_g = 85 ft/d	
U_g (ft/d)	$\nabla P(psi/ft)$	U_w (ft/d)	$\nabla P(psi/ft)$
25	6.5	3.5	5
34	7	4.6	6
50	8	5.5	7
65	9	7	8
77	10	8.2	9

Figure 2.9: Apparent foam rheology with 2 wt% surfactant MA-80I in 210 darcy sandpack (from Rong, 2002). Power-law exponent n is 0.3716 in the low-quality regime and 0.688 in the high-quality regime.

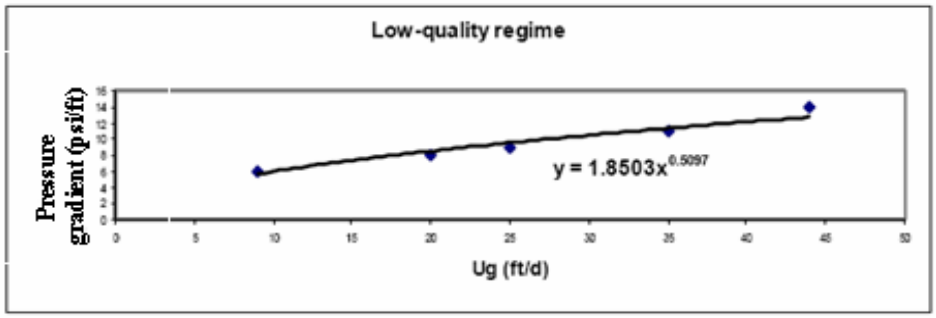

Confidence Interval = 0.214; $\rho = 0.510 \pm 0.214$

Foam rheology: Shear-thinning

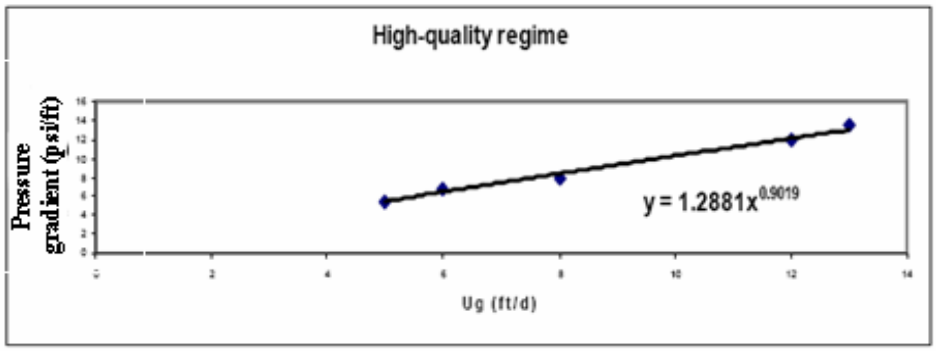

Confidence Interval = 0.211; $\rho = 0.902 \pm 0.211$

Foam rheology: Newtonian

Low-quality regime		High-quality regime	
U_w = 20 ft/d		U_g = 43 ft/d	
U_g (ft/d)	$\nabla P(psi/ft)$	U_w (ft/d)	$\nabla P(psi/ft)$
9	6	5	5.5
20	8	6	6.8
25	9	8	7.8
35	11	12	12
44	14	13	13.5

Figure 2.10: Apparent foam rheology with 0.5 wt% surfactant MA-80I in 210 darcy sandpack (from Rong, 2002). Power-law exponent n is 0.5094 in the low-quality regime and 0.902 in the high-quality regime.

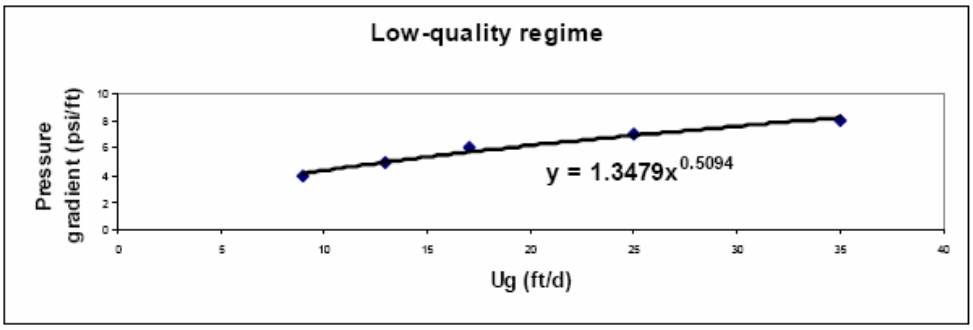

Confidence Interval = 0.115; $\rho = 0.509 \pm 0.115$
Foam rheology: Shear-thinning

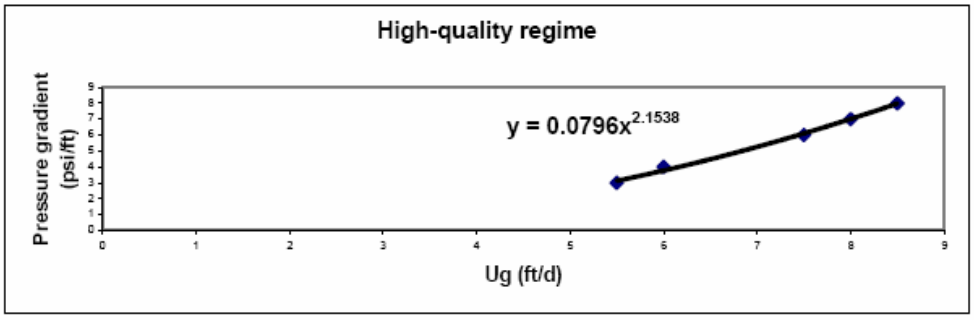

Confidence Interval = 0.360; $\rho = 2.154 \pm 0.360$
Foam rheology: Shear-thickening

Low-quality regime		High-quality regime	
U_w = 15 ft/d		U_g = 35 ft/d	
U_g (ft/d)	$\nabla P(psi/ft)$	U_w (ft/d)	$\nabla P(psi/ft)$
9	4	5.5	3
13	5	6	4
17	6	7.5	6
25	7	8	7
35	8	8.5	8

Figure 2.11: Apparent foam rheology with 0.3 wt% surfactant MA-80I in 210 darcy sandpack (Rong, 2002) Power-law exponent n is 0.5094 in the low-quality regime and 2.1538 (shear-thickening behavior) in the high-quality regime.

Chapter 3: Polymer-Enhanced Foam

3.1 INTRODUCTION

As discussed above, foam is used in for mobility control in EOR (Lake, 1989), acid diversion in well stimulation (Gdanski, 1993; Rossen and Wang, 1999) and recovery of wastes in environmental remediation (Hirasaki *et al.*, 2000; Rong, 2002).

However, foam has a limited lifetime. A possible solution is the use of polymer in conjunction with surfactant to improve foam properties. It is a familiar observation that polymer increases liquid viscosity and slows the rate of liquid drainage from bulk foam over a distance of cm. Whether polymer stabilizes foam in porous media, where water drains rapidly from one pore to the next over a distance of μm, driven by capillary forces, not gravity, is not clear.

3.2 OVERVIEW OF EOR POLYMERS

Several polymers have been applied in reservoirs throughout the world, including polyacrylamide (PAM) or hydrolyzed polyacrylamide (HPAM), Xanthan, hydroxyethylcellulose (HEC), carboxymethylhydroxyethylcellulose (CMHEC), and dextran polyethylene oxide (PEO). However, commercially attractive polymers fall into two generic classes: polyacrylamides and polysaccharides (Lake, 1989).

3.2.1 Polyacrylamides

Polyacrylamide is a water-soluble, high-molecular-weight, synthetic polymer. As applied in EOR, polyacrylamides have undergone partial hydrolysis, and are called partially hydrolyzed polyacrylamides (HPAM).

Polyacrylamide is relatively resistant to microbial attack, and its degradation is mainly through physical breakdown (Seybold, 1994). This is probably related to its extremely high molecular weight, which renders microbial attack difficult. It exhibits permanent permeability reduction (Lake, 1989) in porous media. We found in our experiments that the permeability of Boise sandstone could not be fully recovered after polymer flooding.

Historically, HPAM has been used in about 95% of reported polymer field applications (Lake, 1989). We used HPAM as the polymer additive to surfactant solution in most of our experiments.

3.2.2 Polysaccharides

Polysaccharide is more branched than the HPAM molecule. We used Xanthan gum in some of our experiments.

Xanthan gum hydrates rapidly in cold water without lumping to give a reliable viscosity, encouraging its use as thickener, stabilizer, emulsifier and foaming agent. Xanthan gum is less sensitive to salinity changes and mechanical degradation compared to polyacrylamide (Kohler *et al.*, 1981).

3.3 THE INTERACTION BETWEEN OF POLYMER AND SURFACTANT

Some of the earliest studies on surfactant/polymer interaction in the petroleum literature were in relation to surfactant flooding (Szabo, 1979; Pope *et al.*, 1982). These studies showed that sulfonate and polymer (Xanthan gum or HPAM) coexisted in solution up to a certain salinity, beyond which separate surfactant-rich and polymer-rich phases were formed, suggesting that surfactant and polymer repelled each other. The interfacial tension (IFT) experiments of Austod and Taugbol (1995) and Nilsson *et al.* (1997) indicated no associative interaction between Xanthan and HPAM and dodecyl-o-xylene sulfonate.

These results suggest that, at least for polymer-enhanced foams (PEF's) made of anionic surfactants and Xanthan or HPAM polymer, it is unlikely that polymer molecules would be adsorbed at gas-liquid interface in association with surfactant molecules. We confirm this for one pair of anionic surfactant and HPAM polymer below (Chapter 5). With molecular repulsion between surfactant and polymer, it is also unlikely that polymer molecules would be inside the thin lamella films. Most of the polymer is expected to stay in the relatively thick liquid film on tube wall (Huh and Rossen, 2006) or in Plateau borders. The implication is that the addition of anionic polymer to a foam made of an anionic surfactant would not help improve the foam's stability. On the other hand, the increase in water viscosity may significantly increase the apparent viscosity of foam.

3.4 PREVIOUS RESEARCH ON POLYMER-ENHANCED FOAM

In the literature, a wide range of polymer structures has been employed to study the effects of polymer addition on foam behavior in porous media. Anionic polymers,

such as polyacrylamide and Xanthan gum that are commonly used for enhanced oil recovery, and nonionic polymers such as polyvinyl pyrrolidone, have also been used.

An important early work on polymer-enhanced foam (PEF) was by Sydansk (1994a, b), who studied properties and effectiveness of PEF formed from C_{14}-C_{16} alpha-olefin sulfonate (AOS) surfactant and HPAM polymer. Use of PEF was intended to reduce gas mobility during its injection into a naturally fractured reservoir. High concentrations (0.35 – 0.7 wt%) of polymer were employed. Bulk PEF viscosity, PEF mobility in a Hele-Shaw cell used as an idealized fracture model, and mobility in sandpacks were compared with those for surfactant-free polymer solutions and polymer-free foams. PEF were pre-formed before injection into the fracture model or the sandpack. Results showed that PEF could be much more resistant to water drainage and foam collapse in a 100-cm^3 graduated cylinder than polymer-free foams. Core flooding results also suggested that greatly reduced gas mobility and improved stability of foam (inferred from increased pressure gradient) were due to the polymer addition.

Aarra *et al.* (1997) studied the enhancement of the gas-blocking ability of foam formed from AOS surfactant, with the addition of different polymers. Foam mobility in Berea sandstone and reservoir cores was measured for PEF with Xanthan, polyvinyl alcohol, or HPAM. The best gas blocking performance was observed with Xanthan biopolymer.

For gas control in the Prudhoe Bay field, Thach *et al.* (1996) tested PEF made from AOS or Chevron Chaser CD1045 and HPAM polymer. After laboratory evaluations of bulk-foam stability in a 25-cm^3 graduated cylinder and gas mobility with foam in a sandpack, the PEF was tested in three hydraulically fractured wells to

determine their effectiveness in reducing gas-oil ratio (GOR). In the field, the authors concluded that "gas shut-off with PEF in a hydraulically fractured well has been shown to last for periods of greater than one year."

Dalland and Hanssen (1997) carried out experiments in sandstones to investigate PEF for gas-influx control. As foam-forming surfactants, AOS and a highly fluorinated C_9-alkyl ethoxylated alcohol were employed, together with HPAM polymer. The results showed that strongly improved gas-blockage performance might be obtained by addition of polymer to the foaming-agent solution. In most cases, foams of essentially no gas-blocking ability could be transformed to very efficient gas-blocking agents by adding polymer. However, in some experiments, polymer addition did not result in a better gas-blocking foam, and a concentration effect was observed, in that adding too much polymer could give sharply reduced foam efficiency.

One desired benefit of adding polymer to foam is to increase foam stability to resident oil. Hanssen and Dalland (2000) investigated the reasons for improved oil-tolerance by carrying out foam corefloods with crude oil in the core. Based on their study, comparing results with and without polymer and with and without oil, they concluded that the only effect of polymer addition was to lower oil saturations before and during foam generation and propagation, with increased pressure gradient. The more efficient removal of oil by the low-mobility PEF bank reduced the exposure of PEF to oil, thus prolonging its integrity. In other words, they suggested that there is no intrinsic stabilizing effect of polymer on foam in the presence of crude oil.

In order to remedy the severe gas coning problem that can arise in reservoirs with a thin oil rim below a gas cap, Chukwueke *et al.* (1998) investigated the use of PEF for

gas-blocking, by carrying out reservoir-condition corefloods. The surfactants tested were AOS, a fluoro ammonium hydrocarbon, and an ethoxylated nonionic fluoro surfactant, and HPAM was used as polymer. Eight wells were treated using two foamer systems. The field results varied between a significant reduction in GOR for more than 12 months and a minor GOR reduction for only a few weeks. Judging from laboratory core tests and field tests, the AOS/HPAM combination appeared to perform better than others.

In order to attain pore-level understanding of PEF transport in porous media, Romero *et al.* (2002) carried out micromodel studies to observe movements of PEF in constricted capillaries. PEF was made of AOS surfactant and five different polymers: two HPAM's with different degrees of hydrolyzation; a non-hydrolyzed polyacrylamide; a sulfonated polyacrylamide copolymer; and a hydrophobically modified polyacrylamide. Their study on effects of polymer addition focused on determining whether the two foam-flow regimes illustrated in Figure 2.2 could still be observed: a high-quality regime where pressure gradient is independent of gas flow rate, and a low-quality regime in which pressure gradient is independent of liquid flow rate. PEF in micromodels showed quite different behavior, where the high-quality regime seemed to be absent. This type of behavior was seen in our own experiments with and without polymer, discussed below. It is partially explained by Kim *et al.* (2004).

The effects of HPAM polymer addition on foam made of a variety of surfactants have also been studied by Zhu *et al.* (1998). They measured PEF mobility in sandpacks of varying permeability (130, 50, 13 and 3 darcy) and in sandstone cores of 1.0 and 0.2 darcy. The surfactants investigated were AOS, ethoxylated sulfate, ethoxylated

nonylphenol, ethoxylated alcohol, and linear alkyl sulfonate. In their study, the effects of different liquid hydrocarbons and crude oils on foam stability with and without polymer addition were measured by bulk-foam drainage tests in a 100-cm^3 burette and mobility tests with corefloods. Their results showed that contact with lighter oils resulted in less-stable foam. The addition of polymer, however, reduced the adverse effect of oil contact.

In summary, foam with polymer has been shown to reduce gas mobility in porous media. Some studies focused increased foam stability to oil when polymer was present. Inferences that polymer stabilizes the foam have been based primarily on reduced mobility in porous media and retarded drainage of bulk foams outside porous media. As discussed below, reduced mobility in porous media may reflect increased viscosity of the aqueous phase rather than foam stability, while the drainage rate of bulk foam in glassware is unrelated to stability of foam in porous media. Thus it is still not clear whether polymer stabilizes foam in porous media.

3.5 CENTRAL HYPOTHESIS

This study was motivated by a hypothesis about how polymer interacts with foam in porous media. The hypothesis derived in turn from the observation, discussed in Chapter 2, that steady-state strong-foam behavior appears to comprise two very different flow regimes at high and low foam qualities (Figures 2.2 and 2.3). The high-quality regime is controlled by lamella stability, while in the low-quality regime foam lamellae are relatively stable, bubble size is fixed, and behavior is controlled by gas trapping and mobilization. In the high-quality regime, water saturation S_w is held nearly constant at

the water saturation S_w* corresponding to the "limiting capillary pressure" P_c* (Khatib *et al.*, 1988). In the high-quality regime, applying Darcy's law to the aqueous phase at fixed water saturation S_w* gives

$$\nabla P = \frac{U_w \mu_w}{k k_{rw}\left(S_w^*\right)} \tag{3.1}$$

where U_w is water superficial velocity, μ_w is aqueous-phase viscosity, k is permeability and $k_{rw}(S_w^*)$ is the relative permeability to the aqueous phase at S_w*. As discussed in Chapter 2, these two regimes have been observed in experiments with N_2 and CO_2 foam, in a variety of porous media including sandstones and sandpacks over a wide range of permeabilities, with many surfactant formulations (Alvarez *et al.*, 2001; Mamun *et al.*, 2002; Kim *et al.*, 2004).

Our hypothesis was that polymer affects foam in the high-quality regime by (a) viscosifying the aqueous phase (increasing μ_w) and (b) stabilizing or destabilizing foam lamellae (reducing or increasing S_w*, respectively, thereby changing k_{rw}). One can distinguish between these effects by measuring the viscosity of the aqueous phase separately from the foam (accounting if possible for the effects of shear rate on polymer viscosity). If, upon addition of polymer, ∇P in a given porous medium in the high-quality regime increases more than does μ_w, then polymer stabilizes foam lamellae (reduces S_w* and k_{rw}); if ∇P increases less than does μ_w, then polymer destabilizes the lamellae (raises S_w* and k_{rw}). If measured ∇P data are in the low-quality regime, then the relation between $k_{rw}(S_w)$ and foam stability is less direct, but one would still expect

∇P to reflect water saturation and water viscosity, and one can separate the effects of polymer on each.

An extension to this hypothesis is outlined in Section 2.8. *If* polymer stabilizes foam to the presence of oil, it may reflect a shift in the low-quality regime caused by the increase in viscosity of the aqueous phase, and not a change in the intrinsic stability of foam. This hypothesis can be tested by examining the two flow regimes with and without polymer, and with and without oil.

3.6 OBJECTIVE

In this study we investigate the effect of polymer additives on the stability of foams made from AOS surfactant. Coreflood experiments have been run with both conventional and polymer-enhanced foam, without and with oil. Both sandpacks and Boise sandstone have been used. Foam is generated by co-injecting gas and foamer solution, and pressure gradient is measured at steady state. The effect of polymer on the stability of foam is identified from the pressure gradient generated by foam with and without the addition of polymer, specifically, on the effect of the addition of polymer on the two steady-state foam regimes.

Chapter 4: Experimental Methods

4.1 EXPERIMENTAL APPARATUS

Figure 4.1 shows a simplified schematic of our coreflood apparatus. The apparatus included a liquid pump, gas tank, mass-flow controller, visual cell, core holder, backpressure regulators, data-acquisition system and flow lines.

4.1.1 Pumps

Liquid was delivered by either a syringe pump (model LC-500, ISCO Inc, Lincoln, NE) or a Beckman reciprocating pump (Model 100A, Beckman Instruments Inc., Fullerton, CA) at a constant volumetric flow rate.

The ISCO Model LC-500 is a positive-displacement pump. It has a volume capacity of 500 cc and its maximum working pressure is 3700 psi. The pump can display the pressure of the liquid inside the cylinder with a pressure-transducer cap. It is also possible to set the desired minimum and maximum pressure for the pump to work. The pump stops automatically when pressure is out of this range; it also has a function for automatic purge and refill. The flow rate range is 0-400 cc/hr with the scales of 1.5, 4, 15, 40, 150, and 400 cc/hr. With calibration at 600 psi back pressure (the same back pressure used in our coreflood experiments), the true values of these scales were found to be 1.53, 4.14, 15.5, 37.8, and 145.8 cc/hr, respectively.

The Beckman Model 100A is a dual-piston pump. A uniform flow rate is achieved by means of two cams driven reciprocating pistons, each of which displaces 0.1

cc per stroke. The pump has a maximum pressure drop of 10,000 psi, and a range of flow rates from 0.01 cc/min to 9.99 cc/min. With calibration, the true flow rate under 600 psi back pressure was found to be 1.0812 times of the set value.

4.1.2 Mass-flow controller

A Brooks mass-flow controller (Brooks Instruments Model 5850 E, Emerson Electric Company, Hatfield, PA) was used to regulate the gas injection rate. It has an operational flow range between 0 and 250 standard cc/min (i.e., at 1 atm pressure). Before use in our experiments, it was calibrated using a soap-film bubble meter illustrated in Figure 4.2. By measuring with a stopwatch the time required for the soap film to travel between two calibration marks in the tube, one can obtain the volumetric flow rate of gas of the mass-flow controller. Calibration at 600 psi back-pressure showed that the true flow rate was 1.2467 times of the set value.

4.1.3 Foam generator

In most experiments, foam was pregenerated to accelerate attainment of steady state in the core and minimize entrance effects (Ettinger and Radke, 1992). Either a 2-micron filter (Nupro Company, Willoughby, OH) or a packing of 300-μm beads was used as a foam generator, which was installed upstream of the cores.

4.1.4 Visual cells

High-pressure adjustable-volume visual cells (Temco, Tulsa, OK) were installed in-line to observe bubble sizes. One was set between the outlet of the foam generator and the inlet of the porous medium. The other was placed downstream of the outlet of the

porous medium. Through the visual cells, large bubbles appeared very bright and round, while small bubbles looked dark and opaque because of light scattering through multiple layers of bubbles (Alvarez, 1998). The visual cells were used only for qualitative purposes, e.g. to indicate whether foam was present in the line; no attempt at quantitative measurement of bubble sizes was made.

4.1.5 Core holder

Either a sandpack holder or a Hassler-type core holder was used in the experiments. In either case, the core- or pack-holder was mounted vertically and fluid was injected from the top.

4.1.5.1 Sandpack holder

The stainless-steel pack holder was made using a 1-in outside diameter (0.87 inch inner diameter) stainless-steel pipe as a column and using 1-in Swagelok fittings as the end pieces. The 1-in pipe was connected to a 0.5-in fitting, which was finally connected to a Swagelok connector capable of supporting 0.125-in tubing. The pack holder had three pressure taps along its side to allow the measurement of pressure difference across four sections of the pack holder. The sections were 2.4, 3.6, 3.6, and 2.4 in long, sequentially. Two overlapping stainless-steel screens were placed at each end of the pack holder to contain the sand within the pack holder. The screens used were #200 mesh (75-μm opening).

4.1.5.2 Hassler core holder

This Hassler-type core-holder (Phoenix Instruments, Splendora, TX) had a 0.25-in-thick Viton rubber sleeve. Along the core-holder, there were five pressure taps for pressure measurement. In this study, only three of them were used. They divided the core into four sections, 2.1, 3.9, 3.9, and 2.1 in, sequentially.

4.1.6 Pressure traducer

DP15 variable-reluctance differential pressure transducers (Validyne Engineering Co., Northridge, CA) were used to measure pressure differences across the four sections of the core. Each transducer is constructed of stainless steel with a two-piece body, within which is the sensing plate. The deflection of the plate caused by an applied differential pressure is converted to an output voltage which is measured by a carrier demodulator. The transducers have bleed screws on the side of the body for purging the lines of gas. A bypass valve is located between the higher-pressure and lower-pressure lines (not shown on Figure 4.1) to allow the transducers to be zeroed. Each transducer was calibrated, and the demodulator was adjusted, before each experiment.

4.1.7 Back-pressure regulator

There were two back-pressure regulators (BPR's) in the apparatus. One was a Mity Mite BPR (Grove Valve & Regulators, Oakland, CA) installed the downstream of the gas mass-flow controller, which required a constant differential pressure of 50 psi to work properly. (This BPR is not shown in Figure 4.1) In our experiments, the nitrogen

supply pressure was set to 1500 psi, and the dome pressure of this BPR was set to 1450 psi.

The other BPR was a Temco back-pressure regulator (Figure 4.3) (Model BPR-50, Temco Inc., Tulsa, OK) which was placed at the outlet of the apparatus to maintain a back-pressure of 600 psi downstream of the core. This high pressure moderated the effect of gas expansion during foam injection. Pressure maintenance on the dome of the BPR (not shown in Figure 4.1) was provided by a nitrogen cylinder.

4.1.8 Jerguson cell

In our first experiment, we used a Mity Mite BPR downstream of sandpack. In order to ensure that this BPR worked efficiently, only gas phase was allowed to flow through this BPR in our initial experiments. Therefore, a Jerguson cell (Jerguson Gage Company, Upper Saddle Rive, NJ) with 600 cc internal volume was installed upstream of this BPR as a foam breaker. The cell had two openings, at the top and bottom, respectively. There was a transparent window on one side of the cell so that liquid level inside the cell could be monitored. Foam effluent from the sandpack flowed into the cell through a line from the top of the cell to a location close to the bottom, below the liquid level. Silicon oil initially filled about one third of the cell volume. Foam bubbles broke as they contacted the oil, and then aqueous liquid sank to the bottom of the cell and gas rose to the top. Gas flowed out through a second line out the top to the BPR. There was a third flow line connected to a needle valve at the bottom of the cell (not shown in Figure 4.1). Liquid had to be drained periodically through the needle valve to prevent overflow of both gas and liquid downstream to the BPR. Sometimes draining this liquid from the cell

caused rapid pressure decrease in the system, requiring a long time to bring the apparatus back to steady state. Therefore, in the later experiments, we removed this cell from the system, and replaced the Mity Mite back-pressure regulator with a Temco back-pressure regulator, which worked more effectively even without the foam breaker.

4.1.9 Data acquisition

A data-acquisition system, including a personal computer, data-acquisition card, and software package LabView™, was used to collect the pressure data. The data-acquisition card (National Instruments Corporation, Austin, TX) received electrical signals in volts from pressure transducers and transformed them into digital values. LabView™ (National Instruments Corporation, Austin, TX) displayed the digital values on the computer screen.

4.2 EXPERIMENTAL MATERIALS

4.2.1 Sand

The F-95 and F-125 Ottawa sand were obtained from U.S. Silica (Ottawa, IL). To get a more homogeneous grain distribution, we sieved samples with a series of screens from 20-mesh to 200-mesh, and collected grains from the screen that retained most of the given sample. For F-95 sand we took sand retained by the 80-mesh screen (177-μm opening), and for the F-125 sand we took sand retained from 120-mesh screen (125-μm opening).

4.2.2 Boise sandstone core

Boise sandstone cores were cut from blocks obtained from Gerhard Borbonus Landscaping (Boise, ID). The cores were 1 ft long and 1.83 inch in diameter. To suppress clays, the newly cut core was first fired by putting the core into a furnace at 650°C for 24 hours, and then slowly cooled down before used in the experiments.

4.2.3 Nitrogen

Nitrogen (Matheson Tri-Gas Inc, Austin, TX) was used to maintain the dome pressure of the back-pressure regulator and as gas phase in our experiments. It was stored in cylinders with an initial pressure of 2200 psi. To minimize disruption during experiments, two gas cylinders were connected together with a three-way valve. When one cylinder ran low of gas, another was available to supply gas into the system while the first was replaced.

4.2.4 Brine solution

To further suppress swelling of any clays remaining in the core after firing, 1 wt% sodium chloride was added to de-ionized water for both initially saturating the core with brine and for the water used to make up the surfactant formulations. For experiments with sandpacks, the brine composition was 0.25 wt% sodium chloride and 0.01wt% calcium chloride.

4.2.5 Surfactant

The foaming agent was a sodium alpha olefin sulfonate (AOS), Bio-Terge AS-40 (Stephan Co., Northfield, IL), which was used in earlier studies of the two foam-flow regimes (Alvarez *et al.*, 2001; Rong, 2002). As delivered, it appeared as a slightly viscous, yellow liquid, and, according to the manufacturer, its active concentration was 39%. The CMC of this surfactant is around 0.08-0.12 wt% (Figure 4.4) (Rong, 2002). Our experiments were conducted with the concentration of the surfactant well above its CMC. All concentrations given below are active wt%.

4.2.6 Polymer

Both partially hydrolyzed polyacrylamides (Ciba Specialty Chemicals Corp., Suffolk, VA) and Xanthan (Xanvis™, Kelco Oil Field Group, Houston, TX) were used in our experiments. Both types of polymer are commonly evaluated for EOR (Lake, 1989). The partially hydrolyzed polyacrylamides included relatively low-molecular-weight Alcoflood 254s (MW: 2-5 x 10^5, 4% hydrolysis) and two high-molecular-weight polymers, Alcoflood 835 (MW: 10-12 x 10^6, 2% hydrolysis) and Alcoflood 935 (MW: 8-12 x 10^6, 10% hydrolysis). The molecular weight of Xanthan was 5-7 x 10^6. 0.1 wt% Alcoflood 254s, 0.1 wt% Alcoflood 835, and 0.05 wt% Xanthan were used in our sandpack experiments. The viscosities of these aqueous foam formulations (without gas) were 1.2 cp (Alcoflood 254s), 2.4 cp (Alcoflood 835), and 3.9 cp (Xanvis), respectively. In all cases viscosity was independent of shear rate over the range measured, which was from 0.9 to either 8 or 19 s^{-1}, depending on the formulation. 0.2 wt% Alcoflood 935, with

a viscosity of 6 cp, was used in the Boise-sandstone experiments. Further data on the viscosity of the Alcoflood 935 formulation is given in Chapter 5.

4.2.7 Oil

Decane (Mallinckrodt Baker Inc., Phillipsburg, NJ) or a 37.5°API crude oil (Chevron Research & Technology, Richmond, CA) was used in some corefloods.

4.3 EXPERIMENTAL PROCEDURES

4.3.1 Packing sand

A vibrating packing apparatus was utilized to introduce the Ottawa sand into the vertical pack-holder (steel column). Sand slowly flowed out from a funnel, passing through a set of layered screens (7 sets of screens with 1.5 mm openings, spaced approximately 1 inch apart), and then entered the holder. The layered screens allowed sand to be evenly distributed across the whole area of the holder as sand fell. The holder and funnel were vibrated using a vibrating jig and packed at a rate of approximately 0.5 cm per minute.

When sand reached the desired level in the holder, the flow of sand was stopped. The holder was kept shaking for approximately 15 minutes to allow complete settling of the sand.

4.3.2 Boise sandstone core preparation

A core was cut into a cylindrical shape, with 1.83 in diameter, and approximately 12 inches long, from a larger block of stone. As described above, the core was fired in an

oven at 650°C for 24 hours and then slowly cooled to room temperature. The core was then inserted into the core holder, and both the top and bottom end caps were put into place, to seal off the core.

Hydraulic oil was pumped from a hand pump into the top end cap, to apply an axial pressure of 1500 psi. This pushed the movable plunger securely against the end of the core, which ensured that the ends of the core made good contact with the end plates. Otherwise, the sleeve could possibly squeeze into the gaps between the core ends and the end plates when radial pressure was applied, causing the Viton sleeve to be damaged.

Utilizing the same hand pump, hydraulic oil was introduced into the annulus gap between the Viton rubber sleeve and the core-holder wall. This radial confining pressure was raised to 1500 psi, sealing the Viton sleeve to the surface of the core to prevent the flow of injected fluids on the outer surface of the core.

4.3.3 Porosity measurement

Porosity was measured for each new pack or core (both called a "core" below, for simplicity) as follows.

- Connect the vacuum pump, a burette that is filled with brine solution, and the outlet of the core by a three-way valve. Turn the three-way valve to connect the core to the vacuum pump, and then turn on the vacuum pump overnight.
- Close the valve at the bottom of the core, between the 3-way valve and the core. Switch the three-way valve to connect the core to the burette, and turn off vacuum pump. Open the valve of the burette to allow brine to flow just to

the valve at the bottom outlet of the core (which is still closed). Read the level of brine in the burette.

- Open the valve at the core outlet, allowing brine to be drawn into the core. When the brine level in the burette is stable, record the brine level.
- Calculate the volume of brine drawn out of the burette, and subtract the dead volume in end-caps and tube line to obtain the volume of brine inside core. This is the pore volume of the core.
- Calculate the porosity of the core, i.e. the ratio of the pore volume to bulk volume of the core.

4.3.4 Permeability measurement

Permeability was measured with brine solution after the porosity measurement. Permeability measurement is based on Darcy's law:

$$q/A = (k \Delta\Phi) / (\mu L)$$

$$k = (q \mu/A) / (\Delta\Phi/L)$$

where q is flow rate (cc/s); μ is viscosity of fluid (cp); A is the cross-sectional area of the core (cm^2); L is the length of core; k is permeability (darcy); and Φ is the flow potential, including gravity.

Pressure differences ΔP across the core were measured at several, different flow rates with a pressure transducer with a full scale of 2 psi (diaphragm No. 32). A straight line through origin was fitted to the plot of (q μ / A) and (ΔΦ/L) by the no-intercept

regression model (Jensen *et al.*, 2000). The slope of this line represented the permeability of the core.

4.3.5 Leakage test

Before experiments began, it was important to test for leakage. Air at a pressure of about 600 psi was applied within the interior of the apparatus (flow lines and core or pack) for about 2 hours. If a drop in pressure was detected, fittings were tightened and test was repeated until no leak was detected.

4.3.6 Preparation of polymer and surfactant solutions

Polyacrylamides were obtained as powder or microbeads. To make polymer solution, we started with aqueous salt solution at the desired salt concentration in a beaker with a magnetic stir bar. We turned the stirrer on vigorously enough to generate a vortex, and then lightly sprinkled polymer directly into the vortex. We then covered the beaker and let the solution continue to stir for 24 hours.

To make Xanthan solution, we started with the desired salt solution in a blender (Hamilton Beach, Washington, NC), set at low speed, and then added Xanthan powder and sheared the solution at high speed for 10 minutes. After that, the polymer solution was clarified by filtration through a Millipore filter paper (Millipore, Billerica, MA) with an opening size of 1.2 μm, at 20 psi pressure difference across the filter, using a Fann Filter Press (Model 12 BL, Fann Instrument Company, Houston, TX).

To make polymer-surfactant solutions, the surfactant solution was prepared first in a beaker, by adding the given amount of surfactant to brine and stirring moderately

with a magnetic stir bar. We then slowly added polymer solution to make the desired concentration of both polymer and surfactant. The final formulation was kept stirring for two hours to obtain a homogenous solution, and was then filtered again using a Millipore filter with an opening of 1.2 μm and a pressure difference of 20 psi across the filter.

4.3.7 Viscosity measurements

Before each type of polymer-surfactant solution was pumped into a sandpack or a core, its viscosity was tested using a Contraves Low Shear 30 Viscometer (Contraves AG, Zurich, Switzerland), which is a rotational rheometer based on Couette principles. It analyzes the steady shear stress between a rotating cup and bob. The cup rotates at a prescribed speed, and the stationary bob connected to a torsion wire within the rotating cup measures the shear force. The deflection of the torsion wire reflects the torque, and the amount of torque is indicated on a digital display. Readings can be taken at different shear rates from 0.0174 s^{-1} to 128.5 s^{-1}, and it can be easily converted into units of centipoise using a chart provided with the instrument. The sample size required to fill the cup is approximately 1 cc.

4.3.8 Injection procedure

After permeability measurement, we injected at least 10 pore volumes (PV) of surfactant solution into the core to satisfy adsorption of surfactant, and then gas injection began. Gas and liquid injection rates were set to obtain a specific foam quality at the imposed back-pressure of 600 psi. Steady state was assumed when pressure drop though the core held approximately constant. After steady state was achieved, liquid injection

rate, gas injection rate or both were changed to obtain a new point on a plot such as Figures 2.2 and 2.3.

Oil is easily displaced from sandpacks by high pressure gradients. Therefore, to produce reproducible, fairly constant conditions with oil present, we injected oil along with the foam at a rate of 22% of the aqueous phase volume, which is similar to what Rong (2002) did. Similar method was also used by Zhu *et al.* (1998), who simultaneously injected nitrogen, surfactant solution and oil, with oil injected at a rate of 10% of the aqueous phase volume. This approach avoids the artifact criticized by Hanssen and Dalland (2000), discussed in chapter 3, i.e. that the apparent effect of polymer stabilizing foam may in fact reflect lower residual oil saturation with polymer before foam is introduced.

4.3.9 Data analysis

For each steady-state datum, pressure gradient was calculated from the pressure difference across the third section of the core or pack. Using the third section minimizes the likelihood of entrance artifacts (Ettinger and Radke, 1992) but avoids the possibility of an artifact at the core outlet. Superficial velocities were calculated from injection rates, adjusting the gas velocity for the average pressure in the third section of the core.

The results, (pressure gradient as a function of liquid and gas superficial velocities) were plotted as an XYZ contour plot using Deltagraph™ software (Deltapoint, Inc., Monterey, California). The contour lines were automatically drawn by this software by interpolating linearly inside triangles formed by nearest-neighbor triplets of points.

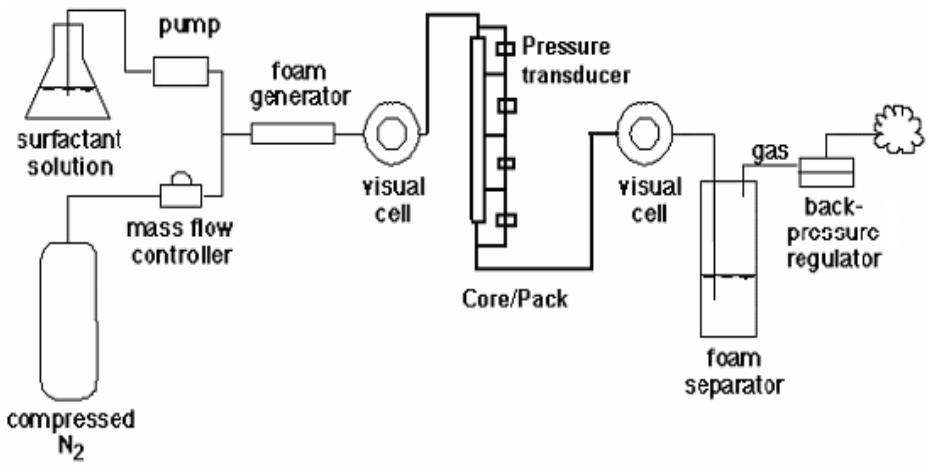

Figure 4.1: Schematic of experimental coreflood or sandpack apparatus for studying foam in porous media.

Figure 4.2: A soap-film flow meter used for calibration of the mass-flow controller.

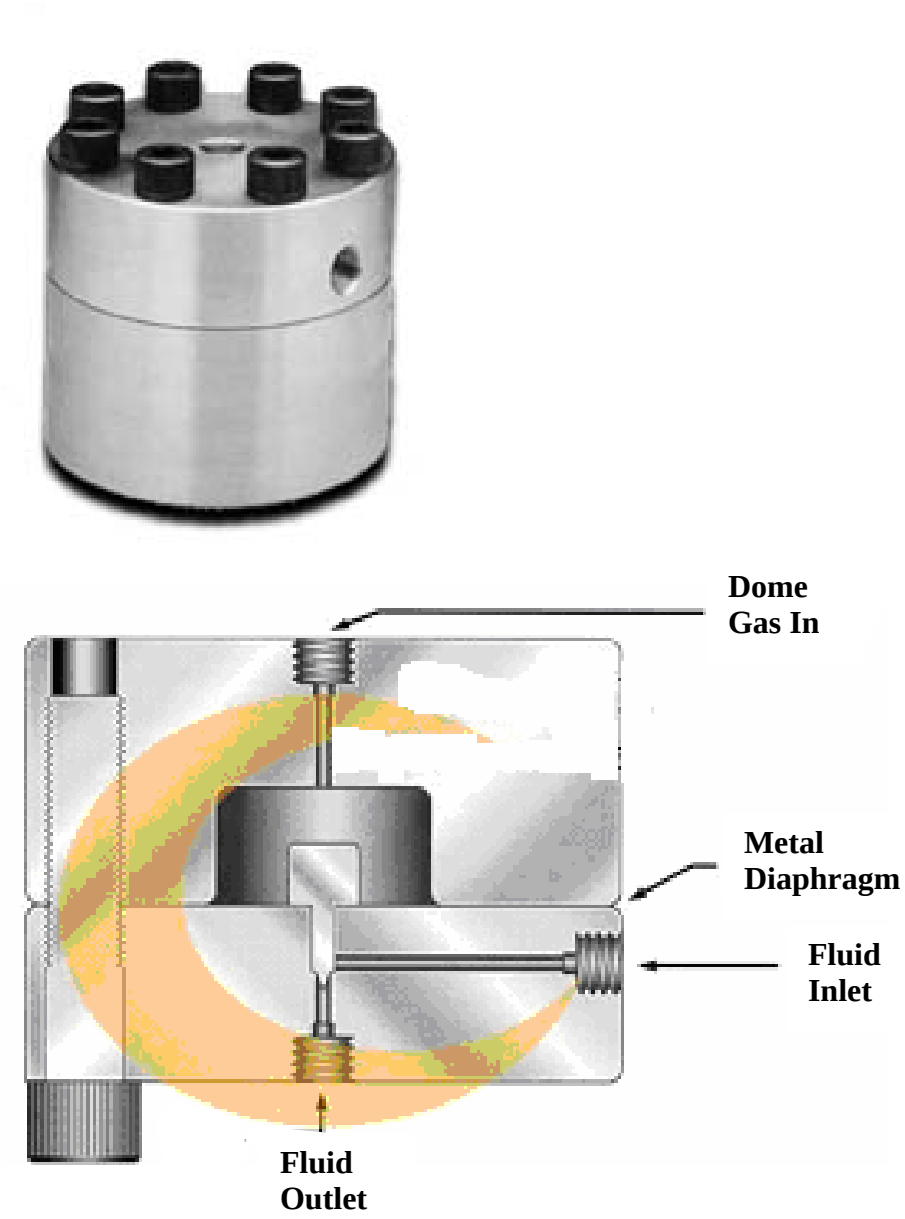

Figure 4.3: Temco back-pressure regulator (BPR-50).

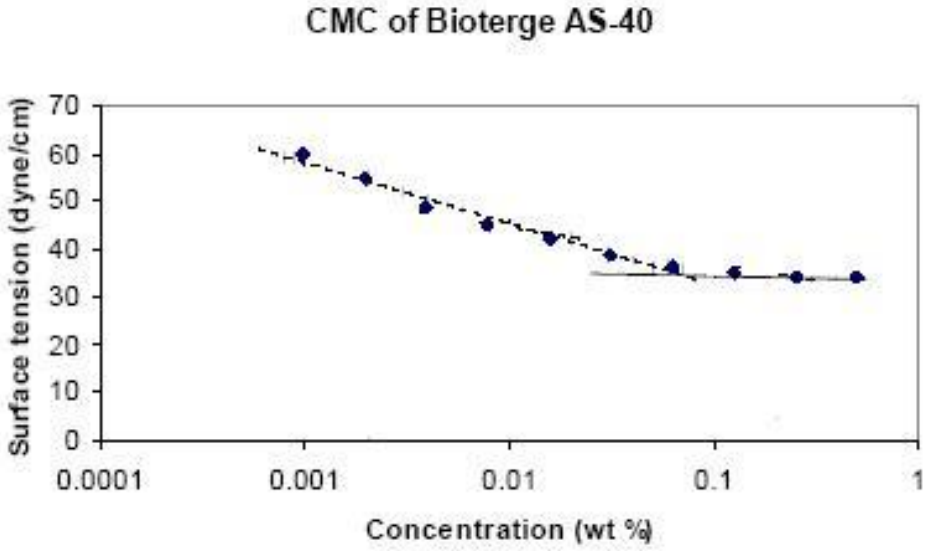

Figure 4.4: The critical micelle concentration (CMC) of Bio-Terge AS-40. The concentrations of surfactant were given as active wt% (Rong, 2002).

Chapter 5: Experimental Results and Discussion

5.1 EFFECT OF POLYMER ON SURFACE PROPERTIES

Polymer can stabilize foam only if polymer resides in the lamellae to stabilize them against drainage. As noted above, it is hard to rationalize how polymer coils could exist in the narrow confines of a lamella (~30-100 nm wide) unless polymer complexes with surfactant at the interface. If polymer does so, it should affect the surface tension of surfactant solution against air. We examined this issue with Alcoflood 935 polyacrylamide polymer using a Du Nouy Interfacial Tensiometer (Central Scientific Company, Inc., Chicago, IL).

Figure 5.1 shows the effect of polymer and surfactant concentrations on surface tension at room temperature of aqueous solutions of surfactant Bio-Terge AS-40 (AOS) with no added salt in this case. There was little effect of polymer on surface tension, and the small effect that was present (higher surface tension with polymer than without) does not suggest positive association between polymer and surfactant at the surface.

We also examined the viscosity of Alcoflood 935-AOS solution using a Contraves Low Shear 30 Viscometer (Contraves AG, Zurich, Switzerland). Figure 5.2 illustrates the effect of polymer and surfactant concentrations and shear rate on viscosity. At 1 wt% NaCl, surfactant had virtually no effect on polymer-solution viscosity, and shear-thinning effects began above about 200 s^{-1} at a polymer concentration of 0.1 wt%. According to Lake (1989), the characteristic shear rate for single-phase flow in a 1-darcy porous medium at a superficial velocity of 1 ft/d is about 10 s^{-1}. This shear-rate estimate

is based on the assumption that polymer fully occupies all pores and flows at a moderate velocity. Polymer in thin films between bubbles and pore walls, moving at the velocity of flowing gas in foam, may experience a higher shear rate. The variety of shear regimes for polymer in water-filled pores, in the films surrounding bubbles, and in the Plateau borders between bubbles makes it difficult to relate rheology measured at fixed shear rate in a rheometer to that experienced in foam in porous media. Our corefloods with Alcoflood 935 polymer were conducted at 0.2 wt% concentration of polymer. According to Figure 5.2, at this concentration, in 1% NaCl brine, behavior is Newtonian up to a shear rate 5 to 10 times that estimated using the formula of Lake (1989).

5.2 EXPERIMENTS IN SANDPACKS

As noted above, our plan was to characterize the effect of polymer on foam by its effect on the two steady-state strong-foam regimes illustrated in Figures 2.2 and 2.3. We chose initially to conduct corefloods in sandpacks to avoid having to distinguish foam effects from polymer permanently altering the permeability of the medium, as can happen at lower permeabilities (Lake, 1989) (and as we observed in Boise sandstone, as discussed below). While the permeability of sandpacks is much higher than in most oil reservoirs, and pressure gradients lower, foam shows the same basic trends in behavior in sandpacks as in consolidated core: two flow regimes (Figure 2.2; Alvarez *et al.*, 2001; Rong, 2002); foam collapse at a limiting capillary pressure (Khatib *et al.*, 1988); foam generation at a minimum pressure gradient (Gauglitz *et al.*, 2002); and other steady states at pressure gradient below that of the strong-foam state (Gauglitz *et al.*, 2002).

Our first experiments were conducted in sandpacks of permeability 6.6 and 16.6 darcy. Figure 5.3 shows the behavior of foam without polymer in a 6.6-darcy sandpack. There appears to be a high-quality regime (vertical ∇P contours) at lower liquid superficial velocity U_w. At higher U_w (right-hand side of the plot) the ∇P contours are not horizontal as expected in the low-quality regime (*cf*. Figures 2.2 and 3.2), but show decreasing ∇P as U_w increases at fixed gas superficial velocity U_g. Similar behavior is reported by Romero *et al*. (2002) and Kim *et al*. (2004). There is one other aspect of these results that is unexpected. Rather than a smooth transition from the high-quality to low-quality regimes (Figures 2.2 and 2.3), one finds a drastic increase in ∇P between them. Figure 5.4 plots a transect through the ∇P data of Figure 5.3 at $U_g \sim 9$ ft/d. ∇P increases gradually with U_w in the two low-U_w data points, as expected in the high-quality regime (*cf*. Figures 2.2 and 2.3), and decreases gradually in the two data at high U_w. Between these pairs of data there is a drastic increase in ∇P, which implies an extremely shear-thickening response to increasing U_w. Normally, one would associate this sort of behavior with hysteresis resulting from a foam-generation event (Gauglitz *et al*., 2002). But we found the ∇P data on both sides of the jump in ∇P to be reproducible. We have no explanation for this behavior. Figures 5.3, 5.5 and 5.6 show the same abrupt jump in ∇P with polymer in a 6.6-darcy pack and without polymer in a 11.8-darcy sandpack. Both plots also show decreasing ∇P as water superficial velocity increases in the low-quality regime.

Comparison of Figures 5.3 and 5.5 shows that the polyacrylamide polymer *de*stabilized foam in the 6.6-darcy sandpack in the absence of oil. One would expect

pressure gradient to increase slightly given the slightly higher viscosity of the low-MW polyacrylamide polymer compared to water, but pressure gradient was lower at all superficial velocities.

Figures 5.7 to 5.9 show data for this surfactant formulation in a 16.6-darcy sandpack with, respectively, 0.1 wt% high-MW polyacrylamide (MW~10-12 x 10^6); 0.05 wt% Xanthan (MW~5-7 x 10^6); and foam without polymer in the same sandpack after the polymer-foam experiments in that pack. The solution of surfactant and high-MW polymer had a viscosity of 2.4 cp, while the solution of surfactant plus Xanthan had viscosity 3.9 cp.

With higher-MW polymer (Figure 5.7), values of ∇P were comparable to those in Figure 5.9, i.e. without polymer. The values of ∇P in Figure 5.8, with Xanthan polymer (3.9 cp viscosity for the aqueous phase) are likewise comparable to those on Figure 5.9. Again, one concludes that polymer *de*stabilized foam (increases water saturation and k_{rw}), while the increase in the viscosity of the aqueous phase partially compensated for this effect.

Comparison of these figures suggests that without oil, polymer increases the foam pressure gradient by a factor less than it increases the viscosity of the aqueous formulation alone (or does not increase pressure gradient at all). This suggests that ***polymer destabilizes foam modestly***, raising water saturation S_w and water relative permeability k_{rw} (Eq. 3.1), ***but the increase in the viscosity of the aqueous phase partially compensates for this effect in the measured pressure gradient***.

5.3 EXPERIMENTS IN BOISE SANDSTONE

We also conducted experiments in a 0.94-darcy Boise sandstone core (Gerhard Borbonus Landscaping, Boise, ID) with Alcoflood 935 polyacrylamide polymer, the polymer used to prepare Figures 5.1 and 5.2.

With lower permeability than sandpacks (about 1 darcy v. several or tens of darcy) there is a greater chance of polymer adsorption altering the permeability of the medium (Lake, 1989). We found that injection of many pore volumes of 0.1 wt% polymer solution (in 1 wt% NaCl), followed by many pore volumes of polymer-free brine, reduced the permeability of our first Boise core from 1.59 darcy to 0.94 darcy, a decline of about 40%. Subsequent injection of 0.2-wt% polymer solution had no further effect on permeability. The second Boise core had an initial permeability of 1.67 darcy. We did not measure its permeability after polymer injection, but it probably decreased by about the same amount as the first core.

Figure 5.10 shows the behavior of foam made with 0.39 wt% active Bio-Terge AS-40 in 1 wt% NaCl brine in the first Boise sandstone core. The two regimes look much as they do in Figures 2.2 and 2.3, with no abrupt jump in ∇P in the high-quality regime, and virtually horizontal contours in the low-quality regime. Figure 5.11 shows the behavior of the same formulation in the same core with 0.2 wt% Alcoflood 935 polymer added to the surfactant formulation. The low-quality regime is nearly unchanged by the addition of polymer. There is an increase of about a factor of 2 in ∇P in the high-quality regime (vertical contours at low U_w). The viscosity of the liquid phase is about 6 cp with this polymer, however (Figure 5.2). If polymer left the stability

of foam unchanged, as reflected in P_c* and S_w*, ∇P would then be expected to increase by roughly a factor of 6 (Eq. 3.1). The fact that ∇P increases by much less than this means that ***the presence of polymer destabilized foam by an amount sufficient to raise S_w* and $k_{rw}(S_w$*) by about a factor of 3***.

Figure 5.12 shows the behavior of the same foam formulation with no polymer or oil in the second Boise sandstone core. The pattern is substantially similar to that in the first Boise core. The high-quality regime appears to extend to higher liquid superficial velocity in Figure 5.12 than in Figure 5.10, but this may be an artifact of interpolation: data were taken at higher liquid and gas superficial velocities (U_w = 1.5, U_g = 1 ft/d) in this case than in Figure 5.10, and contours constructed around these data extend the high-quality regime. In this case, unlike Figure 5.10, the core had not yet contacted polymer when this foam was injected. Figure 5.13 shows the same foam formulation with 0.2 wt% Alcoflood 935 polymer added, but not oil, in the second Boise core. The pattern of the data in this figure is consistent with Figure 5.11 and is reminiscent of Figures 5.3, 5.5, 5.6, 5.8, and 5.8. As with Figure 5.11, polymer did not increase the pressure gradient with foam as much as expected from the viscosity of the polymer solution alone. Over most of the range of superficial velocities it had little or no effect on pressure gradient. At high gas superficial velocity and low liquid superficial velocity, addition of polymer produced a small increase in pressure gradient, but less than the increase in the viscosity of the aqueous solution. Therefore, as with Figure 5.11, we conclude that ***the presence of polymer destabilizes foam, but the increase in aqueous-solution viscosity partially or fully compensates for this effect***.

5.4 EXPERIMENTS ON THE EFFECT OF OIL IN SANDPACKS

One goal of this work was to examine the effect of oil on foam both with and without polymer. We used decane as the oil in the initial tests.

These experiments on the effect of oil on foam with and without polymer were conducted in a 3.67-darcy sandpack. The surfactant formulation was the same as before (0.39 wt% active Bio-Terge AS-40 in 0.25 wt% NaCl and 0.01 wt% $CaCl_2$ brine). Polymer-foam solutions in this portion of the study contained 0.05 wt% Xanthan polymer in the surfactant formulation, one of the formulations discussed above (see Figure 5.8). However, with this batch of polymer solution the viscosity of the aqueous surfactant formulation with polymer (without gas) was 4.6 cp, rather than 3.9 cp as cited above. The viscosity varies slightly from one batch of mixed polymer solution to another.

Figure 5.14 shows behavior with no polymer and no oil in the 3.67 darcy sandpack. Figure 5.15 shows behavior with decane but no polymer. Decane reduced the pressure gradient with foam moderately here, i.e. by about 30-40%. Thus decane does destabilize this foam in the sandpack. ∇P is lower in Figure 5.15 than in any of the plots presented so far at any permeability.

Figure 5.16 shows the same system with decane and with Xanthan polymer in the foam formulation. Pressure gradient was actually a little lower than without polymer. ***Polymer did not stabilize foam in the presence of decane***. In fact, given that the aqueous phase is 4.6 times as viscous in Figure 5.15 as in Figure 5.14, polymer must have *de*stabilized foam, reflected in a rise in water saturation and water relative permeability (Eq. 3.1).

Figure 5.17 shows the behavior of foam without polymer or oil in the same sandpack as the preceding figures, after that sandpack had contacted both polymer and oil. Evidently some oil remained in the pack; the pressure gradient is less than in Figure 5.14. Thus foam is sensitive to even the relatively small residual oil saturation left behind in this sandpack at high pressure gradient.

5.5 EXPERIMENTS ON THE EFFECT OF OIL IN BOISE SANDSTONE

Our final experiments were conducted using a 0.94-darcy Boise sandstone core with two oils, decane and a sample of 37.5°API crude oil. Initial tests (shaking 100 ml of surfactant solution in a 500 ml plastic bottle), with and without polymer, with and without decane or crude oil, suggested that this crude oil is more detrimental to foam than is decane, and that polymer does aid the stability of the foam. In these experiments we used Alcoflood 935 polyacrylamide polymer, used to prepare Figures 5.1 and 5.2.

Figure 5.18 shows the behavior of foam without polymer but with decane. The data have lost the characteristic trends of the low- and high-quality regimes. Pressure gradient was substantially reduced in what used to be the low-quality regime, but increased somewhat at the lowest liquid injection rates (upper-left portion of figure). Similar trends to Figure 5.18 were observed in experiments with CO_2 foam described by Kim *et al*. (2004), as well as (in the low-quality regimes) in Figures 5.3, 5.5 and 5.6 above. Emulsions between oil and surfactant solution can substantially change the rheology of foam and in some cases increase the pressure gradient over that in the absence of foam (Yang and Reed, 1989). Over most of the range of injection rates, however, ***the addition of decane reduced the pressure gradient with foam.***

Figure 5.19 shows the behavior of foam with polymer and added decane. The presence of polymer had virtually no effect on pressure gradient with foam and oil (Figure 5.18). ***This polymer did not stabilize the foam to the presence of decane in this Boise core***.

Figure 5.20 shows the effect of the injection of the 37.5° API crude oil on the foam without polymer. As with decane, ***the addition of crude oil destabilized the foam*** (*cf*. Figures 5.12 and 5.20). Figure 5.21 shows the effect of addition of polymer to the aqueous solution in the presence of crude oil. As with Figures 5.18 and 5.19, ***this polymer did not stabilize the foam in the presence of crude oil in this Boise core***.

5.6 DISCUSSION

5.6.1 Rheology of foam with polymer

According to Eq. 3.1, foam rheology in the high-quality regime is effectively set by the rheology of the aqueous phase, with S_w fixed at S_w* (Rossen and Zhou, 1995; Alvarez *et al.*, 2001). With water saturation fixed at S_w*, water relative permeability is fixed, while its viscosity may respond to shear rate. Therefore, foam with polymer in the aqueous phase would be expected to be shear-thinning in the high-quality regime as the polymer solution itself is shear-thinning.

In the low-quality regime, foam rheology is controlled by the mobility of gas bubbles, and foam behavior is shear-thinning even if the aqueous phase is Newtonian (Rossen and Wang, 1999; Alvarez *et al.*, 2001). However, Huh and Rossen (2006) found that foam with a shear-thinning liquid shows more highly shear-thinning behavior

because the aqueous film with shear-thinning rheology coats the pores filled with gas bubbles.

5.6.2 Explanation for foam behavior in the low-quality regime

Most of our experimental results failed to reflect the behavior observed by Alvarez *et al.* (2001) and Rong (2002) (Figures 2.2 and 3.2): rather than ∇P independent of either gas superficial velocity (high-quality regime) or liquid superficial velocity (low-quality regime), ∇P decreased upon increasing liquid superficial velocity at fixed gas superficial velocity. Similar behavior was observed in some cases with CO_2 foam above the critical pressure of CO_2 (Kim *et al.*, 2004). We can explain the new behavior in part, with earlier theoretical work of Hirasaki and Lawson (1985) and de Vries and Wit (1990), by considering gas mobility in the low-quality regime.

5.6.2.1 Model of Hirasaki and Lawson

In this section we apply the derivation of Kim *et al.* (2004), using the viscosity we measured for one of our polymer solutions. Hirasaki and Lawson (1985) proposed a reasonable conceptual mode for foam flow in a natural porous medium which is a bundle of parallel cylindrical capillaries of the same radius, without constrictions. They assumed that bubbles are at least as wide as the capillaries and are separated by short slugs of liquid. Then, they derived an equation for the apparent viscosity:

$$\frac{\mu_{app}}{\mu} = L_s n_L + 0.85\frac{(n_L R)}{(r_c/R)}(3\mu U/\sigma)^{-1/3}\left[(r_c/R)^2 + 1\right] + (n_L R)(3\mu U/\sigma)^{-1/3}\sqrt{N_s}\frac{(1-e^{-N_L})}{(1+e^{-N_L})} \quad (5.1)$$

where L_s, R and r_c are the length of liquid slug, radius of the capillary tube and radius of curvature of gas-liquid interface, respectively; σ is surface tension; μ is liquid viscosity; n_L is the number lamella per unit length; U is the interstitial velocity of bubbles; and N_s and N_L are dimensionless groups. The three terms in above equation represent the resistance for foam flowing caused by the liquid slug, the distortion of the interface under flow, and surface-tension gradient, respectively.

For a foam comprising individual lamellae with bubbles touching one another, L_s = 0. Then, the above equation becomes:

$$\mu_{app} = \left[0.85\frac{n_L}{r_c}(r_c^2 + R^2) + n_L R\sqrt{N_s}\frac{1-e^{-N_L}}{1+e^{-N_L}}\right]\left[\frac{\sigma\mu^2}{3}\right]^{1/3} U^{-1/3} \quad (5.2)$$

where

$$r_c = R\left[\frac{1}{3(1-\pi/4)}\frac{1-\Gamma}{\Gamma}\right]^{1/2}\left[\frac{r_B}{R}\right]^{3/2} . \quad (5.3)$$

In the Eq. 5.3, following Hirasaki and Lawson, Γ is foam quality in gas-filled pores (i.e. excluding water in water-filled pores) and r_B is equivalent radius of bubble if unconstrained by the pore and allowed to take a spherical shape. For bubbles larger than pores, $n_L = (3/4)\ \Gamma\ R^2/r_B^3$. According to Hirasaki and Lawson, $N_s = \beta/r_c$, where

empirical factor $\beta = 5$ cm. $N_L = (L_B/r_c)\,(3\mu U/\sigma)^{-1/3}/\,(N_s^{1/2})$. L_B is length of thin liquid film on the capillary wall. When bubbles are touching, $L_B = \Gamma/n_L - 2r_c + [(4-\pi)\,(r_c^2/R)]$.

The definition of apparent viscosity from Hirasaki and Lawson is

$$\mu_{app} \equiv R^2 \nabla P / (8U) \tag{5.4}$$

Applying equation 5.2 to our cases, with the viscosity of polymer-surfactant solution μ_{pf} in place of the viscosity of liquid phase in Hirasaki and Lawson (1985), and combining equation 5.2 and 5.4, one can obtain pressure gradient as a function of the velocity of bubbles under the assumption that all gas and water flow in foam through all pores with the same size.

For example, assume that R = 10 μm, $r_B = 2.5R$, $\mu = 0.006$ Pa s, $\sigma = 0.035$ N/m, and U = 2.27 ft/day, we can obtain the plot of pressure gradient and liquid velocity, as shown in Figure 5.22.

Figure 5.22 shows that pressure gradient decreases with increasing liquid velocity at constant gas velocity, which is the same trend seen in many of our experiments (*cf*. Figures 5.3, 5.5-5.9, 5.15-5.17, 5.19-5.21). One can obtain effective viscosity from ∇P in Figure 5.22 using Eq. 5.4; the result is in Figure 5.23. As pointed out by Kim *et al*. (2004), in Hirasaki and Lawson's model, an increase in liquid velocity causes a decrease in apparent viscosity of foam because bubbles can slide over a thicker liquid film on the wall more easily than a thinner film. However, in real porous media, the relationship among pressure gradient, velocity and apparent viscosity is much more complex. Nonetheless, Figure 5.23 illustrates that increasing liquid velocity at constant gas velocity

could reduce the resistance to the movement of foam bubbles, and cause a decrease in apparent gas viscosity.

5.6.2.2 Model of de Vries and Wit

de Vries and Wit (1990) conducted foam experiments to investigate the rheology of foam, and they also formulated a semi-quantitative model to explain the behavior they found. Their model was a simplified description of foam in a single capillary, coupled with an extension to foam flow in a bundle of identical parallel capillaries. de Vries and Wit's reasoning is similar to that of that of Kim *et al.* (2004), based on Hirasaki and Lawson's (1985) model: the film of water along the wall in gas-filled pores gets thicker as U_w increases, which reduces the resistance to movement of gas. Therefore, pressure gradient decreases with increasing U_w in the low-quality regime. Kim *et al.* (2004) provide a critique of the details of the model.

Figure 5.24 shows the fit of the model of de Vries and Wit to their experimental data. Their data fell into two regimes. Kim *et al.* (2004) re-plotted de Vries and Wit's experimental data in the style of Figures 2.2 and 2.3, shown here as Figures 5.25 and 5.26, and found their two flow regimes were similar to the high-quality and low-quality regimes. Figure 5.25 shows the type like Figures 2.2 and 2.3, but Figure 5.26 shows the trend seen in our experiments: pressure gradient decreasing with increasing liquid velocity at fixed gas velocity.

We replotted our data in the low-quality regime based on the axes $[(U_g/U_w)^{4/3}, (k\nabla P/U_g^{1/3})]$ proposed by the theory of de Vries and Wit (1990) (Figure 5.24). In Figures 5.27 and 5.28 the data lie on a single trend, as de Vries and Wit predicted for foam below

the “break point". In other cases (Figures 5.28 to 5.30) there is more scatter in the trend, as with de Vries and Wit's own data below the "break point" (Figure 5.24). The model cannot explain all our experimental results.

5.6.3 Possible explanations of destabilization of polymer on foam lamella

Polymer causes foam lamella to break probably in two ways. First, in porous media, when foam moves from the pore constriction to the pore body, the lamella is stretched , which exerts a higher disjoining pressure, and then fluid surrounding the sand grains is needed to flow into the stretched lamella to prevent its thickness from falling below h_{cr} (Jimenez and Radke, 1989). However, there is no sufficient time for fluid to transport along the channel and in the Plateau borders into lamella to heal the thinning of a lamella due to higher resistance with addition of polymer. Therefore, polymer makes lamella break more easily. Second, with polymer only in the Plateau borders as discussed in section 5.1, an osmosis pressure would exist, which causes diffusion of water from lamella to Plateau border. So, with addition of polymer, lamella becomes thinner.

5.7 CONCLUSIONS

We began this study intending to investigate whether polymer stabilizes foam without oil based on the effect of polymer on the two foam-flow regimes, and with a hypothesis for why polymer might stabilize foam in the presence of oil based on its effect on the two regimes. In most cases we did not observe the two conventional regimes illustrated in Figures 2.2 and 2.3. Nonetheless, the following conclusions can be drawn from this study:

- For the polymers (Xanthan and partially hydrolyzed polyacrylamide), oils (decane and 37.5° API crude oil), and surfactant (Bio-Terge AS-40, an alpha-olefin sulfonate), tested here, it appears from coreflood pressure gradient ∇P that polymer *de*stabilized foam somewhat, raising water saturation S_w and water relative permeability k_{rw} (Eq. 3.1). Any increase in pressure gradient ∇P observed resulted from the increased viscosity of the aqueous phase. In all cases examined, this increase was less than predicted from the increase in the viscosity of the aqueous phase alone.
- For the same polymers and surfactant, polymer did not stabilize foam in the presence of decane or 37.5°API crude oil.
- The two regimes were observed with and without polymer in Boise sandstone, but not in the sandpacks or in any of the cases with oil present. At the limit of, or in the place of, the high-quality regime, there was sometimes an abrupt jump upwards in ∇P as though from hysteresis and a change of state. In the low-quality regime, ∇P was not independent of liquid superficial velocity, but decreased with increasing liquid superficial velocity. This curious behavior in the low-quality regime was also found in studies of CO_2 foam; an explanation is offered by Kim *et al.* (2004).
- The model of de Vries and Wit (1990) predicts two flow regimes, as pointed out by Kim *et al.* (2004). Some of our experiments appear to fit de Vries and Wit's model for the low-quality regime reasonably well, but some of our data show scatter where de Vries and Wit predict a single trend.

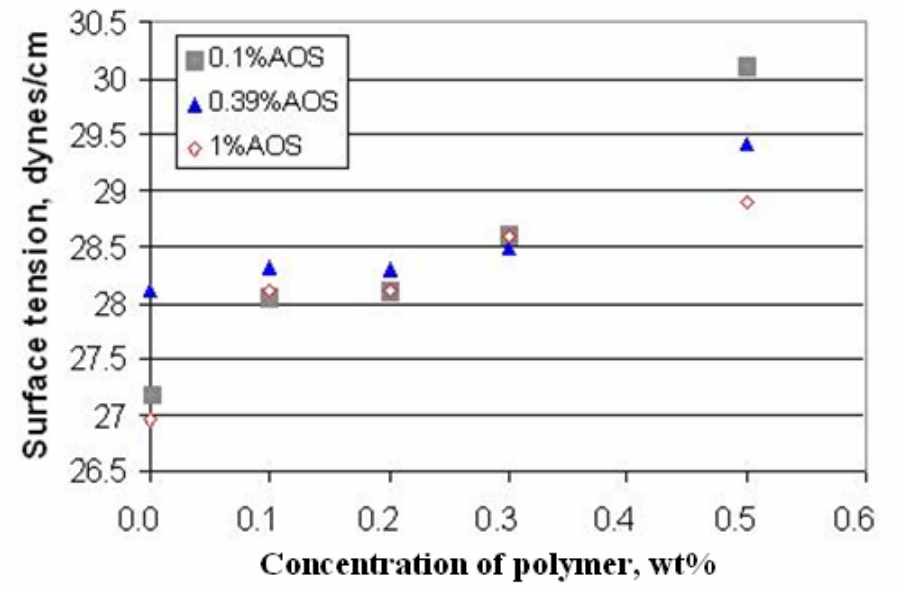

Figure 5.1: Effect of wt% concentrations of Alcoflood 935 polyacrylamide polymer and Bio-Terge AS-40 surfactant on surface tension at room temperature. No added salt.

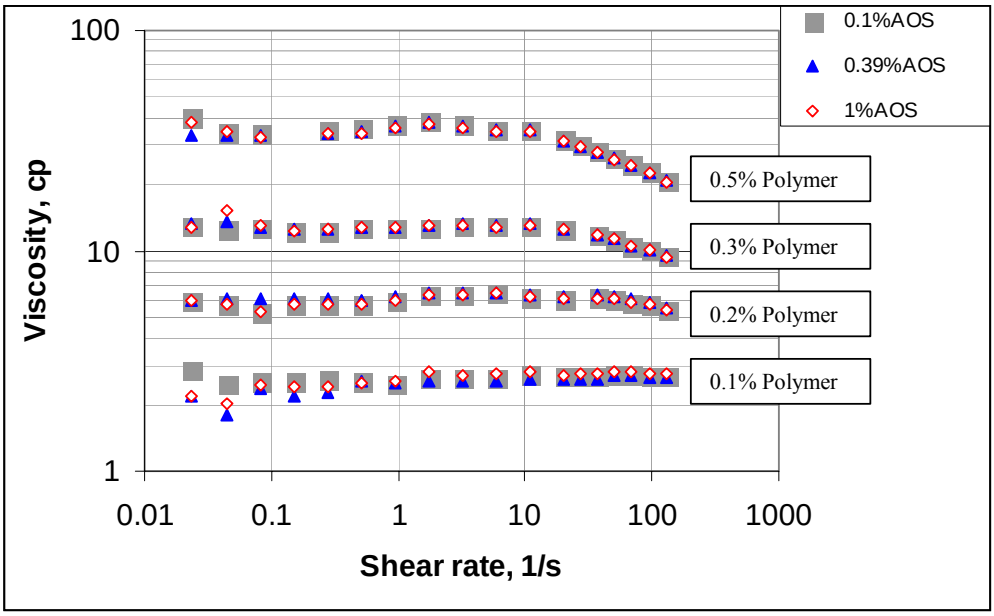

Figure 5.2: Effects of shear rate and concentrations of polymer and surfactant on viscosity of surfactant and polymer solutions; 1 wt% NaCl in all cases.

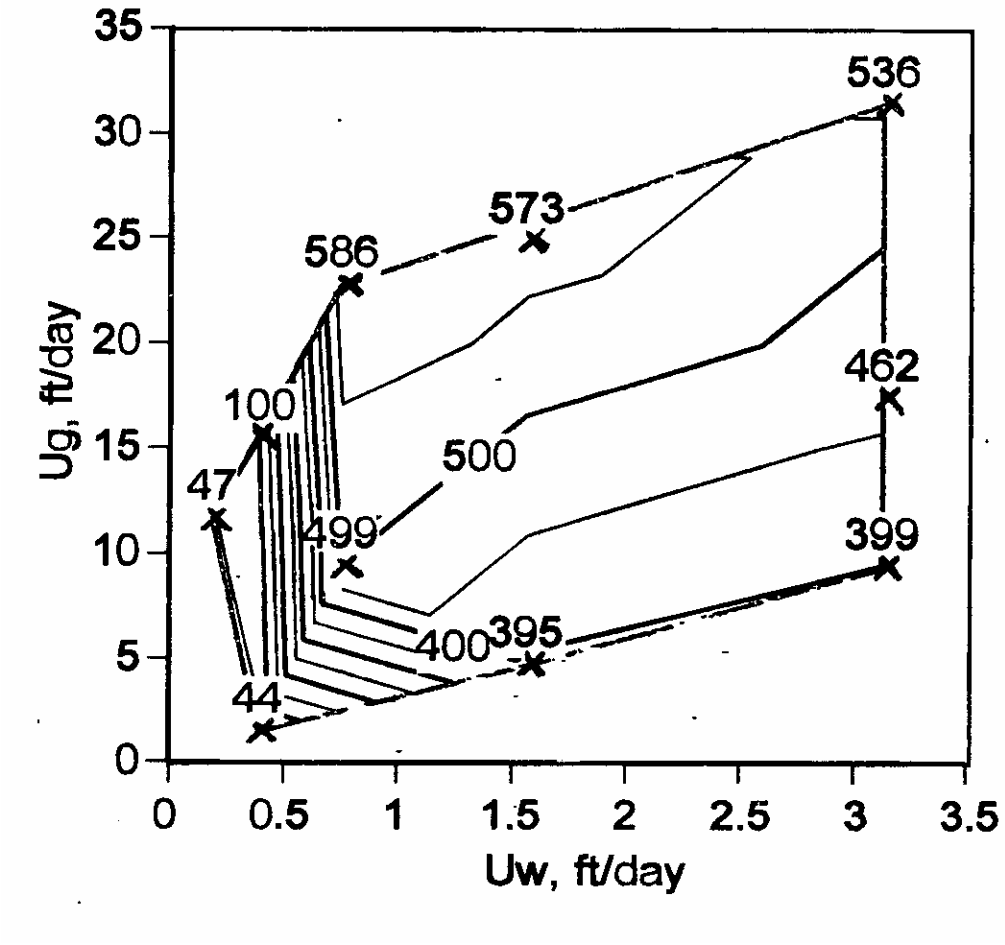

Figure 5.3: Steady-state pressure gradient as a function of superficial velocities of gas (U_g) and water (U_w) for N_2 foam without polymer or oil in a 6.6-darcy sandpack. Surfactant is 0.39 wt% active Bio-Terge AS-40 in 0.25 wt% NaCl and 0.01 wt% $CaCl_2$. In this figure and those that follow, the x symbols represent individual data, and the numbers above them the measured values of pressure gradient (psi/ft).

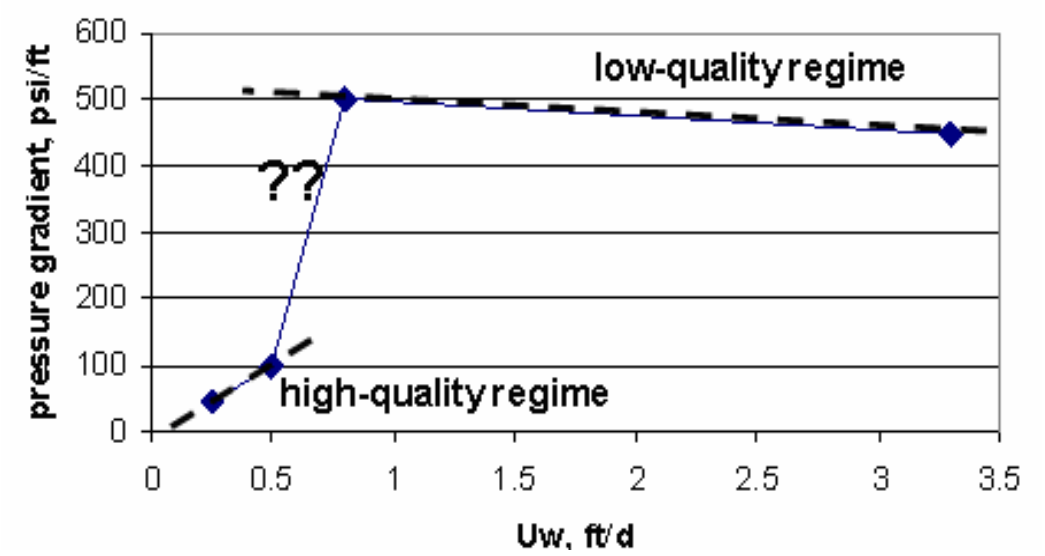

Figure 5.4: Approximate transect through ∇P data of Figure 5.3 at 1 U_g ~ 9 ft/d, showing apparent abrupt jump between high-quality regime and low-quality regime.

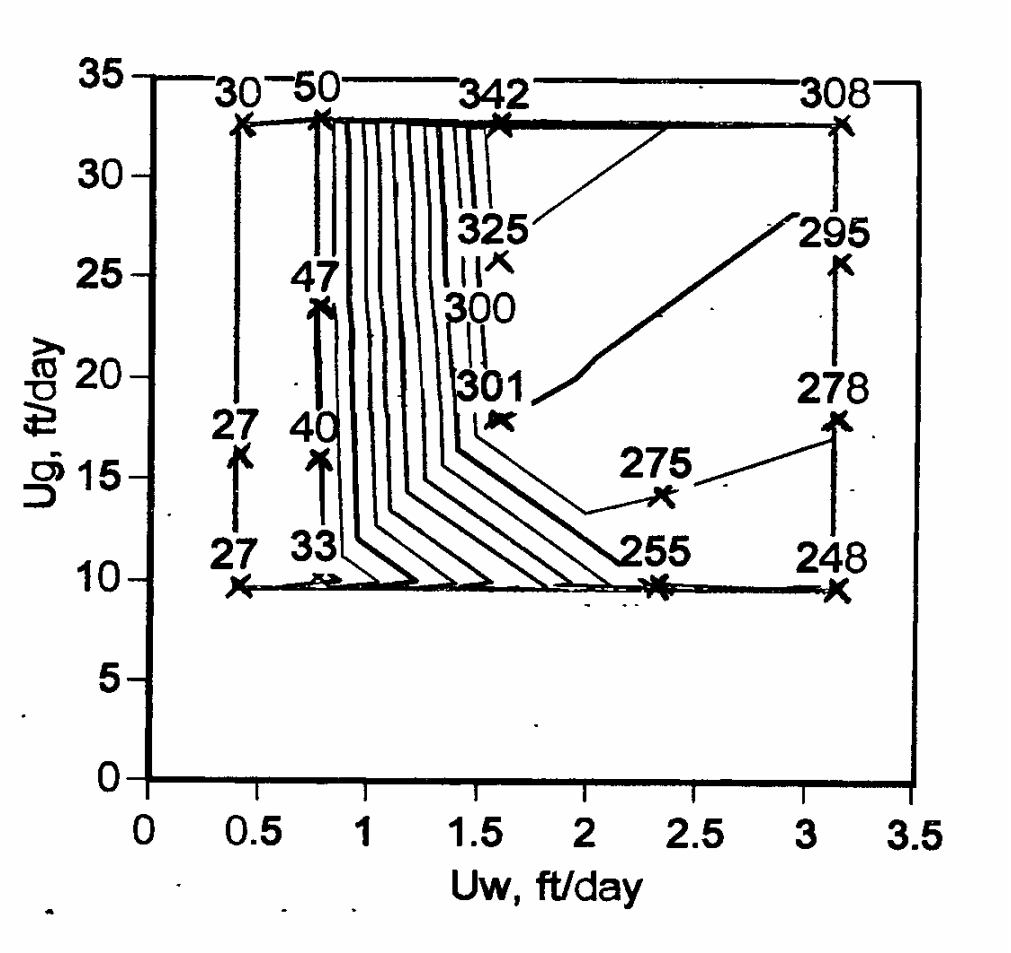

Figure 5.5: Steady-state pressure gradient as a function of superficial velocities of gas (U_g) and water (U_w) for N_2 foam with 0.1 wt% low-MW polyacrylamide polymer, Alcoflood 254s (2-5 x 10^5), in a 6.6-darcy sandpack. Surfactant is 0.39 wt% active Bio-Terge AS-40 in 0.25 wt% NaCl and 0.01 wt% $CaCl_2$.

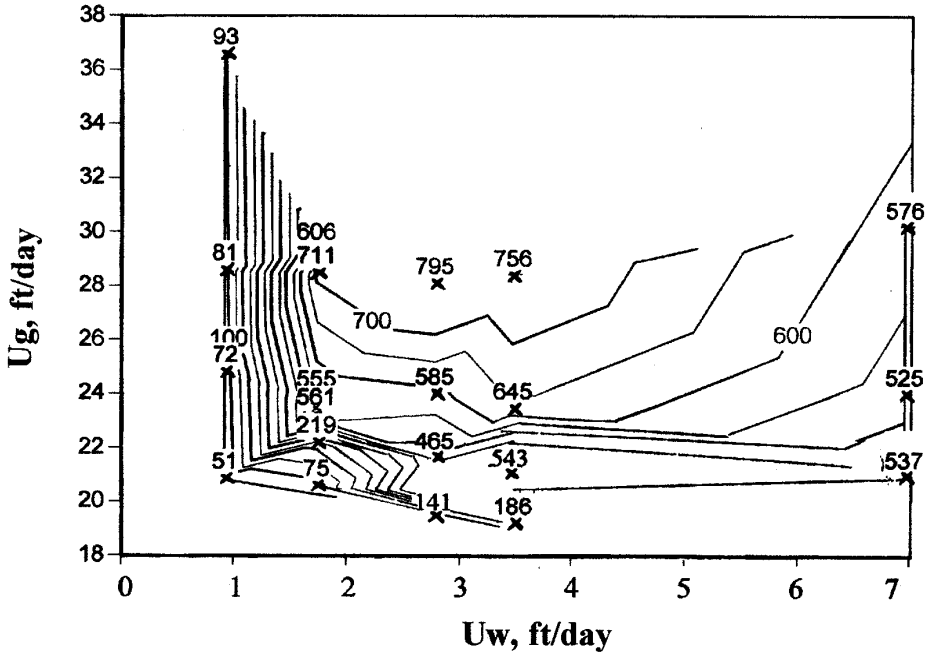

Figure 5.6: Steady-state pressure gradient as a function of superficial velocities of gas (U_g) and water (U_w) for N_2 foam with 0.39 wt% active surfactant in brine with 0.01 wt% $CaCl_2$ and 0.25 wt% NaCl in an 11.8-darcy sandpack.

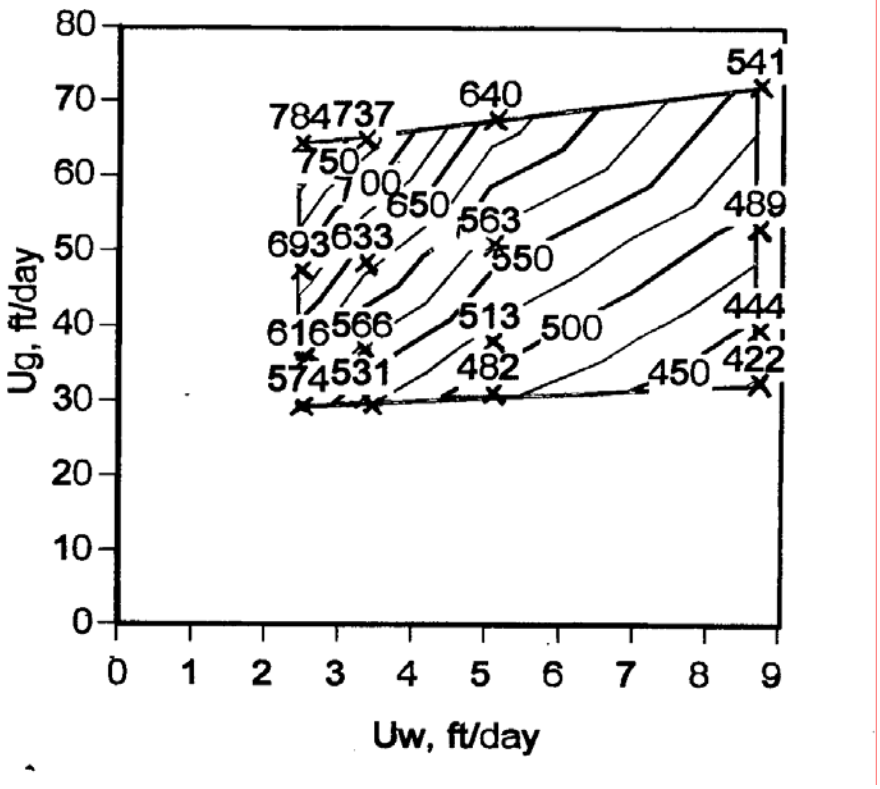

Figure 5.7: Steady-state pressure gradient as a function of superficial velocities of gas (U_g) and water (U_w) for N_2 foam with 0.1 wt% high-MW polyacrylamide polymer, Alcoflood 835 (MW ~ 10-12 x 10^6) in a 16.6-darcy sandpack. Surfactant is 0.39 wt% active Bio-Terge AS-40 in 0.25 wt% NaCl and 0.01 wt% $CaCl_2$.

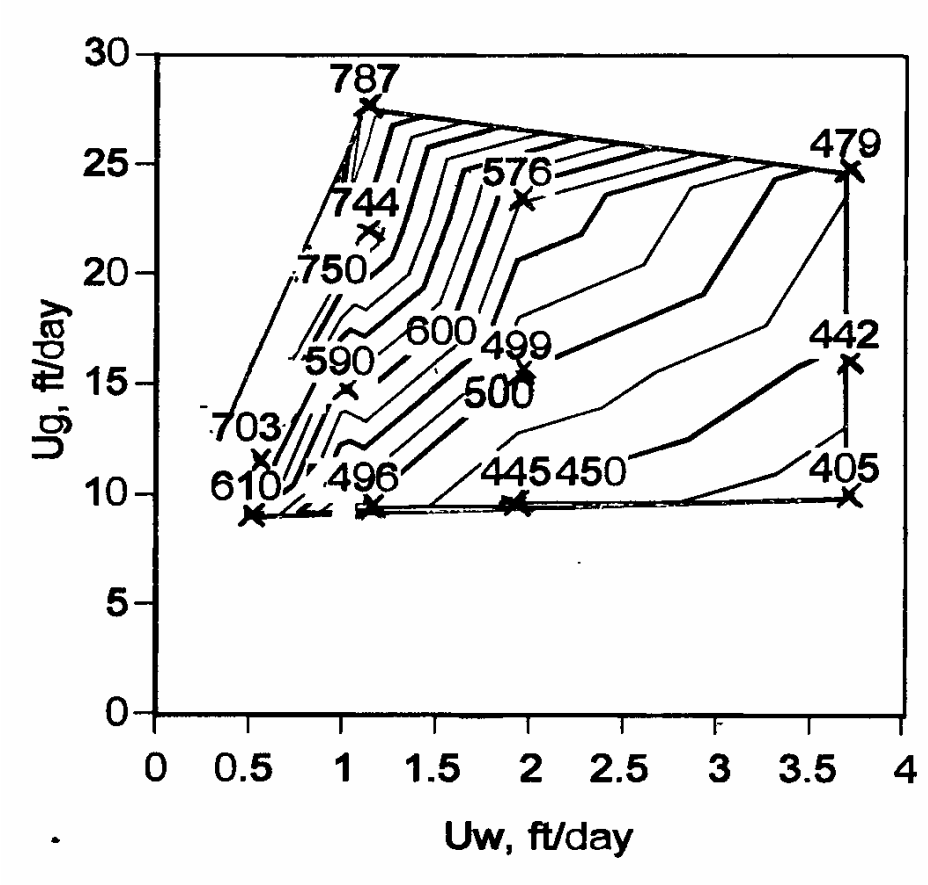

Figure 5.8: Steady-state pressure gradient as a function of superficial velocities of gas (U_g) and water (U_w) for N_2 foam with 0.05 wt% Xanthan polymer in a 16.6-darcy sandpack. Surfactant is 0.39 wt% active Bio-Terge AS-40 in 0.25 wt% NaCl and 0.01 wt% $CaCl_2$.

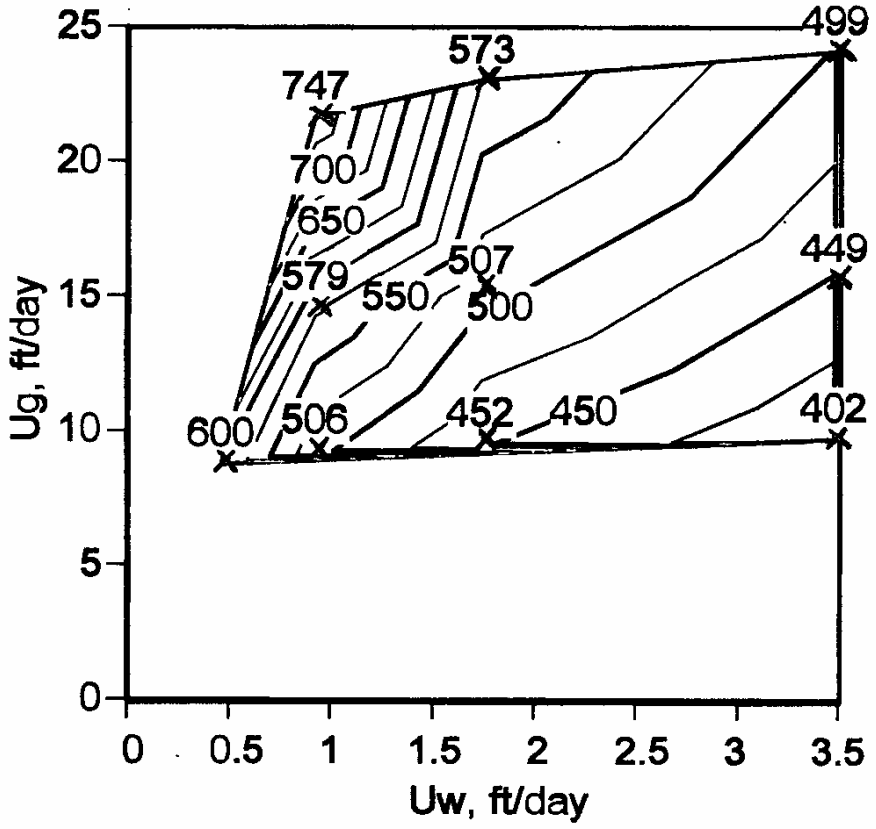

Figure 5.9: Steady-state pressure gradient as a function of superficial velocities of gas (U_g) and water (U_w) for N_2 foam without polymer in a 16.6-darcy sandpack, into which polymer foam had previously been injected. Surfactant is 0.39 wt% active Bio-Terge AS-40 in 0.25 wt% NaCl and 0.01 wt% $CaCl_2$.

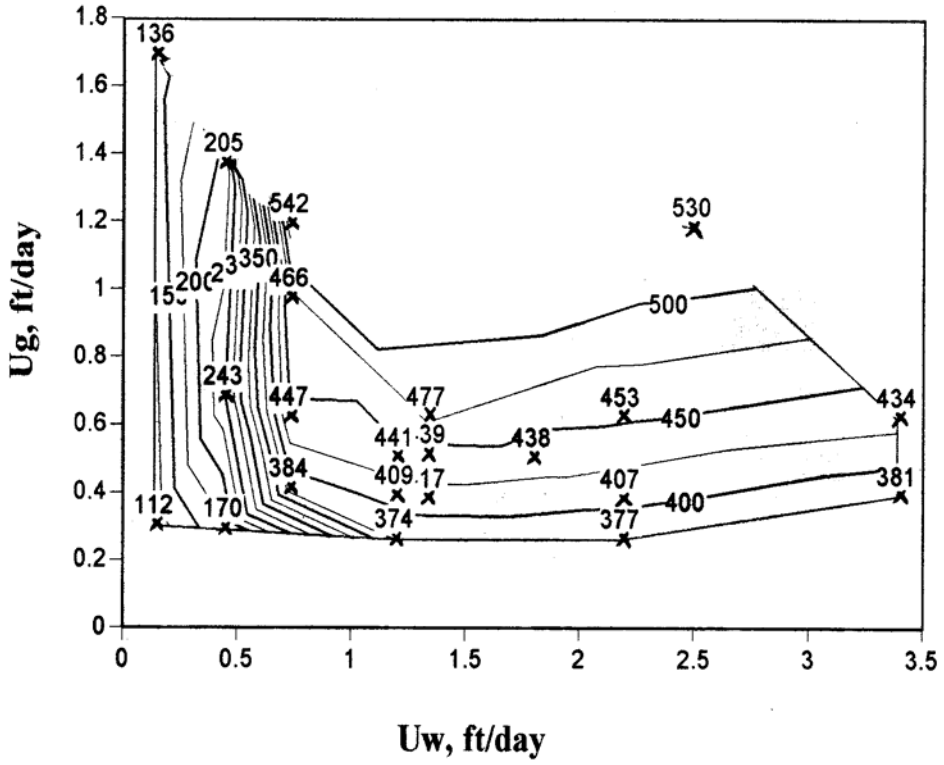

Figure 5.10: Steady-state pressure gradient as a function of superficial velocities of gas (U_g) and water (U_w) for N_2 foam with 0.39 wt% active surfactant in brine with 1 wt% NaCl in the first Boise sandstone core (k = 0.94 darcy).

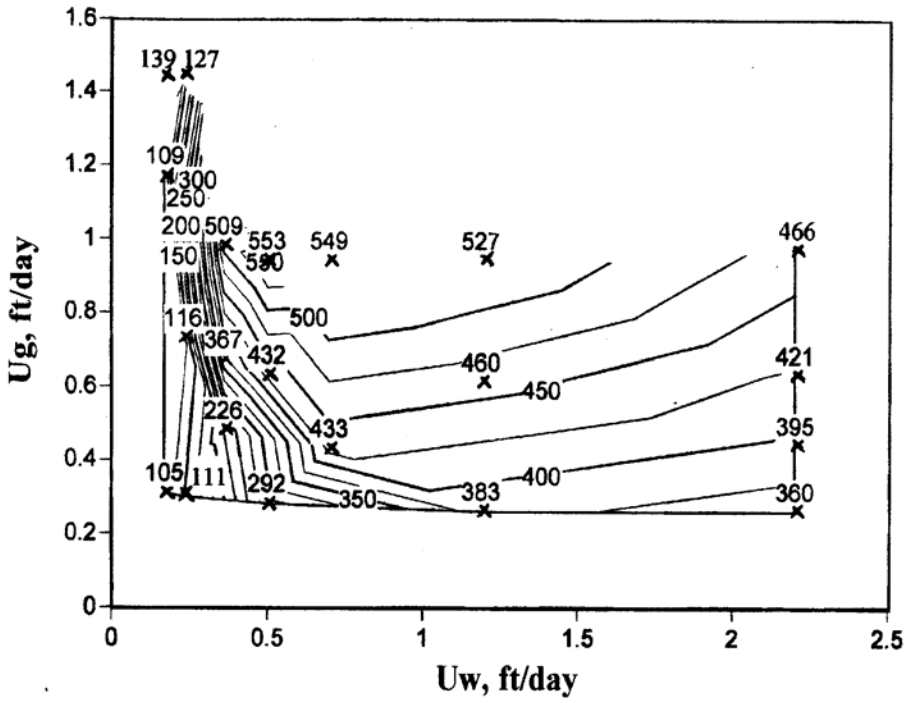

Figure 5.11: Steady-state pressure gradient as a function of superficial velocities of gas (U_g) and water (U_w) for N_2 foam with 0.39 wt% active surfactant with 0.2 wt% Alcoflood 935 polymer in 1 wt% NaCl brine in the first Boise sandstone core.

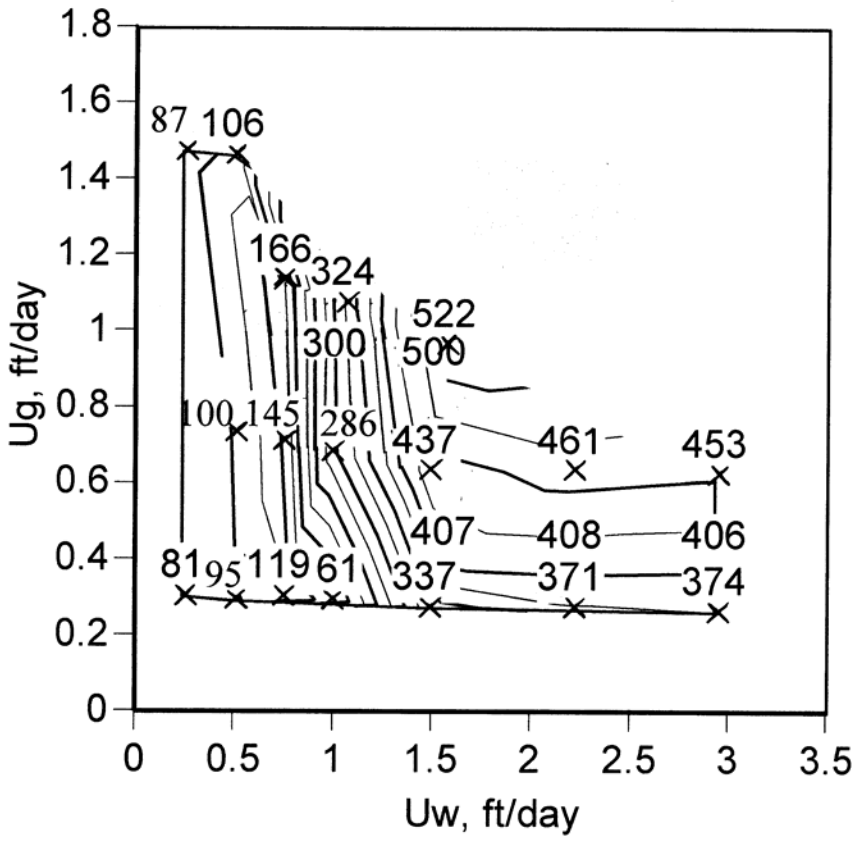

Figure 5.12: Steady-state pressure gradient as a function of superficial velocities of gas (U_g) and water (U_w) for N_2 foam with 0.39 wt% active Bio-Terge AS-40 surfactant in brine with 1 wt% NaCl, in the second Boise sandstone core.

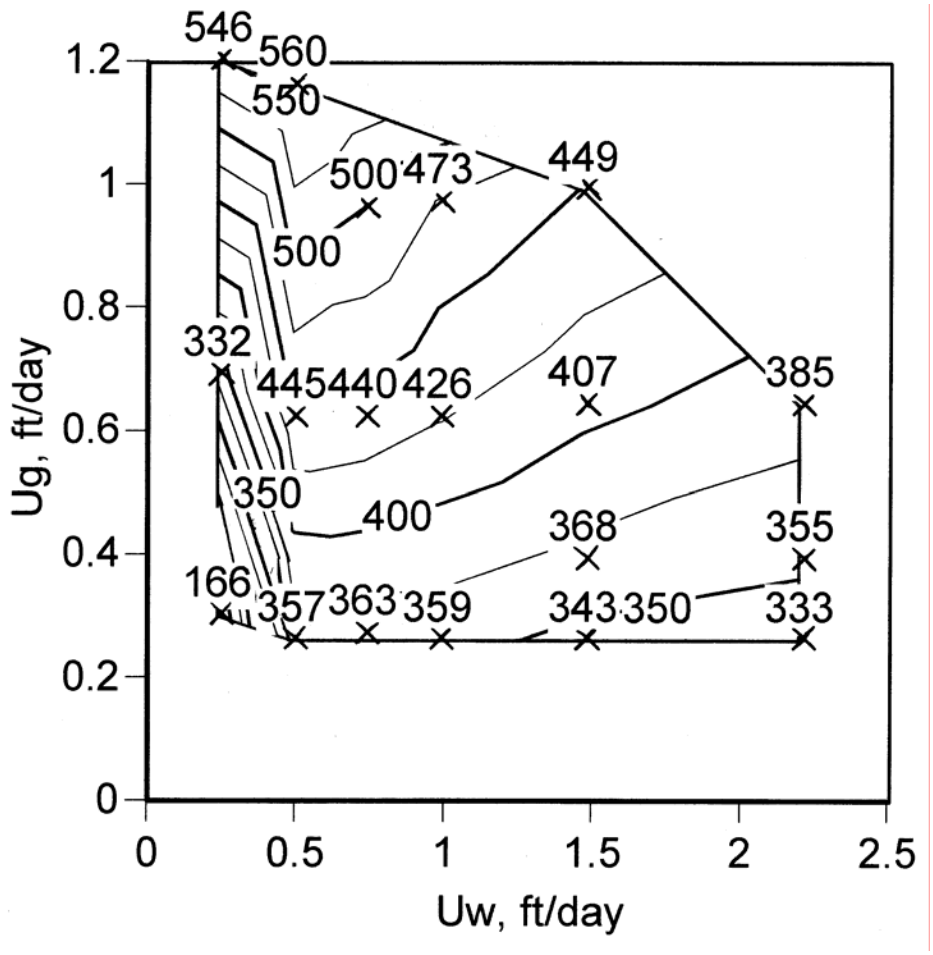

Figure 5.13: Steady-state pressure gradient as a function of superficial velocities of gas (U_g) and water (U_w) for N_2 foam with 0.39 wt% active Bio-Terge AS-40 with 0.2 wt% Alcoflood 935 polymer in 1 wt% NaCl brine in the second Boise sandstone core.

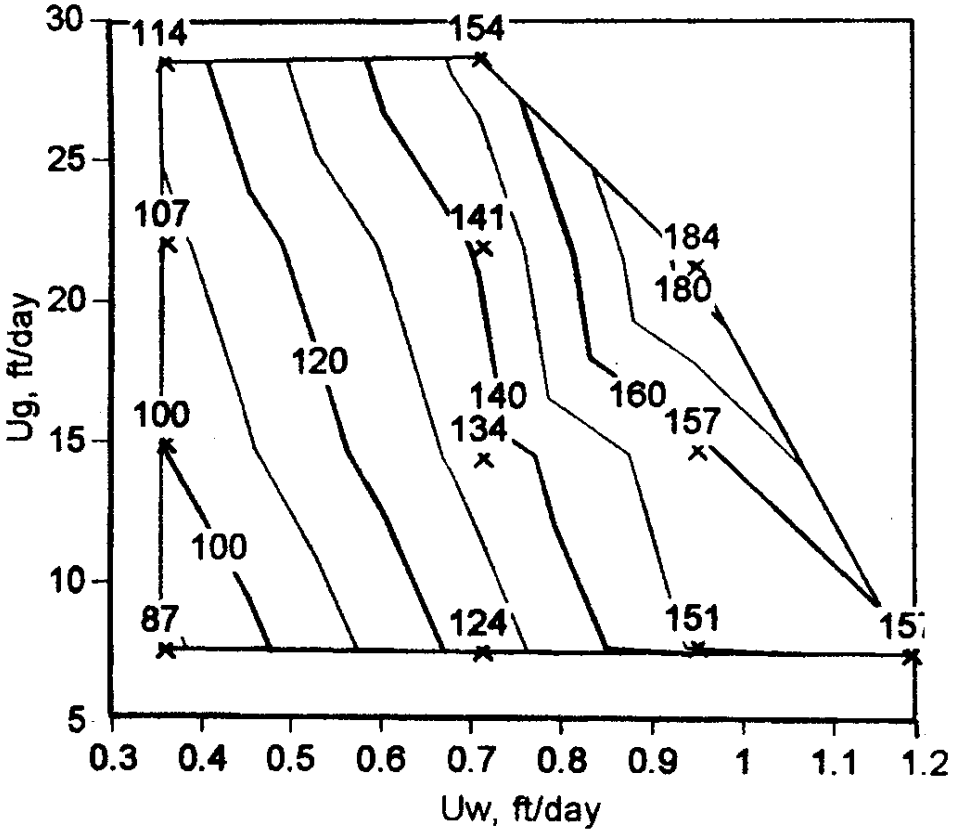

Figure 5.14: Steady-state pressure gradient as a function of superficial velocities of gas (U_g) and water (U_w) for N_2 foam without oil or polymer in a 3.67-darcy sandpack. Surfactant is 0.39 wt% active Bio-Terge AS-40 in 0.25 wt% NaCl and 0.01 wt% $CaCl_2$.

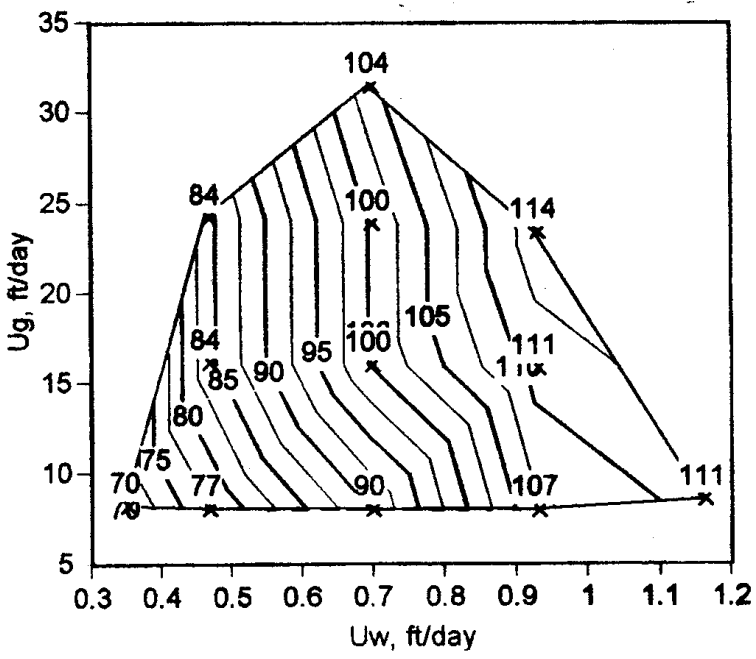

Figure 5.15: Steady-state pressure gradient as a function of superficial velocities of gas (U_g) and water (U_w) for N_2 foam with decane but without polymer, in a 3.67-darcy sandpack. Surfactant is 0.39 wt% active Bio-Terge AS-40 in 0.25 wt% NaCl and 0.01 wt% $CaCl_2$.

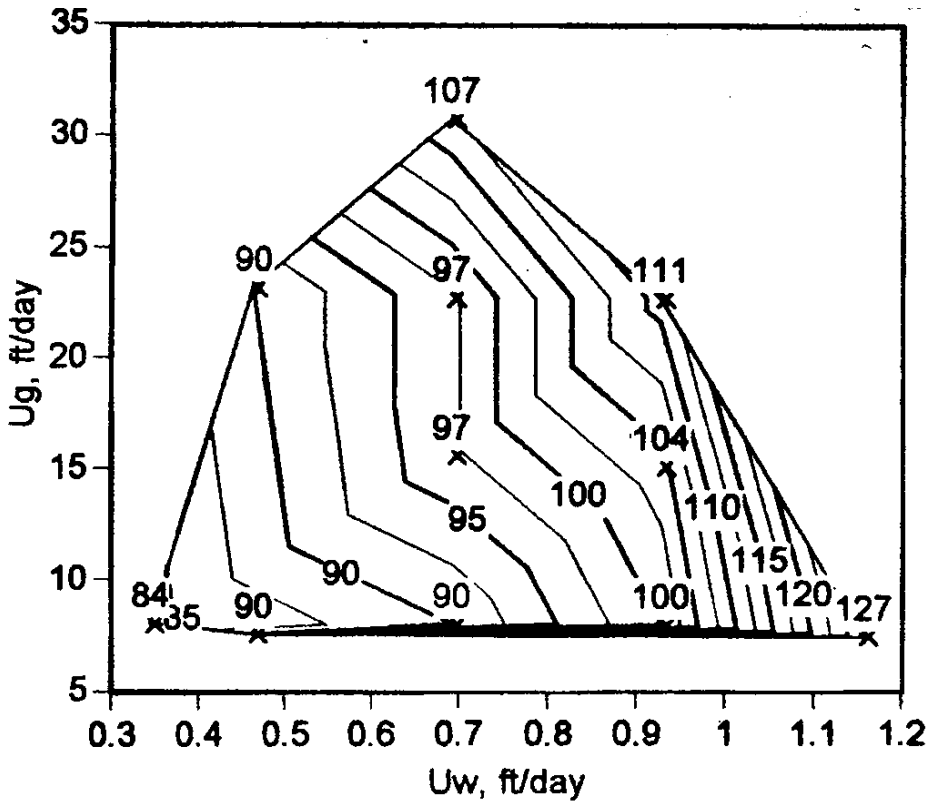

Figure 5.16: Steady-state pressure gradient as a function of superficial velocities of gas (U_g) and water (U_w) for N_2 foam with both 0.05 wt% Xanthan polymer and 22 vol% decane (decane superficial velocity equal to 0.22 times that of surfactant solution) injected into a 3.67-darcy sandpack. Surfactant is 0.39 wt% active Bio-Terge AS-40 in 0.25 wt% NaCl and 0.01 wt% $CaCl_2$.

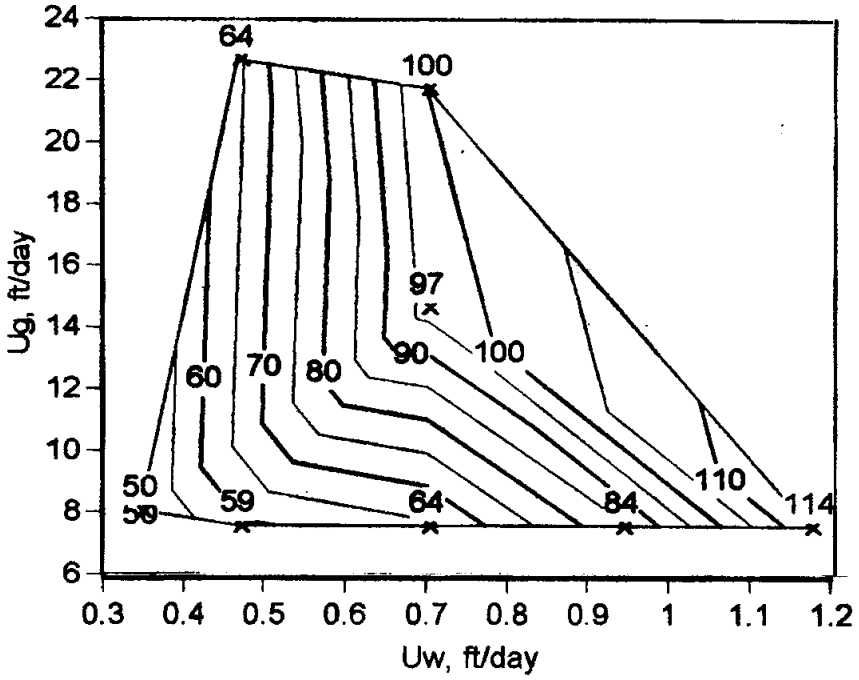

Figure 5.17: Steady-state pressure gradient as a function of superficial velocities of gas (U_g) and water (U_w) for N_2 foam without polymer or oil in a 3.67-darcy sandpack, through which polymer and oil have both been injected previously. Surfactant is 0.39 wt% active Bio-Terge AS-40 in 0.25 wt% NaCl and 0.01 wt% $CaCl_2$.

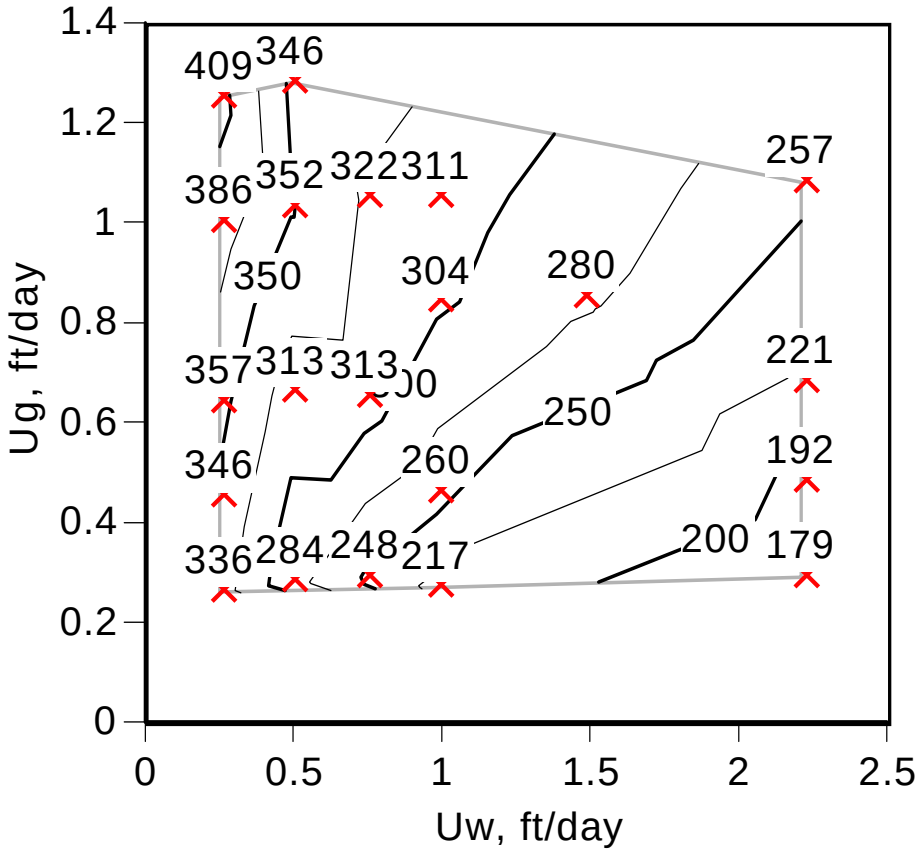

Figure 5.18: Steady-state pressure gradient as a function of superficial velocities of gas (U_g) and water (U_w) for N_2 foam with 0.39 wt% active surfactant in brine with 1 wt% NaCl in the first Boise sandstone core, with decane injected simultaneously with the foam.

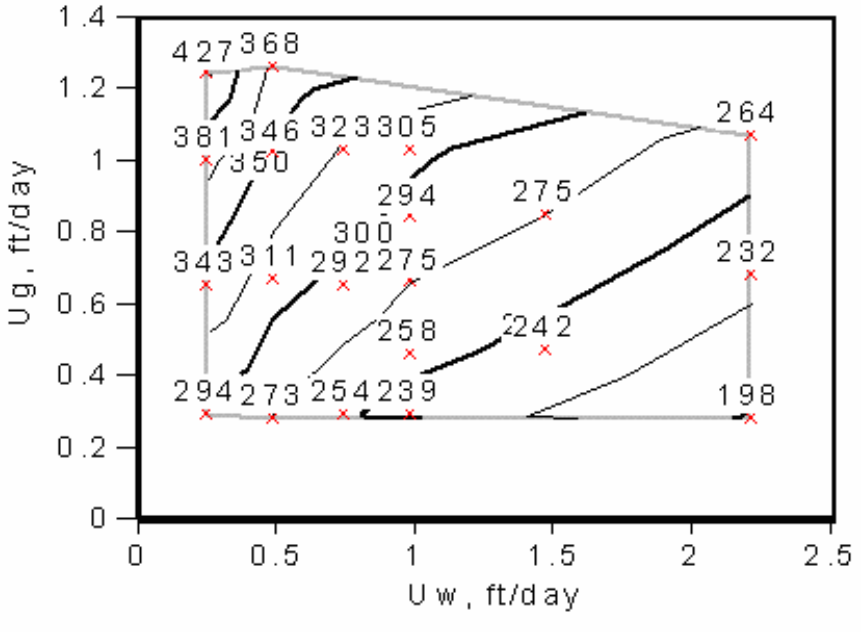

Figure 5.19: Steady-state pressure gradient as a function of superficial velocities of gas (U_g) and water (U_w) for N_2 foam with 0.39 wt% active surfactant and 0.2 wt% Alcoflood 935 polymer in brine with 1 wt% NaCl in the first Boise sandstone core, with decane injected simultaneously with the foam.

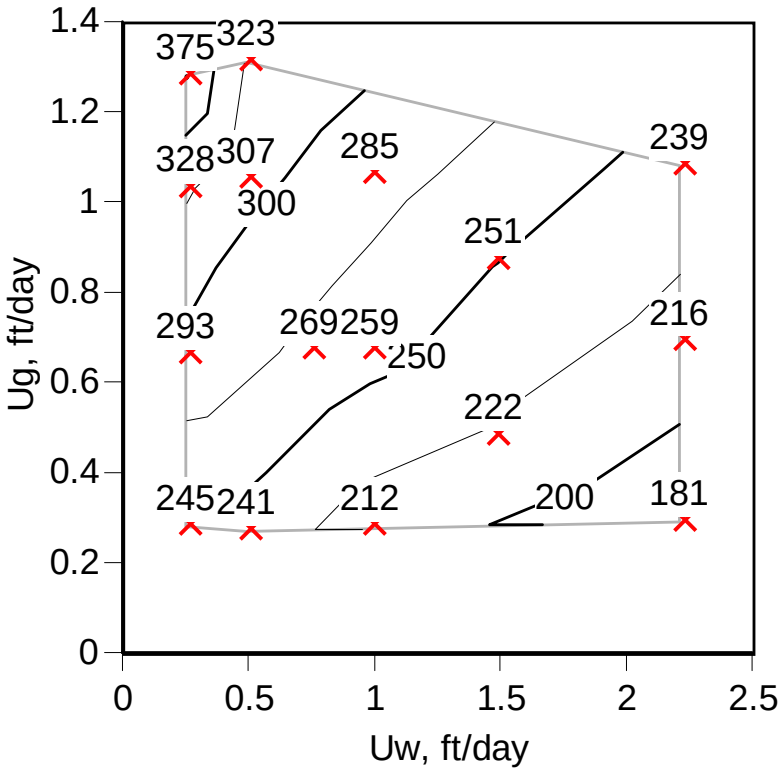

Figure 5.20: Steady-state pressure gradient as a function of superficial velocities of gas (U_g) and water (U_w) for N_2 foam with 0.39 wt% active Bio-Terge AS-40 surfactant in brine with 1 wt% NaCl in the second Boise sandstone core, with 37.5° API crude oil injected simultaneously with the foam.

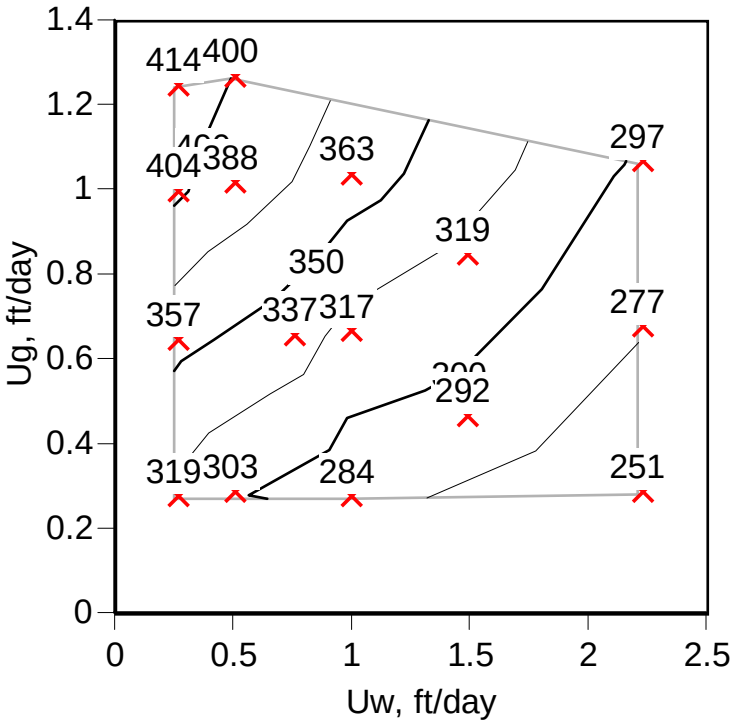

Figure 5.21: Steady-state pressure gradient as a function of superficial velocities of gas (U_g) and water (U_w) for N_2 foam with 0.39 wt% active Bio-Terge AS-40 and 0.2 wt% Alcoflood polymer 935 in brine with 1 wt% NaCl in the second Boise sandstone core, with 37.5° API crude oil injected simultaneously with the foam.

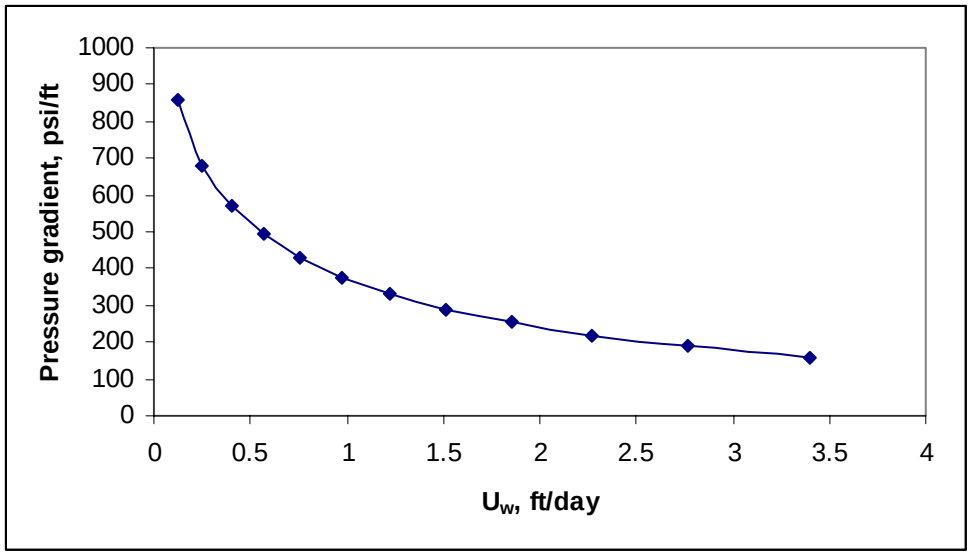

Figure 5.22: The effect of liquid interstitial velocity on pressure gradient at constant gas interstitial velocity.

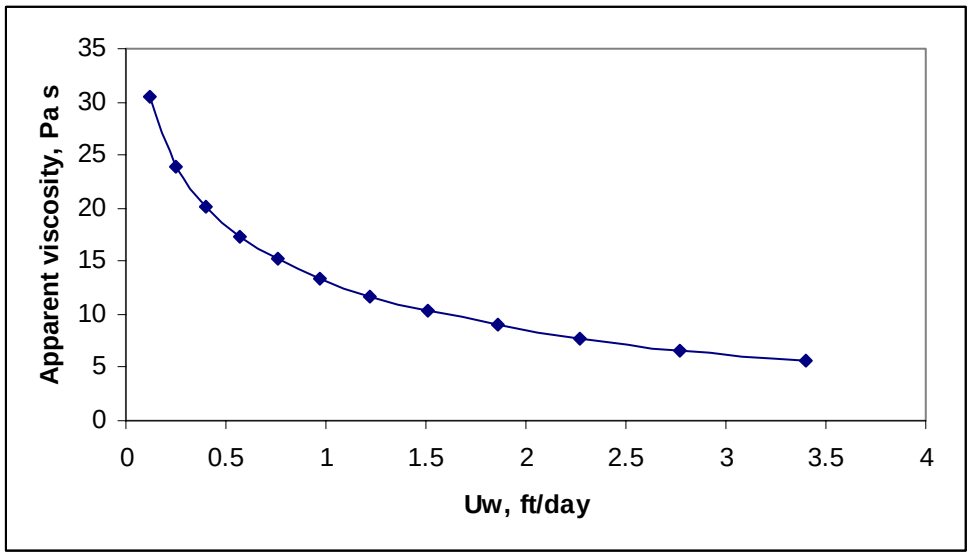

Figure 5.23: The effect of liquid interstitial velocity on effective gas viscosity at constant gas interstitial velocity.

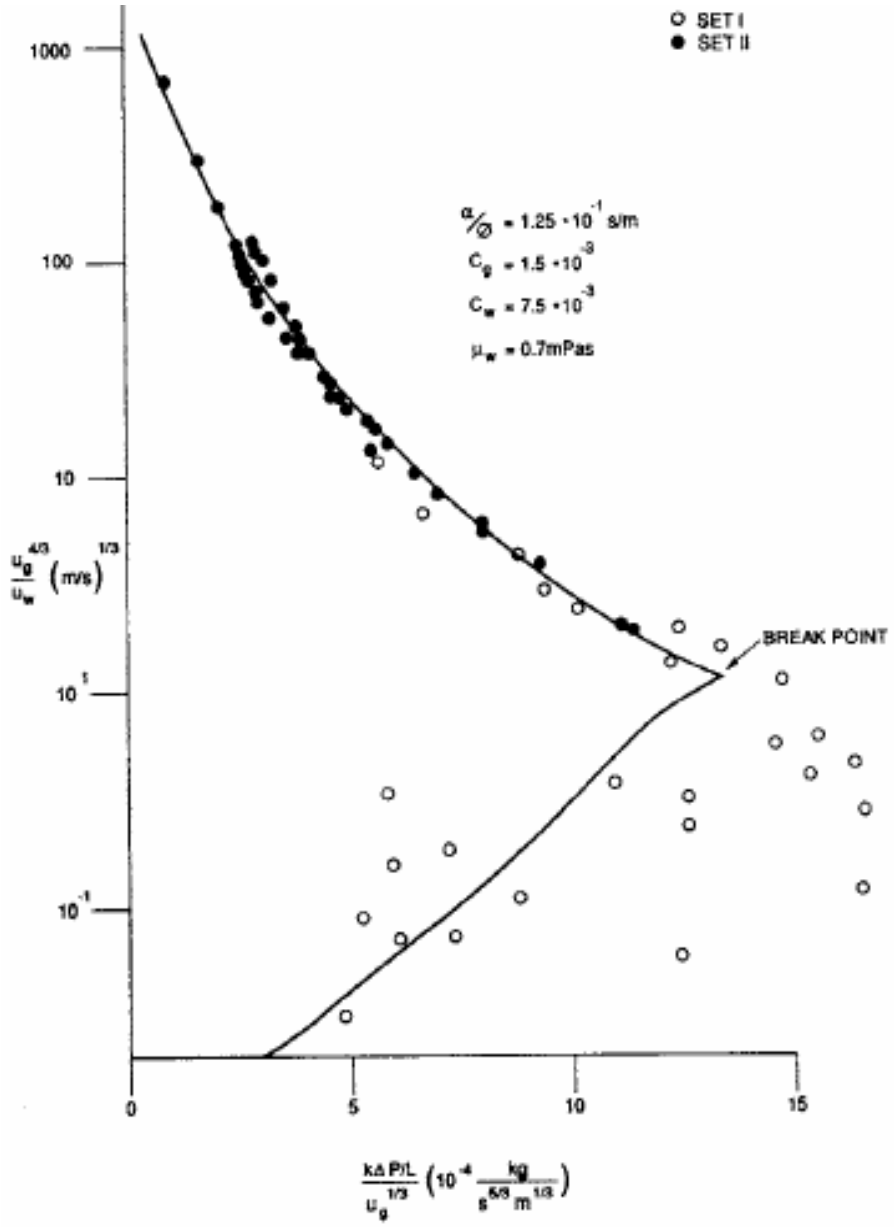

Figure 5.24: The fit between experiment data and the model of de Vries and Wit, from de Vries and Wit (1990). Solid points represent steady-state data and the curves denote theoretical behavior. What de Vries and Wit call the "break point" is the transition between low-quality and high-quality regimes, i.e. foam at the limiting capillary pressure.

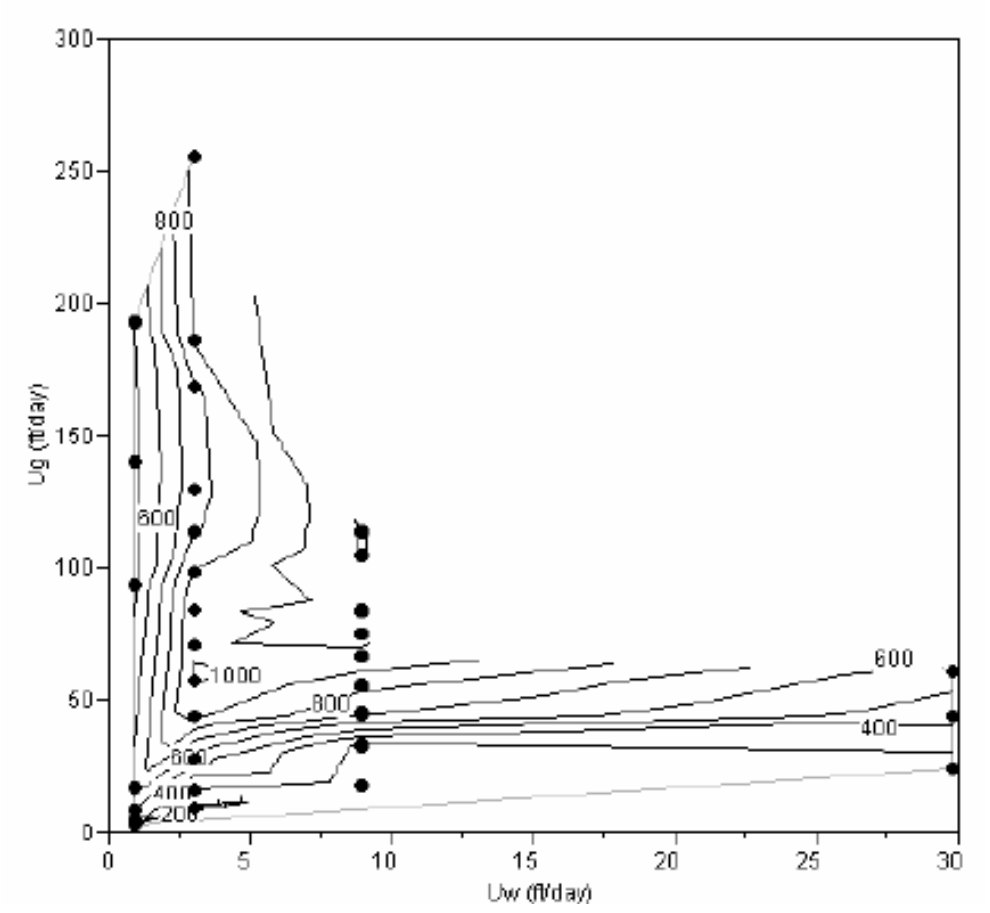

Figure 5.25: Pressure gradient (psi/ft) as a function of gas (U_g) and liquid (U_w) superficial velocities (ft/day) based on data from de Vries and Wit (1990). The porous medium was a sand-pack with permeability 4.26 darcy. Dobanol 91 sulfate surfactant was used at concentration 1%. Solid points represent steady-state data (Kim *et al*., 2004).

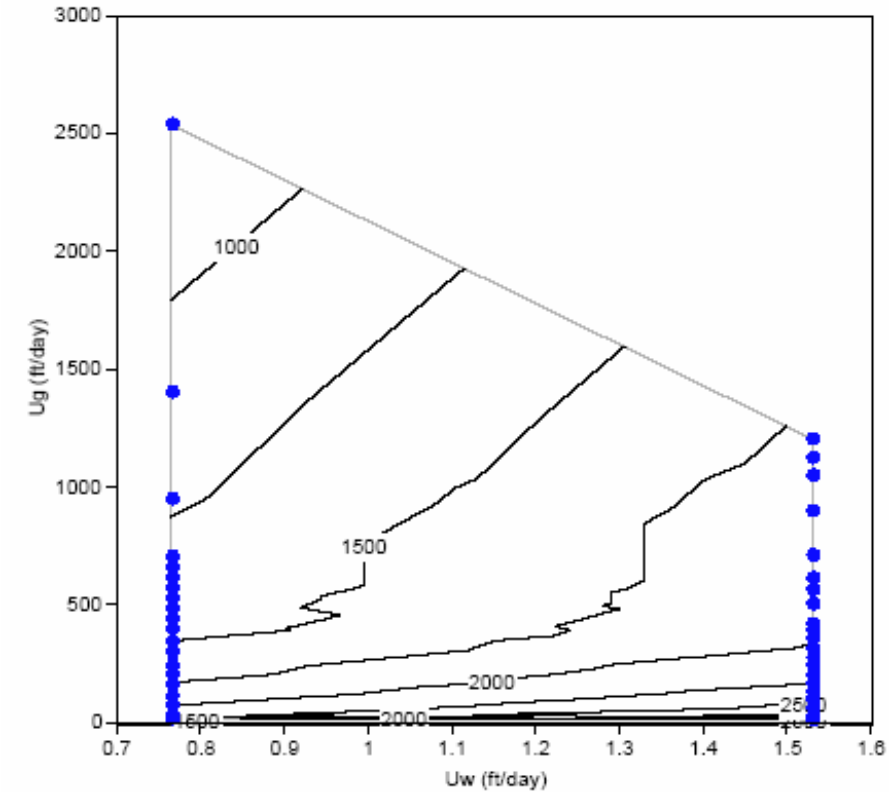

Figure 5.26: Contour plot of pressure gradient (psi/ft) based on data from a second experiment of de Vries and Wit (1990). Porous medium was a Bentheim core and its permeability was 1.22 darcy. Siponate DS 10^{TM} surfactant was used at concentration 0.5%. Solid Points represent steady-state data (Kim *et al.*, 2004).

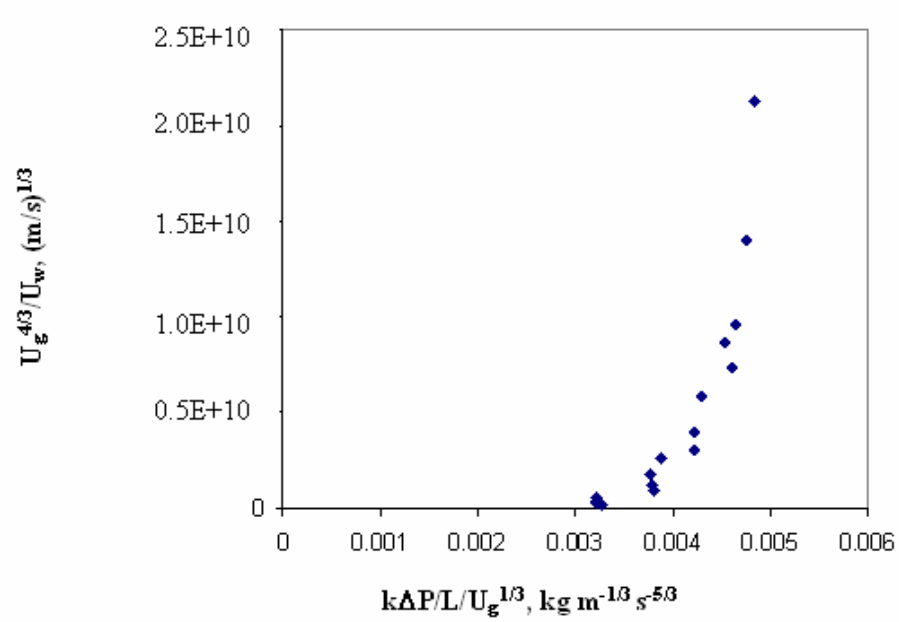

Figure 5.27: Plot of our experimental data in low-quality regime (Figure 5.7) based on the model of de Vries and Wit (1990) (Figure 5.24).

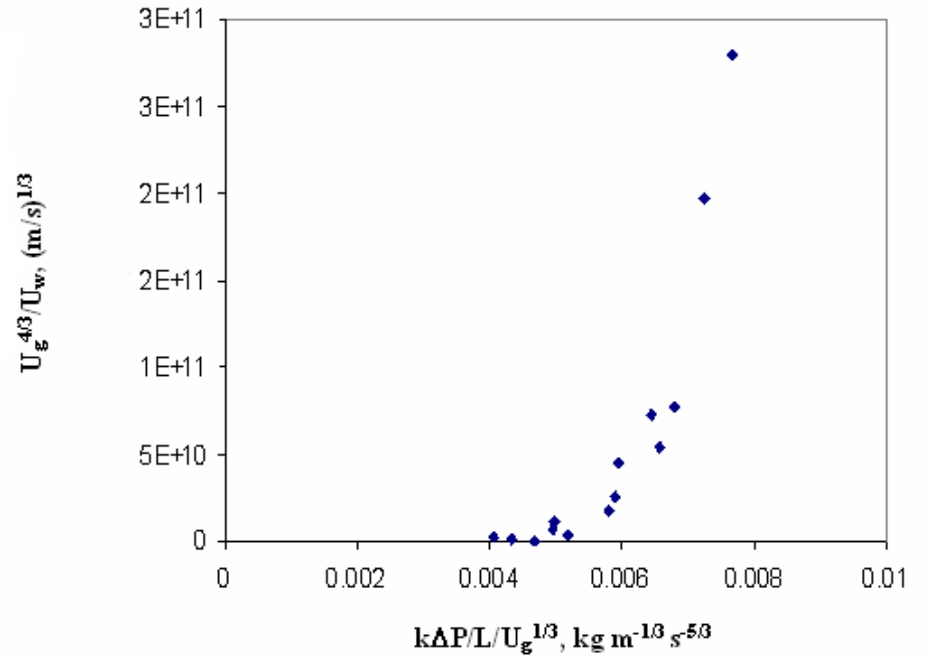

Figure 5.28: Plot of our experimental data in low-quality regime (Figure 5.8) based on the model of de Vries and Wit (1990) (Figure 5.24).

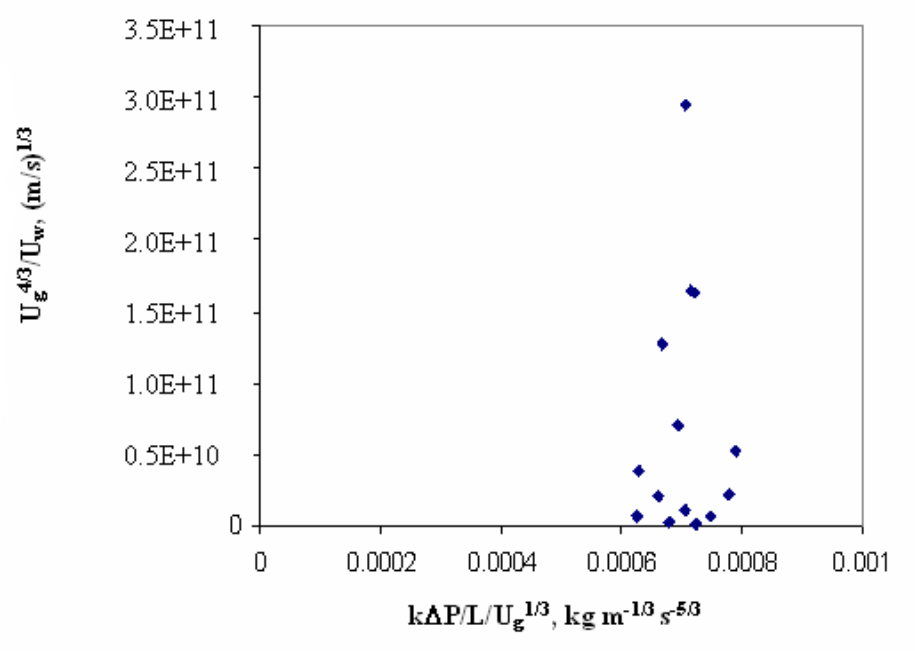

Figure 5.29: Plot of our experimental data in low-quality regime (Figure 5.15) based on the model of de Vries and Wit (1990) (Figure 5.24).

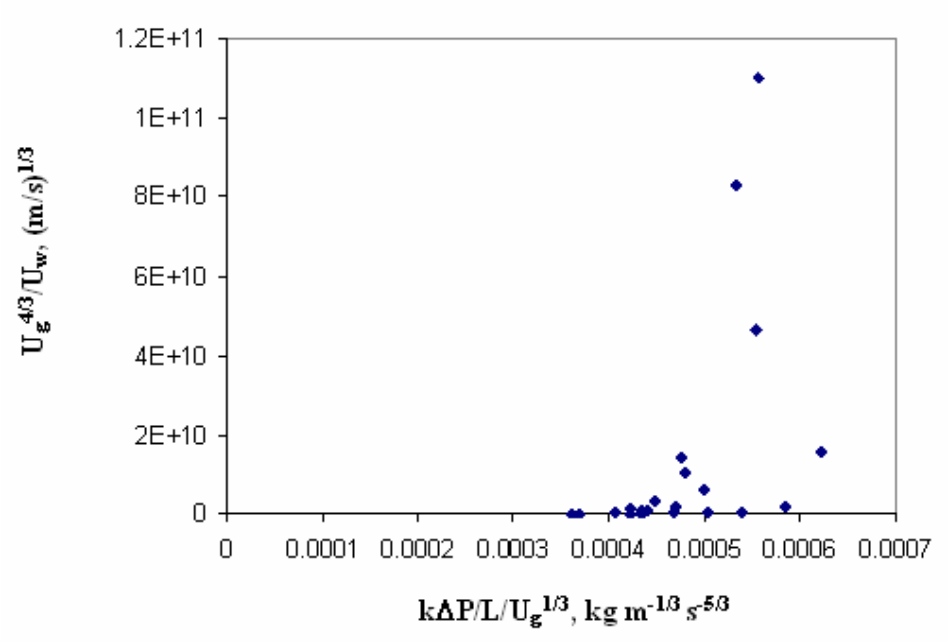

Figure 5.30: Plot of our experimental data in low-quality regime (Figure 5.17) based on the model of de Vries and Wit (1990) (Figure 5.24).

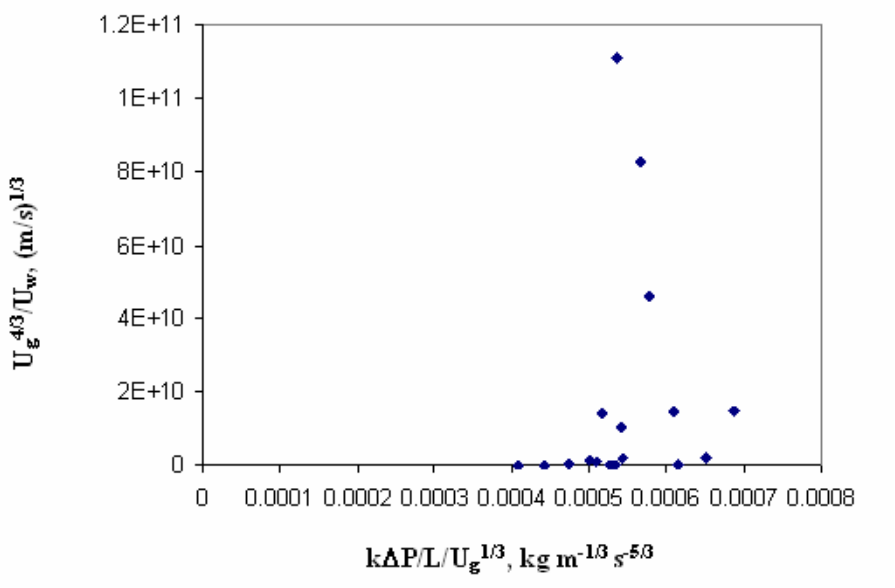

Figure 5.31: Plot of our experimental data in low-quality regime (Figure 5.21) based on the model of de Vries and Wit (1990) (Figure 5.24).

Chapter 6: Simulation Study of Gravity Segregation In Non-Newtonian Foam Processes

6.1 THE PURPOSE OF THIS STUDY

Gas, such as steam, carbon dioxide, nitrogen and re-injected field gas, has been widely used as a driving fluid to improve oil recovery (Lake, 1989). However, the low density of gas in the formation causes gravity override, which leads to poor sweep efficiency. Foam can improve sweep efficiency by increasing horizontal pressure gradient to offset the effect of low gas density. A useful model for gravity override is Stone's model (1982), which describes gravity override during simultaneous water-gas flow. Shi and Rossen (1998) and Cheng *et al.* (2000) extended the model to foam processes with Newtonian rheology. However, as discussed in Section 2.10, foams are non-Newtonian, often in the high-quality regime, and always in the low-quality regime (Figures 2.8-2.9). Therefore, the purpose of this study was to extend the Stone's model (1982) to foam flow with shear-thinning rheology. Specifically, we examined the ability of shear-thinning foam with different foam properties to overcome gravity segregation in homogeneous reservoirs.

6.2 STONE'S MODEL FOR GRAVITY OVERRIDE

In 1982, Stone developed an analytical model to describe steady-state gravity segregation in two-dimensional (2D) (rectangular or cylindrical) gas EOR processes with gas and water injected simultaneously. Jenkins (1984) extended Stone's model and provided a closed-form solution to determine the steady-state saturation profile. This

model assumes that at steady state a reservoir comprises three regions of uniform saturation, with sharp boundaries between them, as illustrated in Figure 6.1: an override zone with only gas flowing, an underride zone with only water flowing, and a mixed zone with both gas and water flowing. In this figure, r_g is the segregation length, i.e. radial position where gas and water are completely segregated. The model also assumes that gravity segregation is controlled by the upwards and downwards movement of gas and water within the mixed zone, that gas is incompressible and that rheology is Newtonian for all phases.

For a rectangular reservoir, according to the model, the distance to complete segregation, L_g, is given by

$$L_g = \frac{Q_{inj}}{k_z \Delta\rho g W \left(\lambda_{rg} + \lambda_{rw}\right)_m} \tag{6.1}$$

where Q_{inj} is total injection rate, k_z is vertical permeability, $\Delta\rho$ is density difference between gas and water phases, g is gravitational acceleration, $(\lambda_{rg}+\lambda_{rw})_m$ is the total relative mobility in the mixed zone, and W is reservoir width. For cylindrical flow,

$$r_g = \sqrt{\frac{Q_{inj}}{k_z \Delta\rho g \pi \left(\lambda_{rw} + \lambda_{rg}\right)_m}} \tag{6.2}$$

where r_g is the radial position at which gas and liquid flows are completely segregated.

6.3 SHI AND ROSSEN'S MODIFICATION OF STONE'S MODEL

Shi and Rossen (1998) showed empirically that Stone's model applies to the process of continuous foam injection, where foam is in the high-quality regime and has Newtonian rheology. They tested the model over a wide range of reservoir permeabilities

and geometries, foam qualities, foam strengths, and other parameters. They assumed that wherever gas and surfactant solution meet, foam is generated there immediately; in other words, they did not consider issues of foam generation (Gauglitz *et al*., 2002). They showed that Stone's equations could be recast as follows. For a rectangular reservoir, Eq. 6.1 is equivalent to

$$\frac{L_g}{L} = \left(\frac{\nabla P_f}{\Delta\rho g}\right)\left(\frac{Hk_x}{Lk_z}\right) = \frac{1}{N_g}\frac{1}{R_L} \tag{6.3}$$

where ∇P_f is the pressure gradient at foam bank, and

$$\nabla P_f\left(r_g\right) = \frac{Q_{inj} f_w \mu_w}{WHk_x k_{rw}\left(S_w{}^f\right)} \tag{6.4}$$

N_g is gravity number, the ratio of the vertical driving force for segregation to horizontal pressure gradient; R_L is reservoir aspect ratio; L and H are reservoir length and height, respectively; k_x is absolute horizontal permeability; ∇P_f is the pressure gradient in the foam bank; μ_w is water viscosity; $k_{rw}(S_w)$ is the same water relative permeability function that applies in the absence of foam; $S_w{}^f$ is the water saturation in the foam bank; f_w is injected water fractional flow of the foam.

For a cylindrical reservoir, Stone's model can be rearranged to give

$$\left(\frac{r_g}{R_e}\right)^2 = \left(\frac{\nabla P_f\left(r_g\right)}{\Delta\rho g}\right)\left(\frac{2r_g Hk_x}{R_e{}^2 k_z}\right) \tag{6.5}$$

or

$$\left(\frac{\Delta\rho g}{\nabla P_f\left(r_g\right)}\right)\left(\frac{r_g k_z}{Hk_x}\right) = N_g\left(r_g\right)R_g\left(r_g\right) = 2 \tag{6.6}$$

with

$$\nabla P_f\left(r_g\right)=\frac{Q_{inj}\, f_w \mu_w}{2\pi r_g H k_x k_{rw}\left(S_w{}^f\right)} \tag{6.7}$$

where N_g, R_L and ∇P_f are evaluated at the radial position r_g at which gas and water flows are completely segregated, and R_e is the outer radius of reservoir.

Rossen and van Duijn (2004) showed that Stone's model applies rigorously as long as the standard assumptions of fractional-flow theory apply, such as incompressible phases, absence of dispersive processes, Newtonian mobilities of all phases, and immediate attainment of local steady-state mobilities.

Shi and Rossen's (1998) version of these equations indicates that the ability of foam to overcome gravity override depends on two dimensionless groups: a gravity number N_g and reservoir aspect ratio R_L. For a given reservoir, gravity segregation depends on N_g alone: specifically, a large value of N_g (low pressure gradient) promotes gravity segregation. Therefore, the only way to control gravity segregation is to provide a sufficient horizontal pressure gradient by increasing injection-well pressure. The ability to raise injection pressure may be limited by concern about fracturing. In a cylindrical reservoir, this limitation is more severe, because of the large pressure gradient near an injection well.

The shear-thinning behavior of foam under some conditions (Alvarez *et al*., 2001; Rong, 2002) may offer a solution to this problem. Shear-thinning rheology reduces pressure gradient near an injection well and allows both higher injection rates and higher horizontal pressure gradient away from the well. Stone's model does not apply in the case of non-Newtonian flow; note, for instance, that a single mobility describes foam in the

mixed zone in Eqs. 6.1 and 6.2. Any extension of Stone's model to non-Newtonian flow depends on finding a representative "average" mobility for the foam bank that adequately replaces the uniform mobility in Stone's Eqs. 6.1 and 6.2. Determining this average mobility is a major focus of this chapter.

6.4 FOAM SIMULATOR

6.4.1 Overview of foam model

STARS™, from the Computer Modeling Group (CMG) of Calgary, Alberta, Canada, is the most widely used commercial foam simulator (Mohammadi and Coombe, 1991 and 1993; Lau and Coombe, 1994; Hanssen *et al.*, 1994; Svorstol *et al.*, 1997; Martinsen and Vassenden, 1999; Vassenden *et al.*, 1999; Cheng *et al.*, 2000; Chalbaud *et al*., 2002). It is a three-phase, multi-component thermal and steam-additive simulator. Grid systems include Cartesian, cylindrical, or variable-depth/variable-thickness. STARS™ provides two general approaches to simulating foam flow. The first is a mechanistic model that incorporates foam creation, propagation, and coalescence effects such as appear in detailed "population balance" models for foam (Falls *et al*., 1988; Kovscek and Radke, 1994; Kam and Rossen, 2003). The second approach models steady-state foam behavior in terms of parameters that directly describe the two strong-foam regimes shown in Figures 2.2 and 3.3 (Cheng *et al*., 2000). In our study, only the second model is used.

In the second STARS™ foam model, the effect of foam on gas mobility is described in terms of a modified gas relative-permeability function. This modification is

represented by a dimensionless interpolation factor FM which rescales the gas relative permeability in the presence of foam. In the simulator, it is assumed that foam exists whenever gas, water and surfactant coexist. The basic input mobility data required in the model are relative-permeability curves and viscosities for gas and water in the absence of foam, the maximum mobility reduction factor fmmob, and interpolation parameters that describe the effects of surfactant concentration, gas velocity, capillary number, and the effect of oil on foam. In this study, for simplicity, oil is assumed to be absent, and the effect of oil on foam is not considered. Also for simplicity, surfactant adsorption on the solid matrix is neglected.

6.4.2 The dimensionless interpolation factor, FM

In STARS™, gas relative permeability with foam k_{rg}^{f} is reduced by a dimensionless interpolation factor, FM, which is related to the product of several functions, as follows:

$$k_{rg}^{f} = k_{rg}^{o}(S_w)\ FM \tag{6.8}$$

where k_{rg}^{o} is the gas relative-permeability function in the absence of foam, and

$$FM \equiv (1 + fmmob\ F1\ F2\ F3\ F4\ F5\ F6)^{-1} \tag{6.9}$$

where parameters are defined as follows:

fmmob	reference (maximum) mobility-reduction factor
F1	surfactant-concentration-dependent function
F2	water-saturation-dependent function
F3	oil-concentration-dependent function (not used here)
F4	gas-velocity-dependent function (not used here)

F5 capillary-number-dependent function

F6 critical-capillary-number dependent function (not used here).

FM varies between FM = 1 (no foam) to FM = $(1 + \text{fmmob})^{-1}$ (strongest foam). In our study, the oil phase is not present, so F3 is not considered. Also, F4 and F6 are not examined here and are set equal to 1.

6.4.2.1 fmmob - maximum reduction in gas mobility

The maximum-mobility-reduction factor fmmob can be obtained by fitting model parameters to experimental data as described by Cheng *et al*., 2000. It is the mobility reduction achieved at the injected surfactant concentration, a reference superficial velocity or capillary number as described below, and zero oil saturation. However, since, as described below, in the STARS™ algorithm FM and gas mobility can only be increased, not reduced, by shear effects (F5 $\leq$ 1), fmmob must be measured at, or extrapolated to, the lowest capillary number one expects to encounter in the simulation.

6.4.2.2 F1 - effect of surfactant concentration

F1 is the surfactant-concentration-dependent function:

$$F1 = \left[\frac{W_s}{fmsurf} \right]^{epsurf} \quad \text{for } W_s \leq \text{fmsurf}$$

$$= 1 \quad \text{for } W_s > \text{fmsurf} \tag{6.10}$$

with parameters defined as follows:

W_s surfactant concentration in the given grid block

fmsurf critical surfactant concentration (same units as W_s) - usually the

injected surfactant concentration

epsurf parameter that controls dependence of gas mobility on surfactant concentration.

According to Eq. 6.10, if surfactant concentration in the grid block is equal to or larger than the critical surfactant concentration, foam has the maximum strength, with F1 = 1; if surfactant concentration is below the critical surfactant concentration foam becomes weaker. Exactly how much weaker depends on W_s, fmsurf and the parameter epsurf (Figure 6.2). If epsurf = 1, foam strength depends linearly on surfactant concentration. However, choosing larger value for epsurf can reduce the effect of dispersion of surfactant on foam strength (Cheng, 2002).

At steady state, surfactant concentration is expected to be uniform at the injected concentration everywhere injected water travels, and Eq. 6.10 is not expected to be important. The simulations of gravity override at the heart of this chapter are at steady state. However, as discussed below surfactant concentration did play a role in whether foam collapses as it should in the override zone. Eq. 6.10 also bears on the unsteady-state simulations shown below used to validate the foam simulator.

6.4.2.3 F2 - effect of water saturation

F2 is a water-saturation-dependent function that controls the behavior of foam in the high-quality regime:

$$F2 = 0.5 + \frac{\arctan\left(epdry * \left(S_w - fmdry\right)\right)}{\pi} \tag{6.11}$$

with parameters defined as follows:

epdry regulates the slope of the gas relative-permeability curve near the critical water saturation

fmdry critical water saturation

S_w water saturation in the grid block.

Water saturation affects foam mobility in the reservoir, especially when the water saturation is close to the critical water saturation fmdry, which is the name STARS™ gives S_w* (Chapter 2). When water saturation is close to the critical water saturation fmdry (S_w*), foam begins to collapse. Since for reasons described below our study focuses on foam in the low-quality regime, the critical water saturation was first set a value very close to irreducible water saturation in reservoir. This ensured that foam was always in the low-quality regime. However, this caused unexpected numerical problems described below. Therefore, we set a higher value for critical water saturation fmdry, below that expected anywhere in the foam bank, but well above the irreducible water saturation.

Figure 6.3 shows a plot of F2 and water saturation for different values of epdry. For large values of epdry, F2 changes very dramatically over a small difference in water saturation in the region around the critical water saturation fmdry. For instance, for epdry = 600, foam breaks within an interval (fmdry ±0.01); for epdry = 200, within an interval (fmdry ±0.03). In the simulations below we used epdry = 600 except where noted. In some cases noted below, long simulation times were reduced by reducing the value of epdry to as low as 200. In these cases water saturation in the foam bank was still higher

then (fmdry + 0.03) within the foam bank except in the top two rows of grid blocks, i.e. except in or near the override zone.

6.4.2.4 F5 - non-Newtonian rheology

F5 is capillary-number-dependent function, which represents shear-thinning behavior of foam in the low-quality regime:

$$F5 = \left[\frac{fmcap}{N_{ca}} \right]^{epcap} \qquad \text{for } N_{ca} \geq \text{fmcap}$$

$$= 1 \qquad \text{for } N_{ca} < \text{fmcap} \tag{6.12}$$

where capillary number N_{ca} is given by

$$N_{ca} = \frac{k \nabla P}{\sigma} \quad . \tag{6.13}$$

fmcap is a reference capillary number, and epcap controls the dependence of mobility on capillary number. Foam gets weaker as pressure gradient increases if epcap > 0. The maximum value of F5 is 1 (Figure 6.4). Therefore, since our goal is to represent shear-thinning flow throughout the foam bank, we set fmcap to a value less than the smallest value of N_{ca} expected to be encountered in a simulation. That further implies that the "reference velocity" at which fmmob is determined (Section 6.4.2.1 above) should correspond to this value of N_{ca}. If foam experiments are conducted in the laboratory at larger value of N_{ca} than may be encountered in the field, fmcap should be the smallest value expected in the simulations and fmmob should be extrapolated to that value of fmcap.

Cheng *et al*. (2000) showed that Eq. 6.12 produces non-Newtonian effects only in the low-quality foam regime. STARS™, they pointed out, cannot represent non-Newtonian behavior in the high-quality regime. The high-quality regime corresponds to S_w near fmdry, where Eq. 6.11 dominates gas mobility. In the high-quality regime, the drastic changes in gas mobility for S_w near fmdry (Eq. 6.11) overwhelm the non-Newtonian effects of Eq. 6.12 and produce Newtonian rheology. Since the purpose of this study is to examine gravity segregation in non-Newtonian flow, we therefore restricted our attention exclusively to the low-quality regime. It is for this reason that we selected fmdry = 0.41, and checked that S_w > fmdry throughout the foam bank in the simulations. We also selected fmcap = 1×10^{-6}, and checked to verify that N_{ca} > fmcap throughout the foam bank in the simulations.

6.4.2.5 epcap and the conventional power-law index n

One can relate epcap to the conventional power-law index n (Bird *et al*., 2002) as follows. Consider a bundle-of-tubes model for rock, where the hypothetical rock comprises N uniform, parallel, cylindrical tubes of radius R, which together give the same porosity and permeability as the real rock. The volumetric flow rate of a power-law fluid flowing through a single tube is (Bird *et al*., 2002):

$$Q = \frac{\pi}{(2m)^{1/n}} \frac{R^{\left[3+(1/n)\right]}}{\left[3+(1/n)\right]} \left(\frac{p_0 - p_L}{L} \right)^{1/n} \tag{6.14}$$

where Q is volumetric flow rate, ($P_0 - P_L$) is the pressure difference along the tube, L is the length of the tube, m is consistency index, and n is power-law index. The volumetric flux u through a rock with N tubes and cross-sectional area A is

$$u = \frac{NQ}{A} = \frac{N}{A}\frac{\pi}{3+1/n}\left(\frac{\Delta P}{2Lm}\right)^{1/n} R^{(3+1/n)} \tag{6.15}$$

Eq. 6.15 can be written as:

$$u = C\nabla P^{1/n} \tag{6.16}$$

where

$$C = \frac{N}{A}\frac{\pi}{3+1/n}\left(\frac{1}{2m}\right)^{1/n} R^{(3+1/n)} \quad . \tag{6.17}$$

Consider the flow of gas in foam as a non-Newtonian fluid. In terms of the foam model in STARS™,

$$u_g = \frac{kk_{rg}^{\ 0}(S_w)}{\mu_g^{\ 0}}\nabla P\left(\frac{1}{1+ fmmob\ F1\ F2\ F5}\right) \tag{6.18}$$

Since for strong foam (fmmob F1 F2 F5) >> 1, F1 = 1 at the injected surfactant concentration, and F2 =1 in the low-quality regime, and further assuming that $k_{rg}^{o}(S_w)$ is nearly constant in the low-quality regime, then, Eq. 6.18 can be written as:

$$u_g = C_1\ \nabla \mathrm{P}\ \frac{1}{\mathrm{F5}} \tag{6.19}$$

where

$$C_1 = \frac{kk_{rg}^{\ 0}}{\mu_g^{\ 0}\ fmmob} \tag{6.20}$$

Combining Eq. 6.19 with Eqs. 6.12 and 6.13,

$$u_g = C_2\ \nabla \mathrm{P}^{(1+epcap)} \tag{6.21}$$

where

$$C_2 = C_1 \frac{k^{epcap}}{fmcap\sigma} \tag{6.22}$$

The comparison of Eqs. 6.16 (applied to flow of the gas phase) and 6.21 implies that

$$n = \frac{1}{1+epcap} \tag{6.23}$$

The relation between n and epcap in Eq. 6.23 may not be exact, to the extent that the assumptions in this derivation are not satisfied, and especially to the extent the $k_{rg}{}^{o}(S_w)$ varies in the low-quality regime.

6.5 VALIDATION OF THE FOAM SIMULATOR

In this section, we first validate the foam model in STARS™ by showing it can match steady-state laboratory data for the two flow regimes. Then we consider the numerical accuracy of the STARS™ simulator by comparing a 1D foam simulation using STARS™ with Newtonian rheology to the fractional-flow solution, which is rigorously correct for the that case. Next, we compare simulations of gravity segregation in 2D foam processes with Newtonian rheology using STARS™ to the segregation length predicted by Stone's model, which is rigorously correct for that case (Rossen and van Duijn, 2004). Finally, we consider the proper level of grid refinement for 2D simulations.

6.5.1 STARS™ foam model compared to steady-state laboratory data

Figure 6.5 (Figure 2.3, repeated here for comparison with the STARS™ foam model) shows pressure gradient as a function of gas and liquid volumetric fluxes for one foam formulation in Berea sandstone, from Alvarez *et al*. (2001). Figure 6.6 shows a fit to the steady-state data of Figure 6.5 using the STARS™ model, from Reme (1999).

Reme used relative-permeability functions for liquid and gas phases without foam based on the data of Persoff *et al*. (1991), and the fitting method was described by Cheng *et al*. (2000). The model fits the nearly vertical pressure-gradient contours in the high-quality regime and nearly horizontal contours in the low-quality regime.

The purpose of our simulation study was to show how non-Newtonian behavior affects gravity segregation, not to fit data for any particular foam. Therefore, in our simulation runs we didn't fit the parameters to laboratory data for foam. To reduce computation time, we choose smaller values for fmmob and epdry than in Figure 6.6. Figure 6.7 shows pressure-gradient contours in the low-quality regime using the STARS™ foam model and base-case parameters from our study. At fixed foam quality, foam shows shear-thinning rheology. Note that although the contours become steep at very low water volumetric flux, all of the chart reflects the low-quality regime; that is, S_w is well above fmdry, and rheology is shear-thinning.

6.5.2 1D foam displacement

6.5.2.1 Overview of fractional-flow methods

With some assumptions, the fractional-flow method can be used to predict the performance of a 1D foam displacements. These assumptions were fully discussed by Zhou and Rossen (1994), which include incompressibility of all the phases as well as of the rock; Newtonian mobilities; immediate attainment of local steady-state; absence of dispersion; and neglecting gradients of capillary pressure and viscous fingering.

In the fractional-flow method, one constructs wave diagrams for the displacement process from fractional-flow curves and the initial and injection conditions. The slope of the wave in the time-distance diagram is equal to the slope of the fractional-flow curve at that saturation, which represents dimensionless velocity of the saturation in the displacement. The velocities of "Buckley-Leverett" shock fronts, discontinuities in saturation, are governed by material balances on water and gas at the shock front, represented by a jump between points on the same fractional-flow curve. The velocity of the "chemical shock," a discontinuity in surfactant concentration, is determined by material balances on water and surfactant at the shock. This shock is represented graphically by a jump between different fractional-flow curves corresponding to the different surfactant concentrations. To obtain the solutions graphically from fractional-flow curves, one requires that the wave velocity increase monotonically from the injection condition to the initial condition. Further details can be found in Zhou and Rossen (1994).

The fractional-flow method provides a way to understand complicated displacements. Also, it provides an exact solution, given the listed assumptions, for comparison with simulation results.

6.5.2.2 Comparison of STARS™ simulator to fractional-flow solution for 1D foam process

In this section we validate the simulator by comparison to the fractional-flow method for conditions on which the fractional-flow method is rigorously correct:

specifically, a case of one-dimensional, rectilinear, incompressible, continuous foam injection with Newtonian rheology (epcap = 0).

6.5.2.2.1 Model parameters

Reservoir and foam parameters used in our simulation are listed in Table 6.1. We simulated foam injection into a brine-filled, rectangular core, 1 ft long and 2 in. on a side, with a total volume of 0.027 ft^3. In this test case, there were 50 grid blocks in the flow, i.e., horizontal, direction. One injector and one producer were placed the first block and the last block, respectively. A sketch of the grid is given in Figure 6.8.

6.5.2.2.2 Fractional-flow solution

In the test case, liquid and gas were injected simultaneously at a constant rate of 0.086 ft^3/hr (volume calculated at atmospheric pressure) into the core initially saturated with brine. The foam quality was 80% and the injection rate 0.00079 ft^3/hr at the core back-pressure, which is maintained constant at 2000 psi. The low injection rate and high back-pressure were chosen to minimize the effects of gas compressibility in the simulation, i.e., to match most closely the assumptions of fractional-flow theory.

Figure 6.9 shows the fractional-flow curves for this 1D foam displacement. The fractional-flow curve without foam is given by

$$f_w = \left(\frac{k_{rg}{}^0(S_w)}{\mu_g} \frac{\mu_w}{k_{rw}(S_w)} + 1 \right)^{-1} \tag{6.24}$$

and the fractional-flow curve with foam is given by

$$f_w{}^f = \left(\frac{k_{rg}{}^f(S_w)}{\mu_g} \frac{\mu_w}{k_{rw}(S_w)} + 1 \right)^{-1} \tag{6.25}$$

where μ_g and μ_w are gas viscosity and water viscosity, respectively, k_{rw} is water relative permeability, $k_{rg}{}^0$ is gas relative permeability without foam, $k_{rg}{}^f$ is gas relative permeability with foam (Eq. 6.8), f_w is water fractional flow without foam, and $f_w{}^f$ is water fractional flow with foam.

Figure 6.9 shows two curves, corresponding to Eqs. 6.24 and 6.25, respectively. One is for foam, and the other one represents the behavior ahead of the foam bank, where there is no surfactant. Three states crucial to the displacement are identified in the figure: J, GB and I. I indicates the initial condition in the core, which is initially saturated with brine (no surfactant), J represents the injection condition with f_w = 20%, and GB stands for the gas bank in front of the foam bank.

Based on the fractional-flow method, with no surfactant adsorption, the velocity of saturation wave at foam bank is equal to the slope of a line from the origin to the injection point J, and this line intersects the foam-free fractional-flow curve at point GB, which represents the water saturation and fractional flow in the gas bank. The velocity of the shock leading the gas bank is represented by the slope of the line from GB point to point I. Further details in how to construct the fractional-flow solution are provided by Zhou and Rossen (1994).

6.5.2.2.3 Comparison of results

Figure 6.10 shows water saturation in the core after 0.3 PV of foam injection. The dashed line represents the results from the simulation, and the solid line represents the

fractional-flow solution. These two approaches should in principle give exactly the same results. However, due to the effects of numerical dispersion, the simulator gives somewhat smeared fronts at the leading edges of the foam bank and gas bank.

Figure 6.11 shows the pressure profiles in the core after 0.3 PV of foam injection. Open symbols represent simulation results (one symbol per grid block). The solid line represents the results from the fractional-flow method. The pressure data throughout the whole core agrees well in these two approaches.

Figure 6.12 is a plot of the surfactant-concentration profile after 0.3 PV of foam injection. It shows the effect of numerical dispersion on surfactant concentration: numerical dispersion smears what should be a sharp front in surfactant concentration. When surfactant concentration in an individual grid block reaches half the injected concentration, foam becomes strong (Figure 6.2). However, there clearly is a high level of dispersion in surfactant concentration in Figure 6.12. If foam strength were a smooth function of surfactant concentration (e.g., if epsurf were 1 in Figure 6.2), the spurious spreading of the surfactant front would lead to a spurious gradual increase in foam strength at the foam front; from Figure 6.12 it is evident that foam would build up gradually over a substantial distance, as surfactant concentration increased. To minimize effects of dispersion of surfactant concentration on the foam displacement, Rossen *et al*. (1999) represented foam strength as a step function of surfactant concentration that jumped from zero to full strength at on-half the injected concentration; Cheng (2002) further discussed the effect of this assumption. In that case, pressure rises in rapid jumps when foam forms in each succeeding grid block, and then pauses until foam forms in the next block. This phenomenon was discussed by Rossen *et al*. (1999). A certain minimum

amount of dispersion in the advance of the foam front is unavoidable because the fronts must advance one grid block at a time.

In our simulations, we set the critical surfactant concentration fmsurf to the half the injected surfactant concentration and set epsurf to 4 (*cf.* Figure 6.2), roughly as Rossen *et al*. (1999) suggest. Larger values of epsurf caused the simulation run times to increase substantially. With epsurf = 4, foam strength increased rapidly but continuously as surfactant concentration rose in each grid block from about one-quarter to one half of the injected concentration.

Reme (1999) pointed out an important paradox. As long as numerical dispersion is present, a large value of epsurf minimizes the effects of dispersion. However, if there is no dispersion, and if it is important to model foam strength with different surfactant concentrations, a smaller value of epsurf should be selected to represent the effect of surfactant concentration on foam strength more accurately. In principle, the effect of surfactant concentration on foam strength should not be important in the steady-state simulations shown below, because at steady state surfactant should be at the injected concentration throughout the foam bank and zero in the override zone. But as discussed below the effect of surfactant concentration and dispersion did play a role in the 2D simulations.

6.5.3 Gravity segregation in 2D with Newtonian rheology

In this section, we compare simulator results with Newtonian rheology (epcap = 0) for gravity segregation in 2D to the model of Stone (1982), which is rigorously correct for this case (Rossen and van Duijn, 2004).

6.5.3.1 Model parameters

Parameters used in this simulation with Newtonian rheology are listed in Table 6.2. We modeled a sector-shaped cylindrical reservoir (one eighth of a cylinder) with the height of 100 ft. The outer radius of the reservoir was 250 ft. There were 100 grid blocks in the radial direction and 20 grid blocks in the vertical direction. Five grid blocks within 8 ft of the wellbore had smaller length (1, 1.2, 1.6, 2 and 2.2 ft long, respectively); beyond that, the size of each grid block was 2.6 ft. The grid model was chosen through an analysis of sensitivity of segregation length to grid refinement, as discussed below.

Two injection wells, one for gas and one for liquid, were placed in the innermost grid block of each layer. This means that the single injection well to be modeled was represented by a total of 40 injection wells in the simulator. This was required in order to guarantee a uniform injection rate and uniform quality along the injection face. (Using a single injection well for gas and liquid, one cannot guarantee uniform quality along the injection well.) Only one producer, which penetrated all 20 layers, was placed in the outermost column of grid blocks. We gave an enormous permeability (10,000 darcy) to the outermost grid block of each layer to represent an open cylindrical reservoir boundary (at the edge of the outermost grid block but one). In early simulations without this modification, at long times enough surfactant was pulled up into the override zone in the top, outermost grid block to create foam there, blocking the override zone and distorting flow throughout the reservoir. With the large permeability in the outermost grid blocks, this problem disappeared.

In these simulations, liquid and gas were injected simultaneously at constant and uniform rate into the reservoir, which was initially saturated with brine (no surfactant).

The total injection rate was set so that in a typical case the segregation length was over 50% of the reservoir radius, for better resolution of the segregation length. The outer boundary of the reservoir was maintained at an elevated, constant pressure of 2000 psi, which minimized the effects of gas compressibility during the foam process and most closely matched the assumptions of Stone's (1982) model. We simulated injection of many pore volumes (150 PV) to ensure that steady state was achieved.

6.5.3.2 Simulation results

6.5.3.2.1 Value of fmdry

As noted above, Eq. 6.12 gives the STARS™ foam model non-Newtonian behavior only in the low-quality regime. Cheng *et al.* (2000) noted that non-Newtonian behavior is possible in the high-quality regime, but it cannot be reproduced by the STARS™ foam model. Therefore we focus our simulation study of gravity segregation in non-Newtonian foams on the low-quality regime. The high-quality regime corresponds to S_w near fmdry. Therefore this strategy argues for choosing fmdry so low that it is not encountered anywhere in the foam bank: to be safest, fmdry just above the irreducible water saturation.

However, we encountered a numerical artifact that required choosing a larger value of fmdry, still below that found anywhere in the foam bank, but well above irreducible water saturation. The reason is as follows.

At steady state in the presence of gravity override, gas mobility is of course extremely high in the override zone. Mathematically (Rossen and van Duijn, 2004), there

is a boundary condition that water is at its irreducible saturation at the top of the reservoir. Simulations with finite grid sizes cannot reproduce that boundary condition exactly, but previous simulations (Shi and Rossen, 1998; Cheng *et al.*, 2000) still fit Stone's model well. Shi and Rossen (1998), working with the UTCOMP simulator with a foam model similar to that in STARS™, showed that two separate mechanisms break foam in the override zone and give gas high mobility there. First, water saturation is low, below fmdry (i.e. S_w* in Shi and Rossen's model). Second, with no surfactant initially in the reservoir and injected water flowing downward under gravity, no surfactant ever reaches the override zone. Shi and Rossen (1998) show that either mechanism working alone prevents foam from forming in the override zone. Shi and Rossen (1998), and later Cheng *et al.* (2000), obtained good agreement between Stone's model and their simulations using UTCHEM and UTCOMP.

In our initial simulations, with epcap set to zero (Newtonian behavior) and fmdry = 0.21, we found deviations in r_g by as much as 15% from Stone's prediction (Table 6.3). Rossen and van Duijn (2004) showed that Stone's model is rigorously correct under the assumptions made, so the deviation must reflect an artifact in the simulations. Moreover, water saturation was distinctly nonuniform in the foam bank, especially toward the upper leading edge of the foam region (Figure 6.13), where Stone's model, and Rossen and van Duijn's proof, predict that it should be uniform.

Investigating the cause of the error in r_g, we found that foam did not break in the override zone in the simulations as it should: both mechanisms identified by Shi and Rossen (1998) failed, at least in part. First, with fmdry set nearly to irreducible water saturation, in the presence of numerical dispersion, the collapse of foam by drying out

was postponed to several grid blocks beyond the point where Stone's model (1982) predicts that segregation should have been complete (Figure 6.14). Second, with numerical dispersion, surfactant concentration in the override zone was also sufficient to sustain foam to the same distance (Figure 6.15) As a result, there were both sufficient surfactant and water in the override zone to sustain foam to a distance of about 190 ft. Thus the escape of gas from the foam bank into and through the override zone was inhibited. The inability of gas to flow out the override zone caused gas to accumulate below the override zone until a point where either S_w approached fmdry or surfactant concentration fell sufficiently; in either case foam broke from that point on, gas flowed freely in the override zone, and segregation proceeded.

To remedy this problem, we raised fmdry to 0.31 and then to 0.41, both still well below the values found in the foam bank, but allowing foam to break more easily in the override zone. Figures 6.16 and 6.17 show the water-saturation profiles throughout the reservoir at steady state and in the override zone (top row of grid blocks). For fmdry = 0.31, S_w falls below fmdry, and foam breaks, in the override zone about 108 ft from the injection well. For fmdry = 0.41, foam breaks in the override zone about 74 ft from the injection well, long before segregation is complete. The results approached Stone's prediction of segregation length better as fmdry increases; see Tables 6.4 and 6.5. Therefore we used fmdry = 0.41 throughout the remainder of the simulations.

6.5.3.2.2 Fit to Stone's model

Table 6.5 compares predicted segregation length to simulation results at different injection rates and values of mobility-reduction factor fmmob, all with fmdry = 0.41. The

fit to Stone's model is not perfect. Moreover, the simulations consistently gave segregation at a larger radial distance than predicted by Stone's model. For a simulation with 100 grid blocks in the horizontal direction and segregation roughly halfway to the outer boundary, an error of ±2% is expected simply from grid resolution. The difference between predicted values and simulation results is larger than this, between 4 and 8%, and represents a level of accuracy that can be expected in the simulations. A bias in the simulation results toward longer segregation distances, in the range of 4 to 8%, should be kept in mind in interpreting the results for non-Newtonian foams. Fits to Stone's model, as reported by Cheng *et al.* (2000), were better with the UTCHEM simulator, to within the range of one or 2 grid blocks (2 to 4%), for a foam bank extending radially over 50 grid blocks).

6.5.4 Grid resolution

To verify the proper level of grid refinement we conducted simulations with different grid refinements. These simulations were conducted using the non-Newtonian foam parameters given in Table 6.2.

Figure 6.18 presents water-phase saturation at steady state in the reservoir with 20 grid blocks vertically and 25, 50, 100, 150 grid blocks along the radial direction, respectively. Complete segregation occurs at 190, 185, 183, and 183 ft, respectively. Thus behavior is independent of grid resolution for 100 grid blocks or more. We used 100 grid blocks in our simulations below.

Figure 6.18 shows water-phase saturation at steady state with 10, 15, 20, and 25 grid blocks along the vertical direction. Complete segregation occurs at 190, 187, 183,

and 183 ft, respectively. Thus behavior is independent of grid resolution for 20 grid blocks or more. We used 20 grid blocks in the vertical direction in our simulations below.

The thickness of the override zone shown in the water-saturation profile is constrained to be at least as thick as one grid block in vertical direction. Jenkins (1984) points out that well beyond the point of segregation the thickness of the override zone h_g is given by

$$\frac{h_g}{H} = \frac{1}{1 + \frac{\left(\lambda_{rg}\right)_g}{\left(\lambda_{rw}\right)_w} \frac{f_w}{1 - f_w}} \tag{6.26}$$

where $(\lambda_{rg})_g$ and $(\lambda_{rw})_w$ are, respectively, the relative mobilities of gas in the override zone and of water in underride zone and f_w is injected water fractional flow. The thickness of the override zone in Figure 6.19 is 30% larger than predicted by Eq. 6.26 even with 25 grid blocks in vertical direction. Shi and Rossen (1998) found using UTCOMP that grid refinement in the vertical direction had little effect on the horizontal distance to the point of segregation, even though it has an obvious effect on the thickness of the override zone. Figure 6.19 confirms this observation.

6.6 GRAVITY SEGREGATION WITH NON-NEWTONIAN FOAM

In this section, we simulate foam displacements with different injection rates, foam qualities, foam strengths and values of the shear-thinning parameter epcap to examine the ability of shear-thinning foam to overcome gravity override. In particular, we relate the segregation distance to the rise in injection-well pressure, and compare shear-thinning cases to Newtonian foams. Also, we present an approximate extension

of Stone's' model to non-Newtonian flow to bypass the need for simulations in making an initial estimate of segregation distance.

The largest effects of non-Newtonian rheology would appear in cylindrical flow, compared to rectilinear flow. Therefore we restrict our interest to cylindrical, homogeneous reservoirs.

6.6.1 Model parameters

The reservoir model, grid model and relative-permeability functions used in these simulations are the same as those used for foam with Newtonian mobility; these and other foam parameters are listed in Table 6.2.

6.6.2 The advantage of shear-shinning rheology

Shi and Rossen (1998) contended that foam does not directly prevent gravity override; it allows attainment of a sufficient horizontal pressure gradient to prevent gravity override (Eq. 6.4). However, attaining this required pressure gradient far from the well may require an injection pressure beyond that allowed by surface facilities or above the formation fracturing pressure. Shear-thinning foam mobility may offer a partial solution to this problem. Shear-thinning rheology reduces pressure gradient near an injection well while maintaining high horizontal pressure gradient far from the well.

Figure 6.20 plots bottomhole pressure at the injection well against segregation length for foams with Newtonian rheology and shear-thinning rheology with epcap = 0.25, 0.5, and 1 (i.e., power-law index n = 0.8, 0.67, 0.5), respectively. The Newtonian results here are based on simulation, not Stone's model, so the artifact discussed in

Section 6.5.3.2.2 should apply equally to all cases. To attain the same distance before segregation, Newtonian mobility requires higher injection pressure than shear-thinning foam, and the difference increases with increasing distance to segregation. The more shear-thinning the foam, the lower pressure gradient required for a given distance. Specifically, at all distances shown, Newtonian mobility requires more than double the injection pressure required for shear-thinning foam with epcap of 1 (n = 0.5). Where injection pressure is a limiting factor, a shear-thinning foam provides far deeper penetration of foam before gravity segregation than does Newtonian foam. This also implies that Stone's model, which assumes Newtonian mobility, is unduly pessimistic applied to foams with shear-thinning rheology.

Figure 6.21 plots the segregation length as a function of volumetric injection rate for epcap = 0 (Newtonian) and epcap = 1. In the example shown, the parameters of the Newtonian and shear-thinning foams are identical except for F5, which is 1 for the Newtonian foam and always less than 1 for the shear-thinning foam (Eq. 6.12). Thus in this particular example the Newtonian foam everywhere has lower mobility than the shear-thinning foam. At fixed injection rate, the Newtonian foam, with lower mobility, gives deeper foam penetration than does the shear-thinning foam, but at the cost of higher injection pressure (Figure 6.20). According to Stone's (1982) model for Newtonian flow at least, at fixed injection rate, reducing mobility always gives deeper penetration before gravity segregation (Eq. 6.2). But if injection pressure is the limiting factor, a shear-thinning foam can perform better than Newtonian foam, and outperform the predictions of Stone's model.

6.6.3 Extension of Stone's model to non-Newtonian flow

One advantage of Stone's model is that it predicts the distance to the point of segregation without the need for computer simulation. Rossen and van Duijn (2004) show that Stone's equation for this distance is rigorously correct for homogeneous reservoirs as long as the usual assumptions of fractional-flow theory apply, including Newtonian rheology. It is desirable to derive an extension to the model to non-Newtonian flow that might give an *approximate* estimate of the distance to the point of segregation without requiring simulation.

In Stone's model, the mixed zone has uniform water saturation and uniform total mobility (Eqs. 6.1 and 6.2). However, in cylindrical flow with shear-thinning rheology, water saturation and mobility vary along the horizontal direction, as shown in Figure 6.22 (b). To apply Stone's model to shear-thinning foam, the key is to find a representative "average" water saturation, from which to calculate a representative "average" total mobility in the foam zone for insertion into Eq. 6.2. Specifically, we seek to determine an "average," or representative, position in the foam bank r/r_g, such that the water saturation and mobility at that position, inserted into Eq. 6.2, gives the correct distance to the point of segregation. We have computed the segregation length by simulation for Cases 1 - 10 in Table 6.6; all these cases have foam quality $f_g = 0.7$ and epcap = 1.0 (n = 1/2), but different injection rates and different values of the reference mobility-reduction factor fmmob. For each case we estimate the best value of r/r_g as follows:

- Determine r_g from the simulation; call it r_{gs}. Specifically, r_{gs} is the radial position of the last grid block invaded by gas in the second row of grid blocks

from the top, i.e. the furthest radial position before all gas flows in the override zone.

- For each grid block at increasing radial distance from the well, take the value of r/r_g for that grid block, and the value of S_w in the middle row of grid blocks at that radial position, from the simulation result. The result is not sensitive to the choice of the middle row of grid blocks, because water saturation is quite uniform along vertical direction in the foam bank (Figure 6.22 (b)).
- Estimate segregation length (r_{ge}) using the mobility at that water saturation as follows:

$$r_{ge} = \sqrt{\frac{8Q_{inj}}{k_z \Delta\rho g \pi \left(\frac{k_{rw}(S_w)}{\mu_w} + \frac{{k_{rg}}^f(S_w)}{\mu_g} \right)}} \tag{6.27}$$

where S_w in the grid block sets $k_{rw}(S_w)$ and ${k_{rg}}^f$ in the grid block is fixed by the value of injected gas volume fraction f_g:

$$f_g = \frac{1}{\frac{k_{rw}(S_w)}{{k_{rg}}^f}\frac{\mu_g}{\mu_w} + 1} \quad . \tag{6.28}$$

- Compare r_{ge} with simulation result r_{gs}:

$$Error = \frac{\left(r_{gs} - r_{ge}\right)}{r_{gs}} \tag{6.29}$$

Figures 6.23 - 6.25 show three of the ten cases examined and illustrate the range of results obtained. They suggest that for this limited range of cases taking the value of S_w at $r/r_g = 0.04$ may give an estimate of r_{ge} that is within about 10% of the value from

the simulation, r_{gs}. This conjecture must be confirmed by testing over a wider range of cases, as illustrated below. In particular, we find that the best value of r/r_g to use depends on epcap, as discussed below.

It is remarkable that the "representative" or "average" position for the purpose of extending Stone's model to non-Newtonian flow is so close to the injection well. A value of $r/r_g = 0.04$ represents only 0.16% of the pore volume of the reservoir contained within $r \leq r_g$. For shear-thinning fluids, the mobility so close to the well is less than that in most of the foam bank. Since in Stone's equation (Eq. 6.2) segregation length is inversely related to total relative mobility, this means that segregation occurs at shorter distance than one would estimate from the mobility one would calculate at a distance further from the injection well, in the middle of the foam bank. We are not sure of the reason for this result. Figures 6.23-6.25 confirm, however, that the larger the value of r/r_g, the more the estimate of r_g exceeds the value from the simulation.

6.6.4 The effect of foam quality

We tested the ability of shear-thinning foam to fight gravity override with 70%, 80% and 90%-quality foam, respectively, at the same total injection rates. Table 6.7 summarizes the segregation length from simulation results. The differences in segregation length among cases in Table 6.7 are within the range of one or two grid blocks. Apart from an error of 2%, comparable to the grid resolution, foam quality has no effect on segregation length. The reason can be seen in Figure 6.26, which repeats the pressure-gradient contour plot of Figure 6.7 with a line of constant superficial velocity

superimposed. For this foam in the low-quality regime, at fixed superficial velocity, pressure gradient is insensitive to foam quality, and therefore so is gravity override.

6.6.5 An empirical correlation between epcap and representative r/r_g

For epcap = 1 (n = 1/2), the water saturation at $r/r_g = 0.04$ gives a representative average saturation and mobility for insertion into Stone's Eq. 6.2. The best value of r/r_g depends on epcap, however. Using the same method described above for epcap = 1, we screened the ratios of r/r_g for foam with different values of epcap and with a fixed foam quality of 70%. Figure 6.27 shows the representative value of r/r_g as a function of epcap or power-law index at this foam quality. There is a roughly linear relation between the representative value of r/r_g and epcap, and a roughly logarithmic relation between the representative r/r_g and power-law index. These correlations should not be extrapolated beyond the range shown; for instance, extrapolating to epcap less than 0.2 would suggest a value of $r/r_g < 0$. (For epcap = 0 (Newtonian rheology), Stone's model indicates that any value of $r/r_g \leq 1$ is representative, because mobility is uniform in the foam bank.) Attempting to use the same value of r/r_g for all values of epcap does not give a good fit to the segregation length. We use this correlation for r/r_g to predict segregation length and compare to simulation results in the next section.

6.6.6 Prediction of gravity segregation without simulation

For non-Newtonian flow, estimating mobility at a given location requires both water saturation and gas superficial velocity. Therefore we start with a method to estimate horizontal superficial velocity.

6.6.6.1 An empirical equation for horizontal velocity

As gas and water move away from the injection well, part of the gas is lost to the override zone and the part of water is lost to the underride zone. For Newtonian fluids in a rectangular reservoir, total horizontal flow in the mixed zone decreases linearly with distance from the well (Rossen and Duijn, 2004); for a cylindrical reservoir, total flow rate through the mixed zone decreases proportionately to the square of radial distance r, because of loss of water and gas to the override and underride zones. For foams, while the horizontal flow rate through the mixed zone decreases, the mixed zone itself does not shrink significantly until a considerable distance from the injection well (*cf*. Figures 6.17-6.19). Therefore, for a cylindrical reservoir, assuming incompressible phases, the total horizontal superficial velocity in the mixed zone decreases with distance from the well roughly as follows:

$$U_{tr} = \left(\frac{4Q_{inj}}{\pi r H}\right)\left[1-\left(\frac{r}{r_g}\right)^2\right] \tag{6.30}$$

where Q_{inj} is the total injection rate, and U_{tr} is the total superficial velocity at position r in the foam bank. The first term on the right-hand side of Eq. 6.30 describes the effect of radial flow. The second term on the right-hand side accounts for the additional decrease of velocity because of loss of gas and water to override and underride zones. Eq. 6.30 would be most accurate for values of r/r_g less than about 0.5, where the foam bank occupies nearly the entire reservoir height, as assumed (*cf*. Figures 6.17-6.19).

6.6.6.2 Estimation process

A goal of this project is to present a convenient method to obtain a reasonable estimate of segregation length using Stone's equation, without having to do simulation, based on estimating total relative mobility at a representative location at a given value of r/r_g. Without simulation, the water saturation and mobility must be determined iteratively. The detailed steps are as follows:

1 For the given value of epcap, determine the representative value of r/r_g.

2 Guess the value of water saturation S_w at this value of r/r_g.

3 Calculate k_{rw} from S_w using the known water relative-permeability function.

4 At the given foam quality, calculate k_{rg}^{f} using Eq. 6.28.

5 Calculate segregation length r_{ge} using Eq. 6.27.

6 Calculate the value of $r = r_{ge}(r/r_g)$ assumed to represent the position of the representative "average" mobility.

7 Calculate U_{tr} at this value of r from Eq. 6.30.

8 Calculate $k_{rg}^{o}(S_w)$ using the known gas relative-permeability function.

9 Calculate $FM = k_{rg}^{f}/k_{rg}^{0}$ using k_{rg}^{f} from step 4 and k_{rg}^{0} from step 8.

10 Calculate F2 using Eq. 6.11.

11 Calculate F5 using Eq. 6.31 (*cf*. Eq. 6.8):

$$FM = \frac{1}{1 + fmmobF2F5} \tag{6.31}$$

12 Calculate capillary number using Eq. 6.12.

13 Calculate pressure gradient using Eq. 6.13.

14 Calculate superficial velocities U_w and U_g using Darcy's law, with pressure gradient from step 13 and mobilities from steps 3 and 4.

15 Calculate total velocity U_{tD}, which is the sum of U_w and U_g from step 14.

16 Check the difference between U_{tr} (step 7) and U_{tD} (step 15). If they are not equal, adjust the estimate of S_w in step 2. Iteration is complete when the guessed value of S_w implies the same values of total horizontal superficial velocity from steps 7 (based on Eq. 6.30) and 15 (based on Darcy's law and mobilities from the STARS™ foam model). The value of r_{ge} from step 5 is then the converged answer.

Table 6.8 compares the values of predicted segregation lengths using the above method and those determined from simulation results for a range of foam parameter values (epcap: 0.25-1.5; fmmob: 3000-5000) and a reservoir with 250-ft outer radius and 100-ft height. Remarkably, the relative differences between the predictions of the algorithm and the simulations are comparable to, or smaller than, in the cases that were used to select the representative value of r/r_g for epcap = 1 (Table 6.6). This algorithm provides a convenient, approximate estimate of segregation distance without running a simulation of the process.

6.6.7.3 Extension to other reservoir geometries

The correlation between the representative value of r/r_g and shear-thinning parameter epcap above is derived from the reservoirs with one particular shape: 100 ft thick, with outer radius 250 ft. Using parameters derived from this reservoir shape, we compared estimated segregation length with simulations for reservoirs of two other

shapes. To model a reservoir 100 ft thick and 500 ft in radius, we used 190 grid blocks in the radial direction. In the vertical direction, there are still 20 grid blocks. Radially, the five grid blocks within 8.2 ft of the wellbore still had smaller size (1, 1.2, 1.6, 2 and 2.4 ft), as before; beyond that, the size of each grid block was still 2.6 ft. Injection rate was higher with this reservoir geometry in order to obtain segregation at a distance least half-way to the larger outer radius. The errors shown in Table 6.9 are mostly within 10%. However, when injection rate was larger than 100 ft^3/hr, the error was larger. In most cases, the estimation process underestimates the segregation distance.

Table 6.10 lists the relative error of predicted segregation length for a reservoir 50 ft tall with outer radius 250 ft. Grid blocks are half as thick as in the other cases; other parameters are same as before. Injection rates are comparable to cases with the thicker reservoir; for Newtonian flow the segregation distance is independent of reservoir thickness at equal injection rate (Eq. 6.2). The errors shown in Table 6.10 are somewhat larger than in Tables 6.8 and 6.9, especially at larger values of epcap.

Tables 6.9 and Table 6.10 imply that the estimation process for r_g should not be extended beyond the range of these and other parameters on which it was based. More study is needed, over a wider range of conditions, to derive a truly general correlation. Nonetheless, the procedure gives an approximate estimate of r_g within the range of parameter values tested, without requiring simulation.

6.7 CONCLUSIONS

Based on our simulation study, we conclude that:

- If injection pressure is limited, shear-thinning foam rheology offers much deeper foam propagation than predicted by Stone's model for Newtonian flow. Shear-thinning rheology reduces pressure gradient near an injection well and allows higher horizontal pressure gradient away from the well.
- At least over the limited range of conditions tested, one can extend Stone's model to non-Newtonian flow using the estimated mobility at a representative "average" location which depends on the degree of shear-thinning behavior (epcap or n). In the cases examined, the representative location was remarkably close to the injection well.
- A method is proposed for estimating the segregation distance for non-Newtonian foams that requires iterative calculation but not computer simulation. Estimates of segregation length in cylindrical flow were within about 15% of the values obtained by simulation over a limited range of conditions tested.
- The STARS™ foam model can accurately reproduce the two steady-state foam-flow regimes seen in the laboratory.
- The STARS™ model accurately fits the (exact) fractional-flow solution for water saturation and pressure a 1D simulation. Numerical dispersion of the surfactant-concentration front is significant, however.
- In 2D cylindrical flow of foam in the low-quality regime, the STARS™ simulator overestimated the segregation distance for Newtonian foams by as much as 8%. This resulted from dispersion of surfactant into the override zone and failure of foam to break promptly by drying out if fmdry was set too

low. Even though the focus of this study was the low-quality regime, it was important that foam break in the override zone.

- The foam model in the simulator assumes that foam generation and propagation are not problems at any pressure gradient if gas and surfactant are present. If foam generation and propagation are prevented by physical processes not accounted for in the simulator, the ability of foam to overcome gravity override would be further limited.

Table 6.1: Parameters used in 1D simulation.

Rectangular reservoir (x, y, z)	0.164 ft, 1 ft, 0.164 ft
Number of grid blocks	1 * 50 * 1
Absolute permeability	530 md
Porosity	0.25
Reservoir temperature	68°F
Initial pressure	2000 psi
Const. pressure at production well	2000 psi
Water density	62.5 lb/ft^3
Gas density	10.2 lb/ft^{3**}
Water viscosity	1 cp
Gas viscosity	0.0144 cp^{**}
Water relative permeability	$0.20\ [(S_w - 0.2) / 0.6]^{4.2}$
Gas relative permeability w/o foam	$0.94\ [(0.8 - S_{w)} / 0.6]^{1.3}$
fmdry	0.3164
fmmob	54958
epdry	2000
fmsurf	0.000143725 (one-half injected concentration)
epsurf	4
epcap	0
fmcap	(not relevant, because epcap is zero (Eq. 6.11))

** determined by simulator

Table 6.2: Parameters used in 2D simulations.

A sector-shape cylindrical reservoir (r, θ, z)	250 ft, 45^0, 100 ft
Number of grid blocks	100 * 1 * 20
Absolute permeability	1000 md
Porosity	0.25
Reservoir temperature	68°F
Initial pressure	2000 psi
Const. pressure at production well	2000 psi
Water density	62.5 lb/ft^3
Gas density	10.2 lb/ft^{3**}
Water viscosity	1 cp
Gas viscosity	0.0144 cp^{**}
Water relative permeability	0.20 $[(S_w - 0.2) / 0.8]^{4.2}$
Gas relative permeability w/o foam	0.94 $[(1.0 - S_{w)} / 0.8]^{1.3}$
fmdry	0.41
fmmob	3000, 5000
epdry	600, except where noted
fmsurf	0.000143725 (one-half injected concentration)
epsurf	4
epcap	varies among cases
fmcap	1×10^6

** determined by simulator

Table 6.3: Comparisons of predicted segregation length with simulation results at different injection rates with fmdry = 0.21 (f_g = 0.7, epcap = 0). Parameter values not listed here are given in Table 6.1.

fmmob	Q_{inj}, ft^3/hr	r_{gSim}, ft	r_{gPred}, ft	Error
3000	8	134	116	13%
3000	10	147	130	12%
3000	18	197	175	11%
3000	25	236	207	12%
5000	5	134	114	15%
5000	10	186	162	13%
5000	15	230	199	14%

Table 6.4: Comparisons of predicted segregation length with simulation results at different injection rates with fmdry = 0.31 (f_g = 0.7, epcap = 0). Parameter values not listed here are given in Table 6.1.

fmmob	Q_{inj}, ft^3/hr	r_{gSim}, ft	r_{gPred}, ft	Error
3000	8	124	116	6%
3000	10	139	130	7%
3000	18	189	175	7%
3000	25	228	207	9%
5000	5	121	114	6%
5000	10	173	162	7%
5000	18	241	218	9%

Table 6.5: Comparisons of predicted segregation length with simulation results at different injection rates with fmdry = 0.41 (f_g = 0.7, epcap = 0). Parameter values not listed here are given in Table 6.1.

fmmob	Q_{inj}, ft^3/hr	r_{gSim}, ft	r_{gPred}, ft	Error
3000	8	121	116	4%
3000	10	137	130	5%
3000	18	186	175	6%
3000	25	225	207	8%
5000	5	119	114	4%
5000	10	170	162	5%
5000	18	236	218	8%

Table 6.6: Parameter values (at 2000 psi) used in simulations for shear-thinning foam. Parameters not listed here have the same values as in Table 6.2.

Case No.	fmmob	epcap	f_g	Q_{inj}, ft^3/hr
1	3000	1	0.7	15
2	3000	1	0.7	20
3	3000	1	0.7	30
4	3000	1	0.7	50
5	3000	1	0.7	60
6	3000	1	0.7	65
7	5000	1	0.7	10
8	5000	1	0.7	15
9	5000	1	0.7	30
10	5000	1	0.7	50

Table 6.7: Comparisons of segregation length at different foam qualities. Parameters not listed here have the same values as in Table 6.2.

epcap = 1, fmmob = 3000

Q_{inj}, ft^3/hr	r_{gSim},ft (f_g=0.7)	r_{gSim},ft (f_g=0.8)	r_{gSim},ft (f_g=0.9)
15	115.9	118.5	118.5
30	160.1	162.7	162.7
50	201.7	206.9	204.3

epcap = 1, fmmob = 5000

Q_{inj}, ft^3/hr	r_{gSim},ft (f_g=0.7)	r_{gSim},ft (f_g=0.8)	r_{gSim},ft (f_g=0.9)
15	141.9	144.5	144.5
30	194.2	196.5	196.5
50	246.2	243.5	246.2

Table 6.8: Comparisons of predicted segregation length with simulation results (f_g = 0.7). Parameters not listed here have the same values as in Table 6.2.

fmmob	epcap	n	Q_{inj} ft^3/hr	r_{gSim} ft	r/r_g	r_{gPred} ft	Error
3000	0.25	0.8	10	124	0.0008	130	-5%
3000	0.25	0.8	25	197	0.0008	198	-1%
3000	0.25	0.8	35	238	0.0008	231	3%
5000	0.25	0.8	10	152	0.0008	154	-1%
5000	0.25	0.8	15	186	0.0008	186	0%
5000	0.25	0.8	25	246	0.0008	235	5%
3000	0.5	0.67	15	137	0.0133	148	-8%
3000	0.5	0.67	30	191	0.0133	198	-4%
3000	0.5	0.67	40	223	0.0133	224	-1%
5000	0.5	0.67	10	139	0.0133	146	-5%
5000	0.5	0.67	15	168	0.0133	173	-3%
5000	0.5	0.67	30	236	0.0133	232	2%
3000	0.67	0.6	15	129	0.0215	137	-7%
3000	0.67	0.6	30	178	0.0215	182	-2%
3000	0.67	0.6	50	230	0.0215	224	3%
5000	0.67	0.6	10	129	0.0215	135	-5%
5000	0.67	0.6	20	181	0.0215	179	1%
5000	0.67	0.6	35	238	0.0215	224	6%
3000	1	0.5	20	132	0.0381	138	-5%
3000	1	0.5	50	202	0.0381	196	3%
3000	1	0.5	65	228	0.0381	216	5%
5000	1	0.5	15	142	0.0381	141	0%
5000	1	0.5	30	194	0.0381	183	6%
5000	1	0.5	50	246	0.0381	223	9%
3000	1.5	0.4	25	126	0.0630	136	-8%
3000	1.5	0.4	50	171	0.0630	173	-2%
3000	1.5	0.4	65	191	0.0630	190	1%
5000	1.5	0.4	15	121	0.0630	128	-6%
5000	1.5	0.4	40	186	0.0630	178	4%
5000	1.5	0.4	65	230	0.0630	213	8%

Table 6.9: Comparisons of predicted segregation length with simulation results for f_g = 0.7, Re = 500 ft; the number of grid blocks in radial direction is 190. Parameters not listed here have the same values as in Table 6.2.

epdry	fmmob	epcap	n	Q_{inj}, ft^3/hr	r_{gSim}, ft	r_{gPred}, ft	Error
600	3000	0.25	0.8	10	124	130	-5%
600	3000	0.25	0.8	25	194	198	-2%
600	3000	0.25	0.8	35	231	231	0%
600	3000	0.25	0.8	100	413	373	10%
600	5000	0.25	0.8	10	153	154	-1%
600	5000	0.25	0.8	15	186	186	0%
600	5000	0.25	0.8	25	244	235	4%
400	3000	1	0.5	20	132	138	-5%
400	3000	1	0.5	50	202	196	3%
200	3000	1	0.5	100	280	255	9%
200	3000	1	0.5	150	332	298	10%
200	3000	1	0.5	200	376	333	11%
200	5000	1	0.5	15	142	141	0%
200	5000	1	0.5	30	194	183	6%
200	5000	1	0.5	50	244	222	9%
200	5000	1	0.5	100	329	288	13%
600	5000	1	0.5	150	397	336	15%
200	3000	1.5	0.4	20	119	126	-6%
200	3000	1.5	0.4	25	129	136	-6%
200	3000	1.5	0.4	50	176	173	2%
200	3000	1.5	0.4	65	197	204	-4%
200	3000	1.5	0.4	100	236	221	6%
200	3000	1.5	0.4	130	259	243	6%
200	3000	1.5	0.4	150	277	256	8%
200	3000	1.5	0.4	200	311	284	9%
200	5000	1.5	0.4	50	205	192	6%
200	5000	1.5	0.4	65	228	210	8%
200	5000	1.5	0.4	100	272	244	10%
200	5000	1.5	0.4	150	322	282	12%

Table 6.10: Comparisons of predicted segregation length with simulation results for f_g = 0.7, H = 50 ft. Parameters not listed here have the same values as in Table 6.2.

epdry	fmmob	epcap	n	Q_{inj}, ft^3/hr	r_{gSim}, ft	r_{gPred}, ft	Error
600	3000	0.25	0.8	10	121	123	-1%
600	3000	0.25	0.8	15	147	148	0%
600	3000	0.25	0.8	25	197	187	5%
600	3000	0.25	0.8	30	215	203	5%
600	5000	0.25	0.8	10	150	145	3%
600	5000	0.25	0.8	15	184	175	5%
600	5000	0.25	0.8	25	243	221	9%
600	3000	1	0.5	25	137	128	7%
600	3000	1	0.5	50	184	167	9%
600	3000	1	0.5	65	207	185	11%
600	5000	1	0.5	15	129	119	8%
600	5000	1	0.5	30	176	154	12%
600	5000	1	0.5	50	220	187	15%
200	3000	1.5	0.4	25	116	110	5%
200	3000	1.5	0.4	50	152	142	7%
200	3000	1.5	0.4	65	191	156	18%
200	5000	1.5	0.4	25	134	122	9%
200	5000	1.5	0.4	40	163	144	11%
200	5000	1.5	0.4	65	197	171	13%

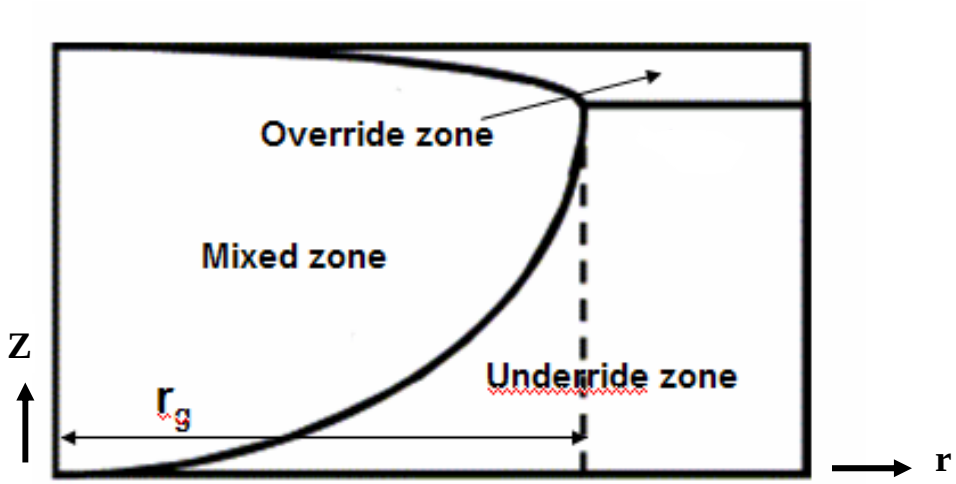

Figure 6.1: Schematic of three zones in the model of Stone (1982) and Jenkins (1984) (cylindrical flow).

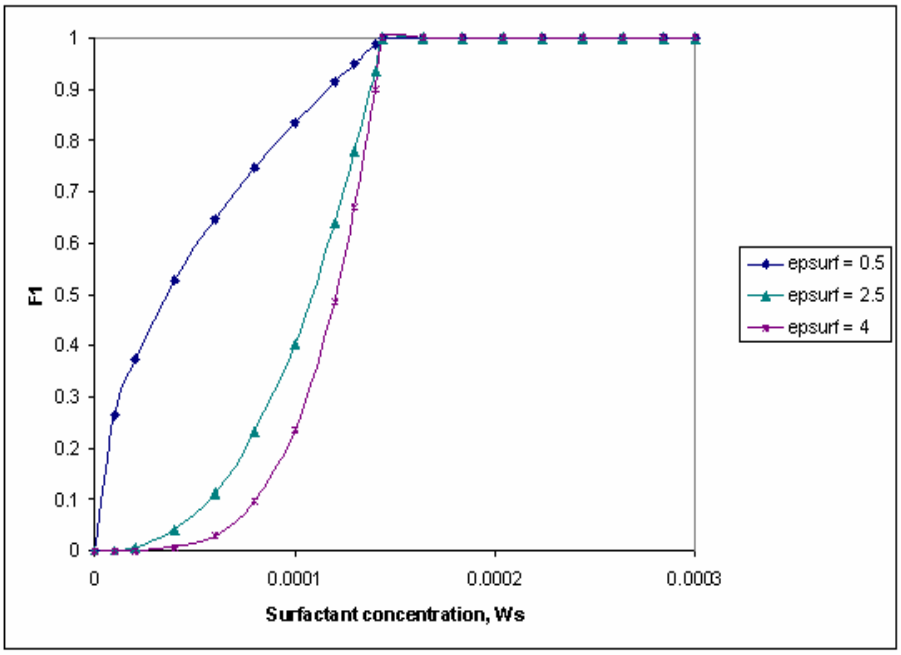

Figure 6.2: Surfactant-concentration-dependent function F1 with fmsurf = 0.000143725.

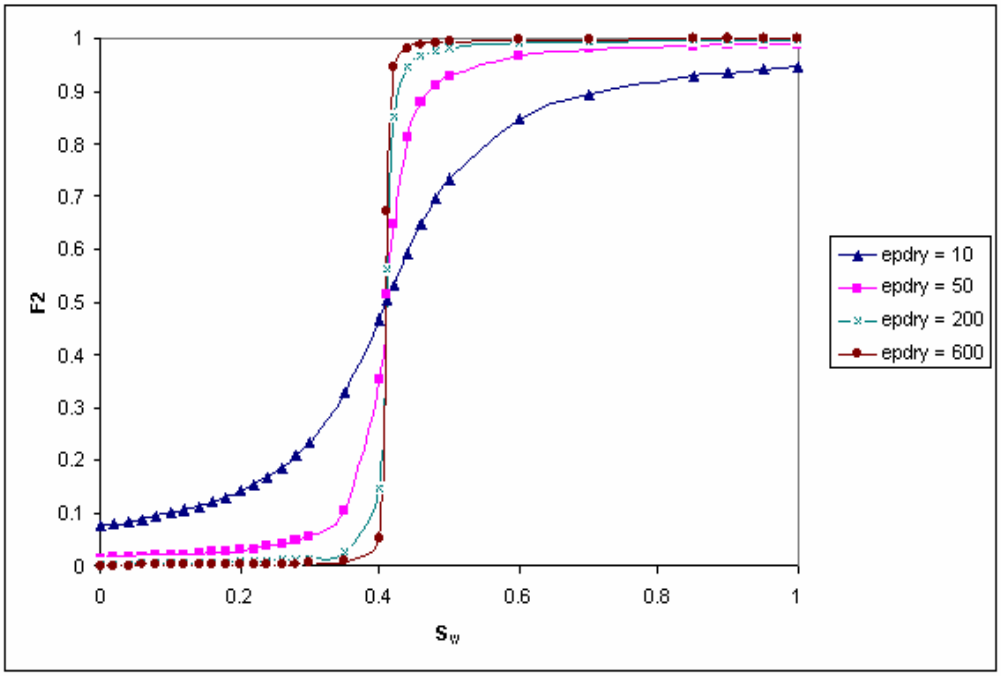

Figure 6.3: Water-saturation-dependent function F2 with fmdry = 0.41.

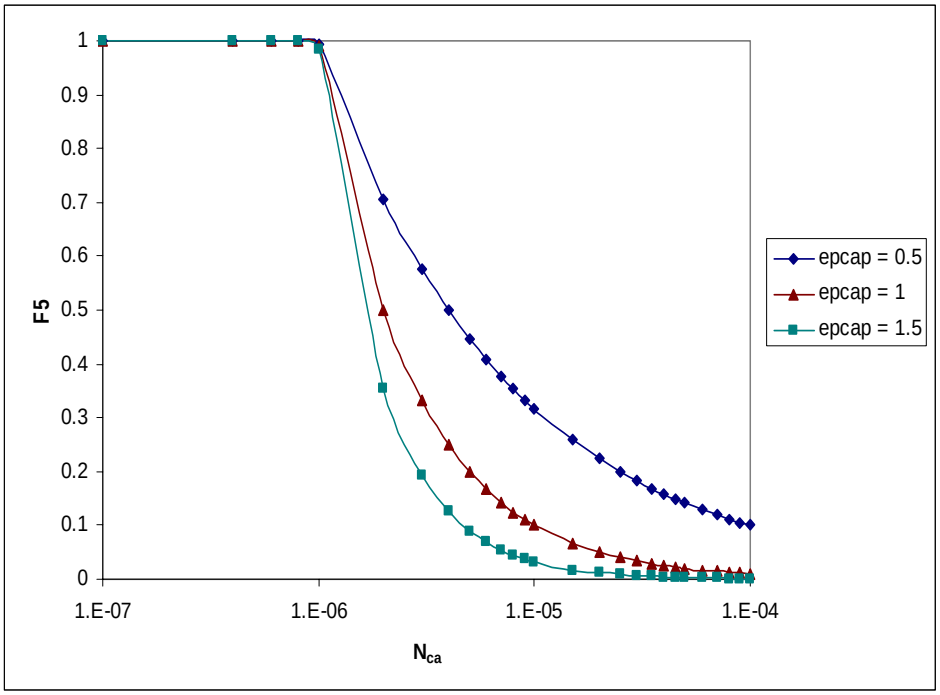

Figure 6.4: Capillary-number-dependent function F5 with fmcap = 1×10^{-6}.

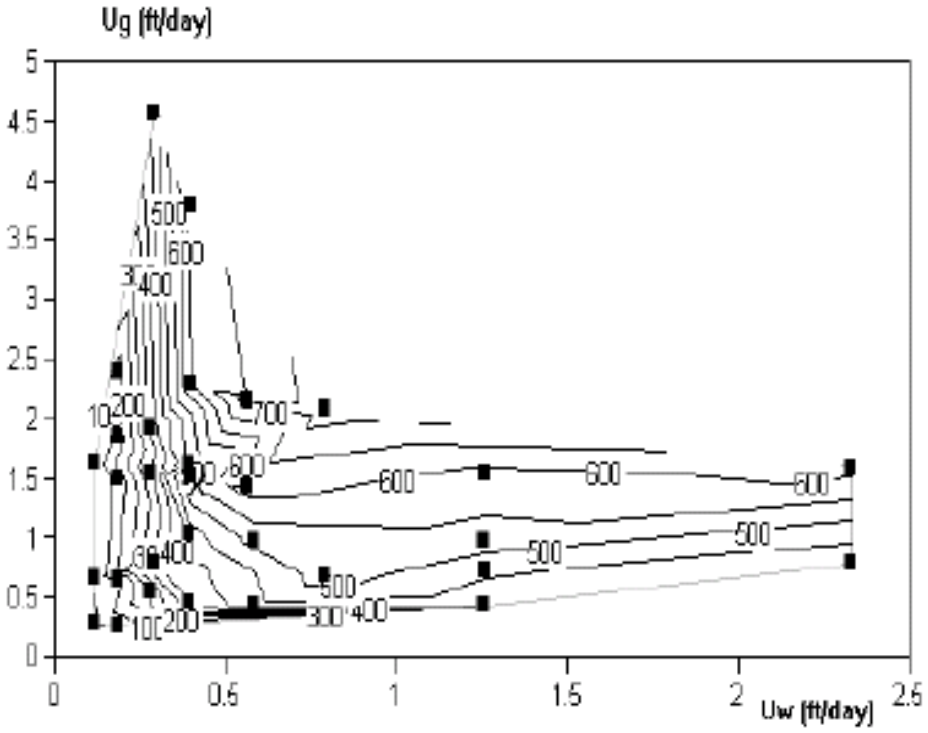

Figure 6.5 Pressure gradient (psi/ft) as a function of gas and water volumetric fluxes, from a study of foam in a Berea sandstone (Alvarez *et al.*, 2001).

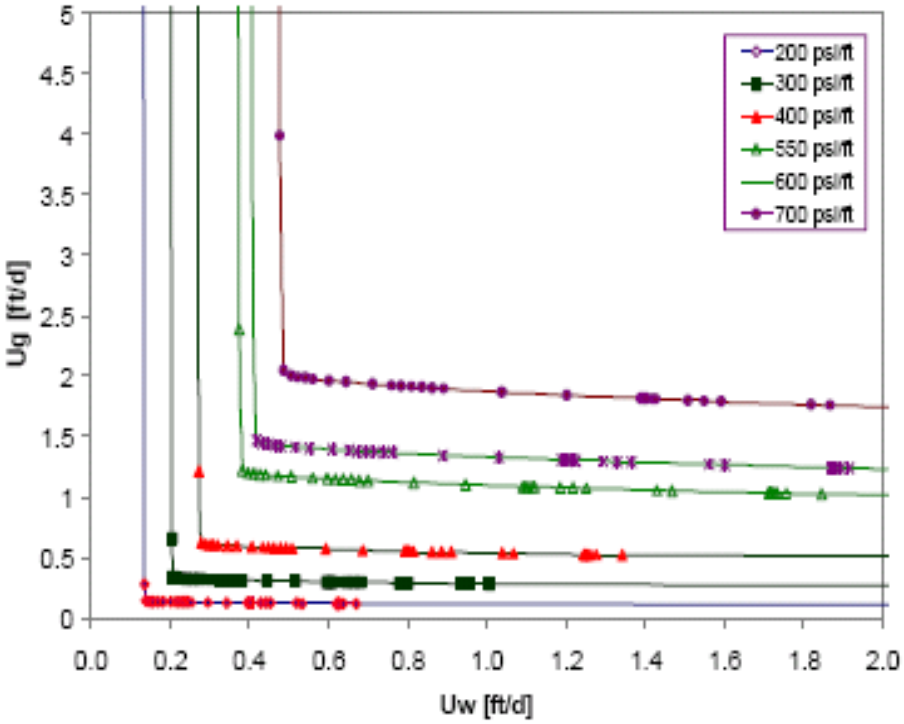

Figure 6.6 Fit to data of Figure 6.5 using parameters of STARS™ foam model: fmdry = 0.316, fmmob = 54985, epdry = 20000, fmcap = 0.0000246, epcap = 1.1215 (Reme, 1999; Cheng *et al*., 2000).

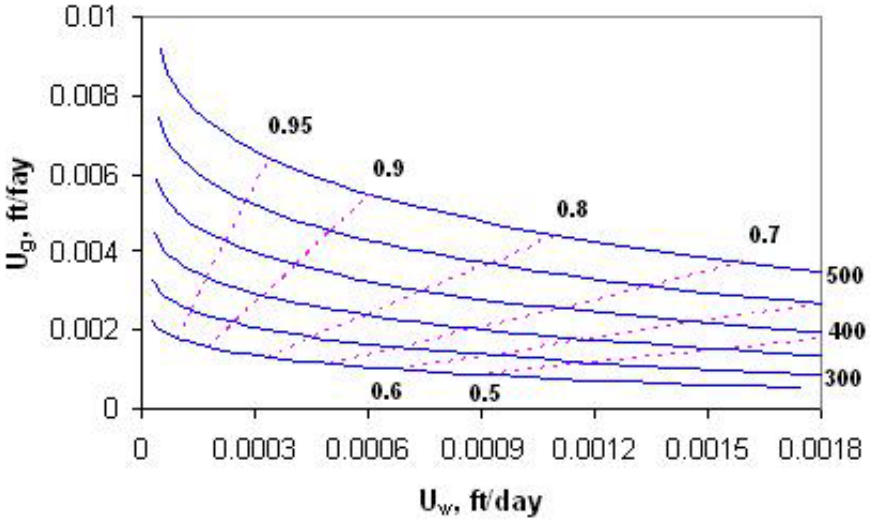

Figure 6.7 Pressure-gradient contours based on STARS™ foam model: fmdry = 0.41, fmmob = 3000, epdry = 600, fmcap = 1 x 10^{-6}, epcap = 1. Solid lines represent contours of constant pressure gradient: 250, 300, 350, 400, 450, 500 psi/ft, from the lower curve to the upper curve, respectively. Dashed lines correspond to the following foam qualities: 0.95, 0.9, 0.8, 0.7, 0.6, 0.5, starting from the left.

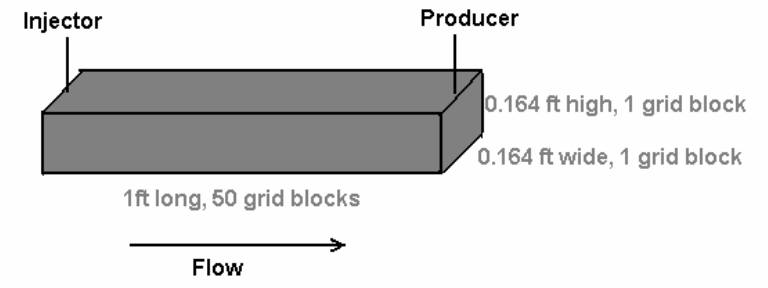

Figure 6.8 Grid model in 1D foam displacement.

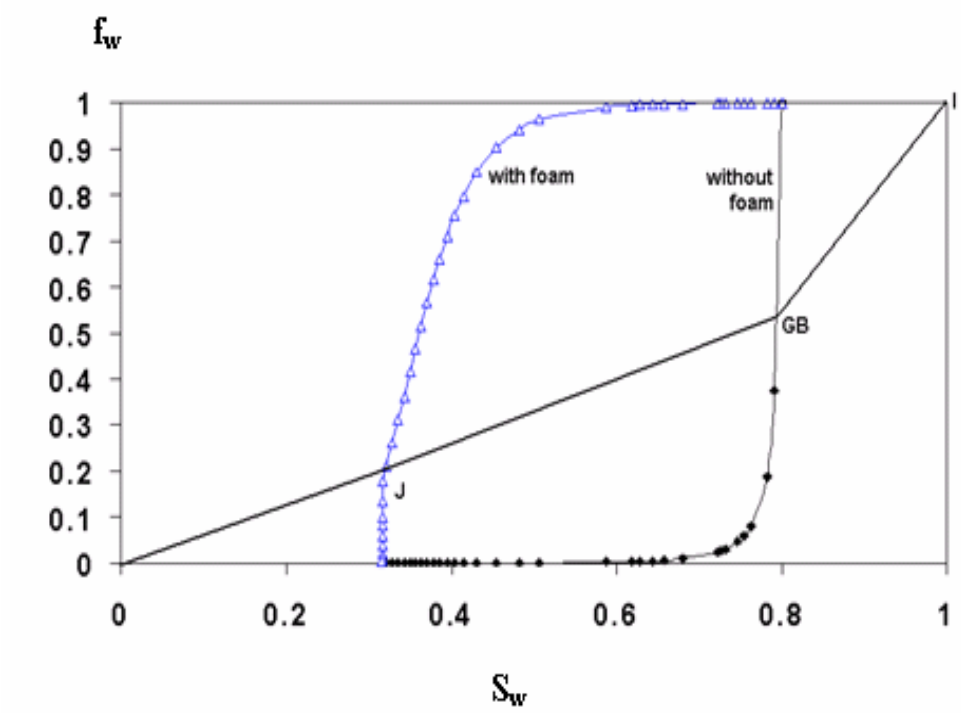

Figure 6.9: Fractional-flow curves and construction of solution for 1D foam displacement with $f_g = 80\%$ ($f_w = 0.2$).

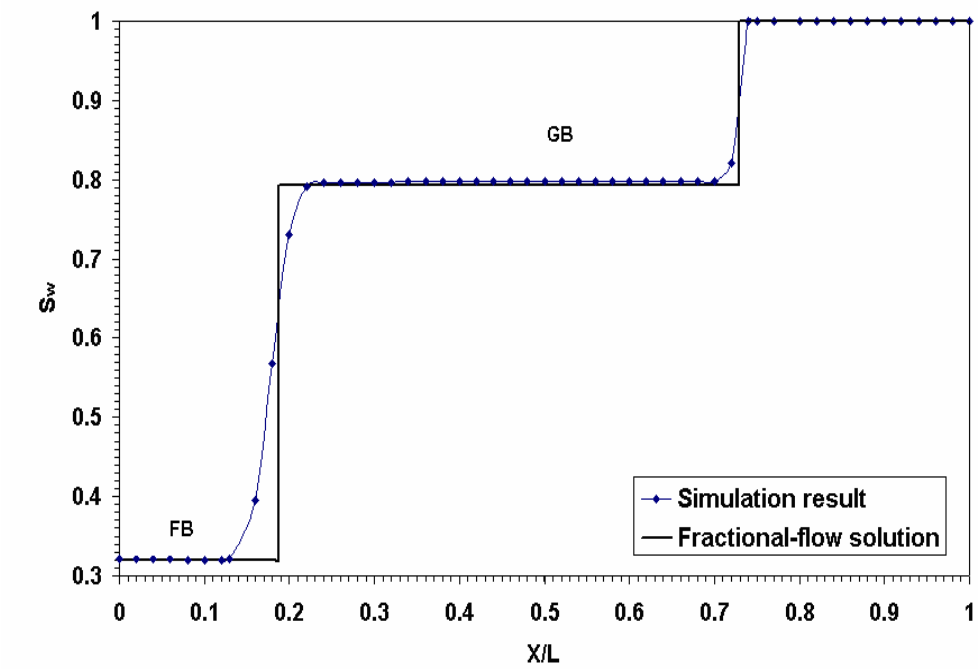

Figure 6.10: Water-saturation profiles in 1D displacement after 0.3 PV foam injection.

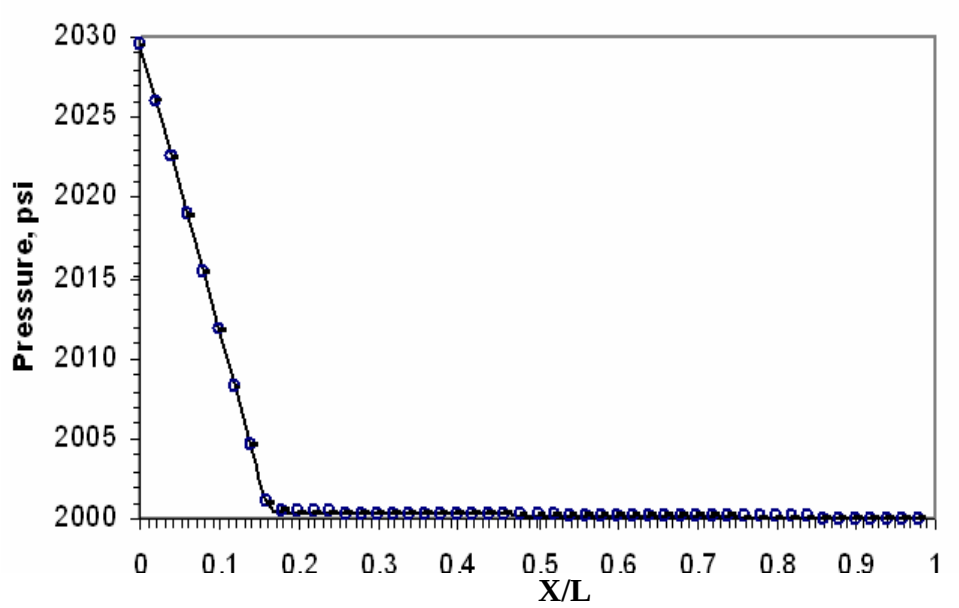

Figure 6.11: Pressure profiles after 0.3 PV foam injection in 1D displacement of Figure 6.10. Open symbols represent the results from simulation (one symbol per grid block). Solid line represents fractional-flow solution.

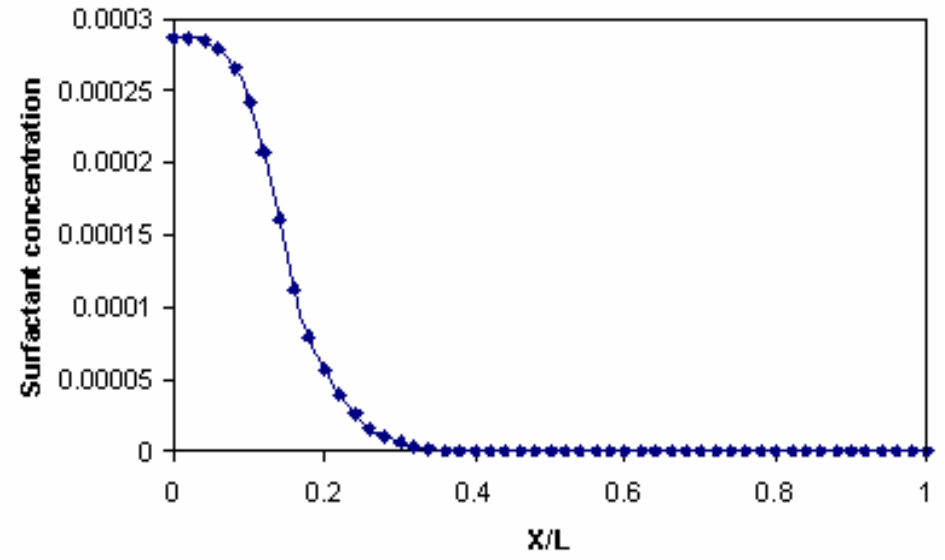

Figure 6.12: Surfactant profile after 0.3 PV foam injection in 1D displacement of Figure 6.10.

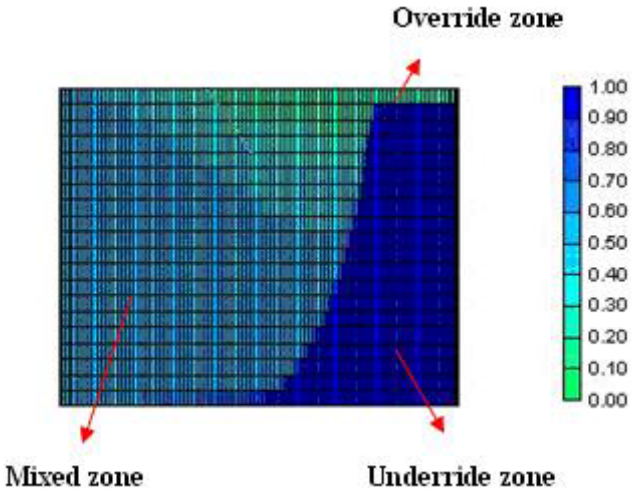

Figure 6.13: Steady-state water-saturation profiles with foam with Newtonian rheology for fmdry = 0.21 (fmmob = 3000, epdry = 600, epcap = 0, $f_g = 0.7$, Q_{inj} = 18 ft^3/hr). Note distinctly nonuniform saturation in foam bank, especially toward the upper leading edge, which reflects an artifact in the simulation.

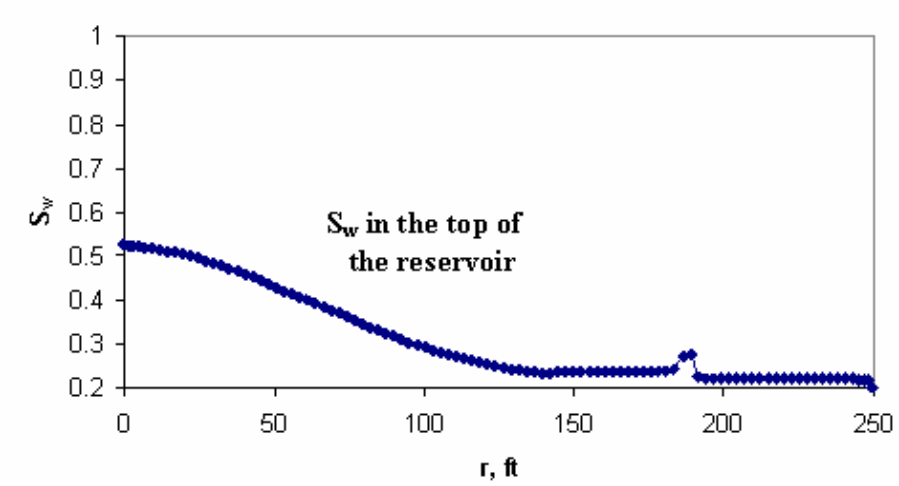

Figure 6.14: Water-saturation profile for top row of grid blocks in Figure 6.13 (fmdry = 0.21, fmmob = 3000, epdry = 600, epcap = 0, $f_g = 0.7$, $Q_{inj} = 18$ ft^3/hr). Note that in the override zone, water saturation does not fall below fmdry = 0.21, or foam break, until about 190 ft from the injection well.

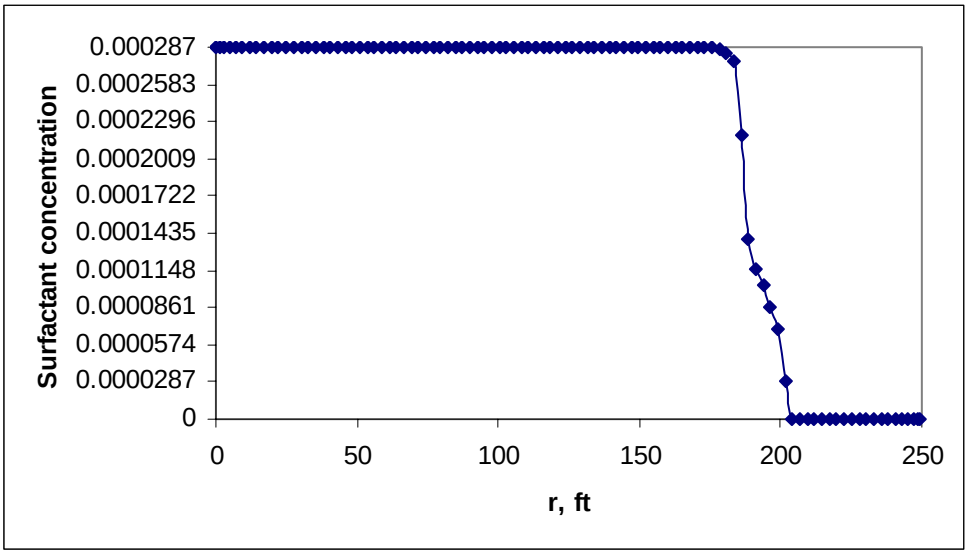

Figure 6.15: Surfactant concentration in top row of grid blocks in Figure 6.13 (fmdry = 0.21, fmmob = 3000, epdry = 600, epcap = 0, $f_g = 0.7$, $Q_{inj} = 18$ ft^3/hr). The injected surfactant concentration is 0.000287. Note that in the override zone, surfactant concentration is sufficient to sustain foam up to about 190 ft from the injection well.

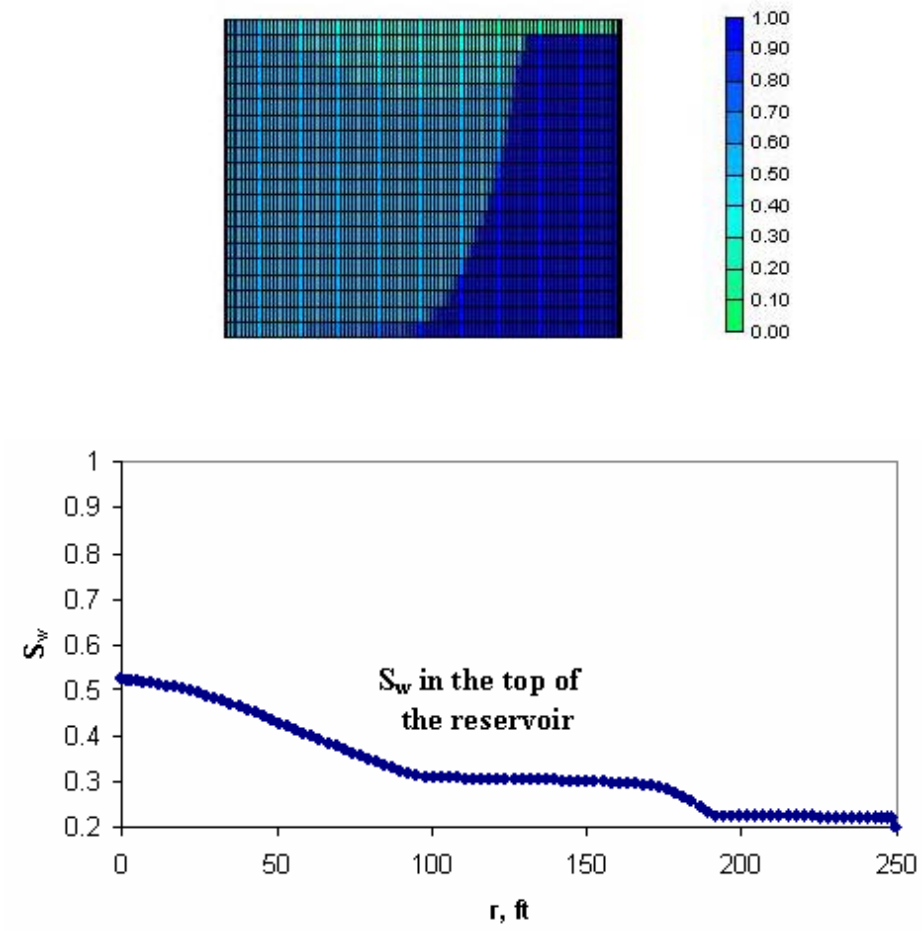

Figure 6.16: Steady-state water-saturation profiles for reservoir and in top row of grid blocks for fmdry = 0.31 (fmmob = 3000, epdry = 600, epcap = 0, $f_g = 0.7$, $Q_{inj} = 18$ ft^3/hr). In the override zone, water saturation falls below fmdry = 0.31, and foam breaks, about 108 ft from the injection well.

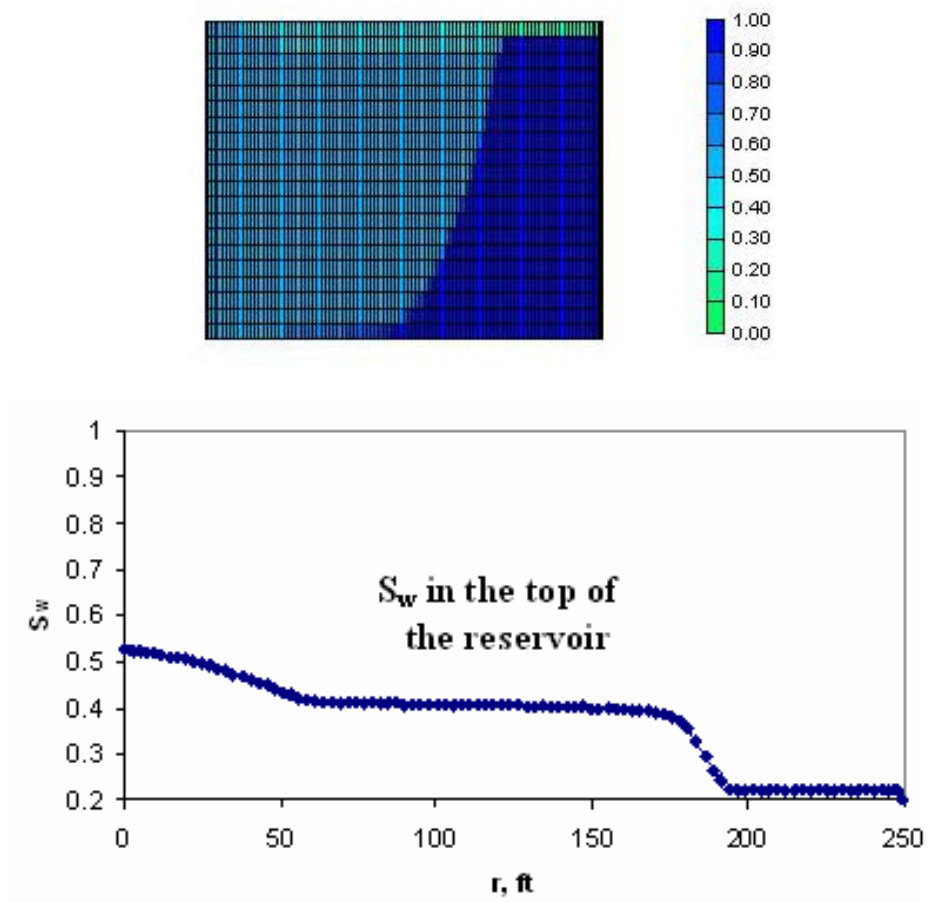

Figure 6.17: Steady-state water-saturation profiles for reservoir and in top row of grid blocks for fmdry = 0.41 (fmmob = 3000, epdry = 600, epcap = 0, $f_g = 0.7$, $Q_{inj} = 18$ ft^3/hr). In the override zone, water saturation falls below fmdry = 0.41, and foam breaks, about 74 ft from the injection well.

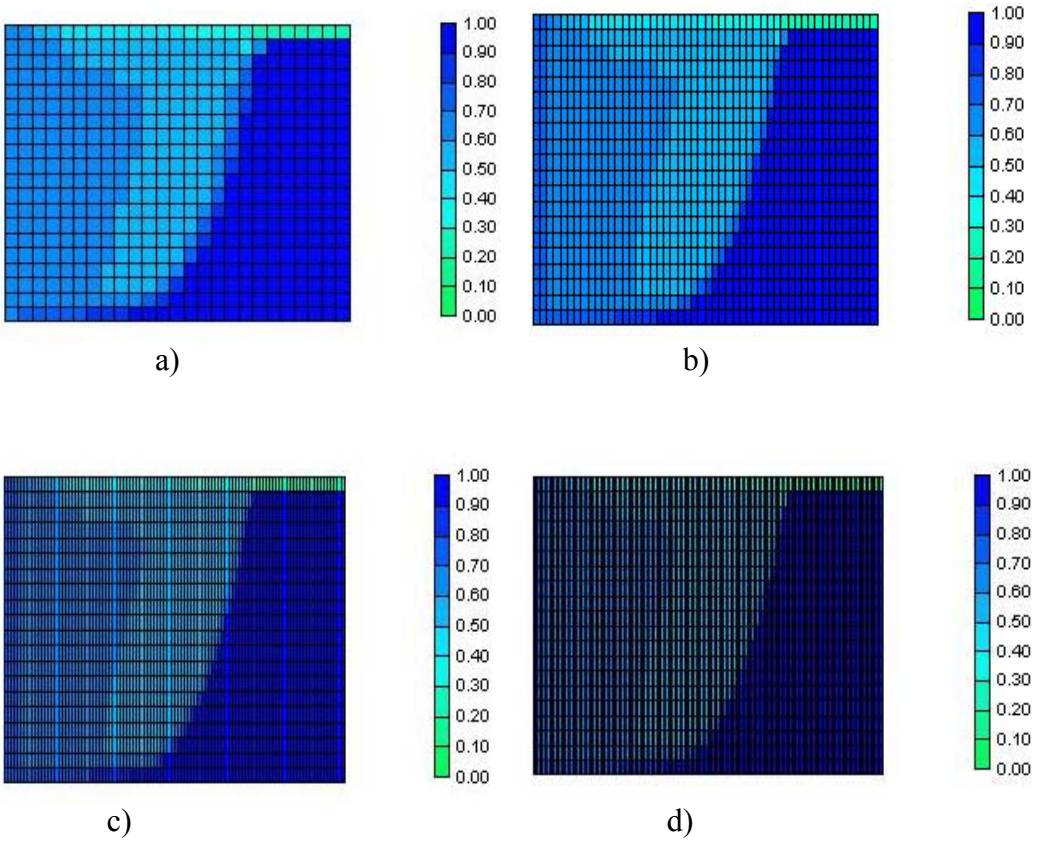

Figure 6.18: Steady-state water-phase saturation profiles from simulations using different grid-block refinements in radial direction. a) 25 grid blocks; b) 50 grid blocks; c) 100 grid blocks; d) 150 grid blocks (fmmob = 3000, epcap = 1, $f_g = 0.7$, $Q_{inj} = 40$ ft^3/hr).

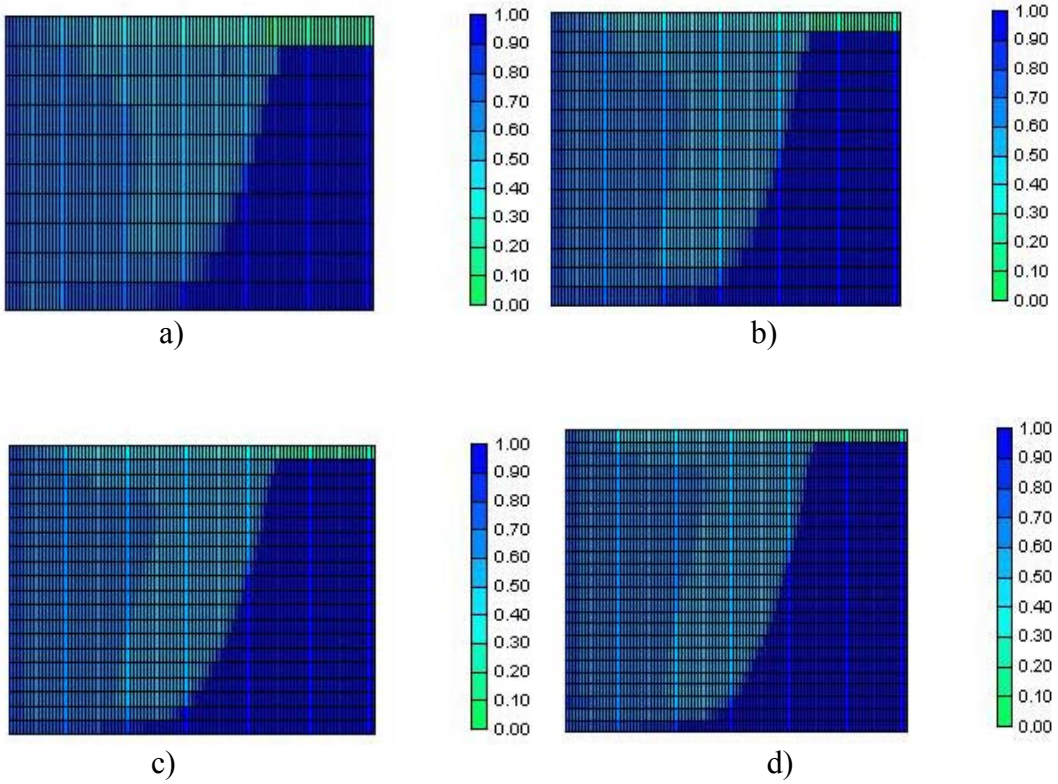

Figure 6.19: Steady-state water-saturation profiles from simulations using different grid-block refinements in vertical direction. a) 10 grid blocks; b) 15 grid blocks; c) 20 grid blocks; d) 25 grid blocks (fmmob = 3000, epcap = 1, f_g = 0.7, Q_{inj} = 40 ft^3/hr).

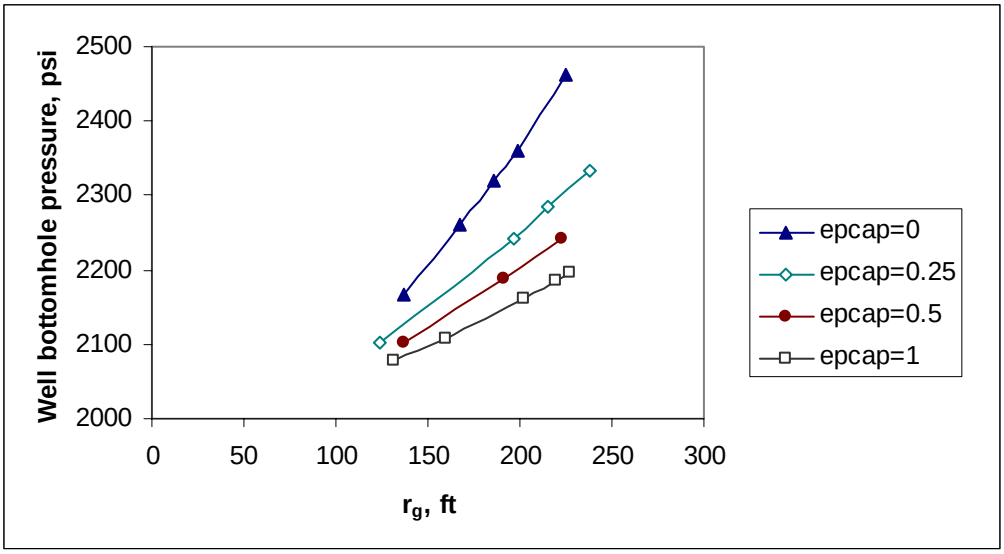

Figure 6.20: Bottomhole pressure required to achieve a given segregation length in cylindrical flow. Solid triangles represent simulation results for foam with Newtonian behavior (fmmob = 3000, epcap = 0, f_g = 0.7, fmdry = 0.41) and other symbols represent simulation results for shear-thinning foam. Note that back-pressure is 2000 psi.

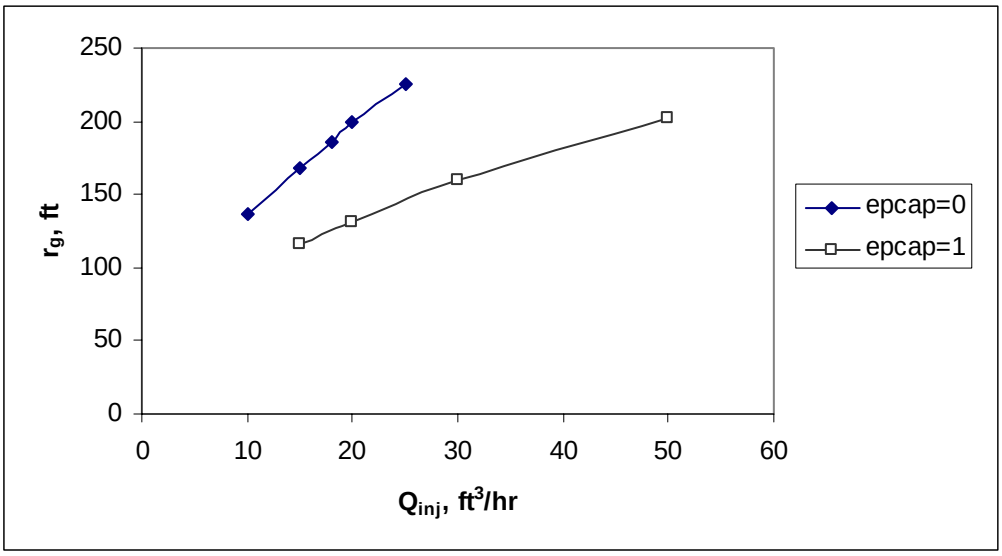

Figure 6.21: Segregation length as a function of injection rate. Solid square dots represent simulation results for foam with Newtonian behavior (fmmob = 3000, epcap = 0, f_g = 0.7, fmdry = 0.41) and empty square dots represent simulation results for shear-thinning foam (fmmob = 3000, epcap = 1, f_g = 0.7, fmdry = 0.41).

a) Newtonian foam

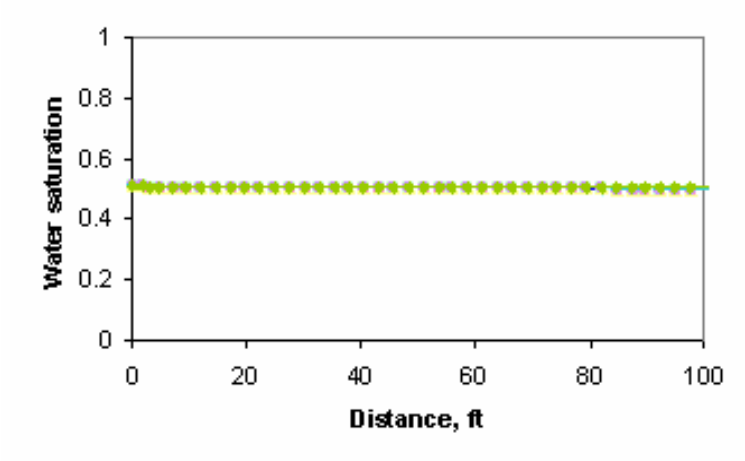

b) Shear-thinning foam

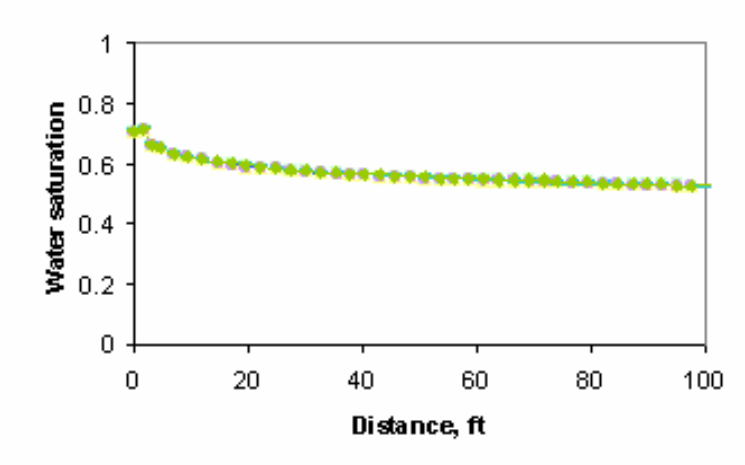

Figure 6.22: Steady-state water-saturation distribution at the 5th, 10th, and 15th layers of the reservoir for foam with shear-thinning rheology and with Newtonian rheology (fmmob = 4000, epcap = 1, f_g = 0.7, Q_{inj} = 20 ft^3/hr). The results for different layers appear as one trend because they lie on top of each other.

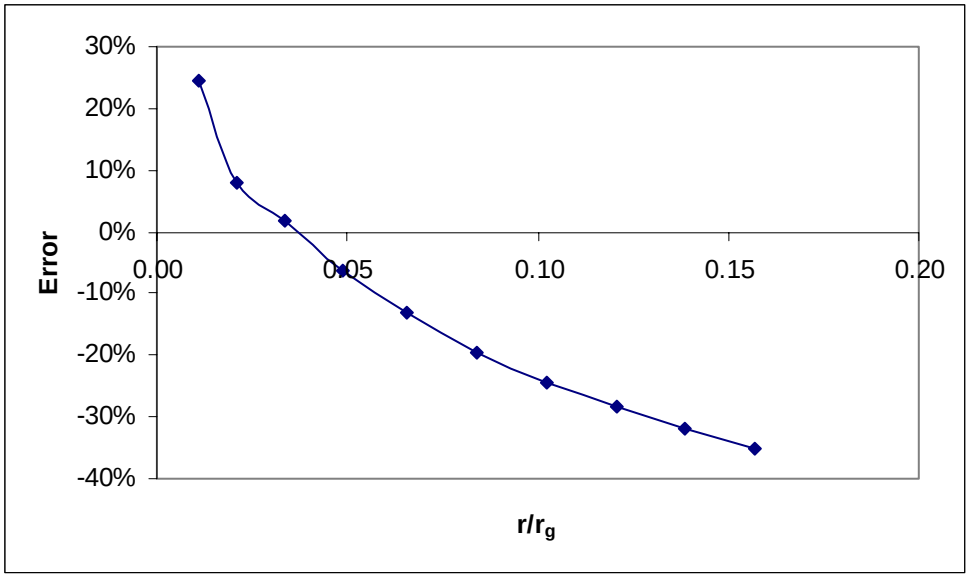

Figure 6.23: Relative error (Eq. 6.29) in predicted segregation length from Eqs. 6.27 and 6.28 with different values of r/r_g; simulation case 8 (Table 6.6).

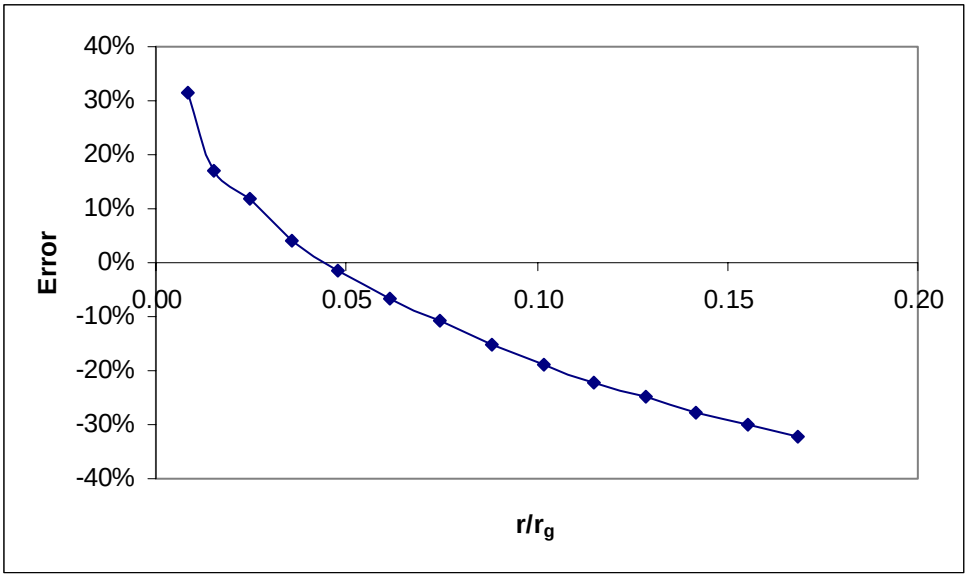

Figure 6.24: Relative error (Eq. 6.29) in predicted segregation length from Eqs. 6.27 and 6.28 with different values of r/r_g; simulation case 9 (Table 6.6).

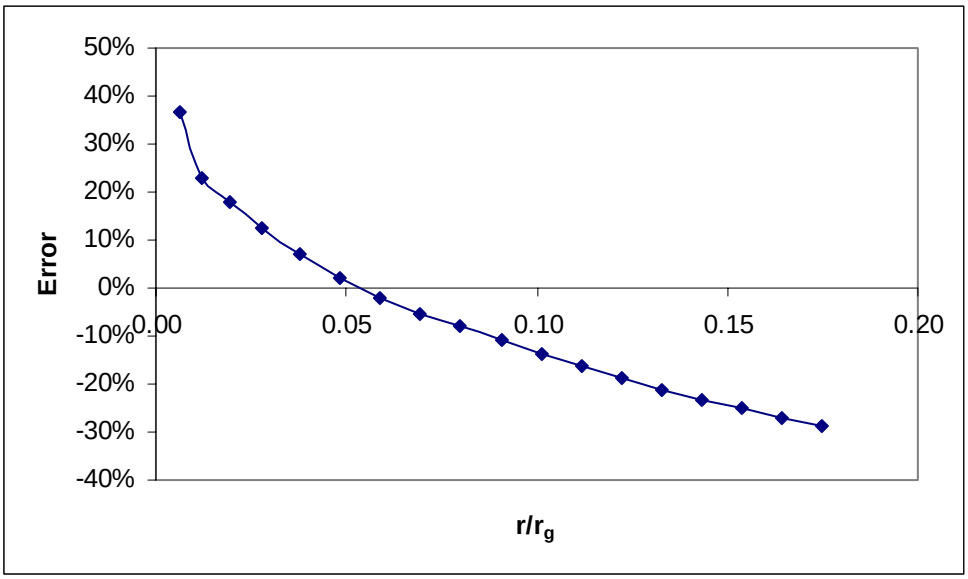

Figure 6.25: Relative error (Eq. 6.29) in predicted segregation length from Eqs. 6.27 and 6.28 with different values of r/r_g; simulation case 10 (Table 6.6).

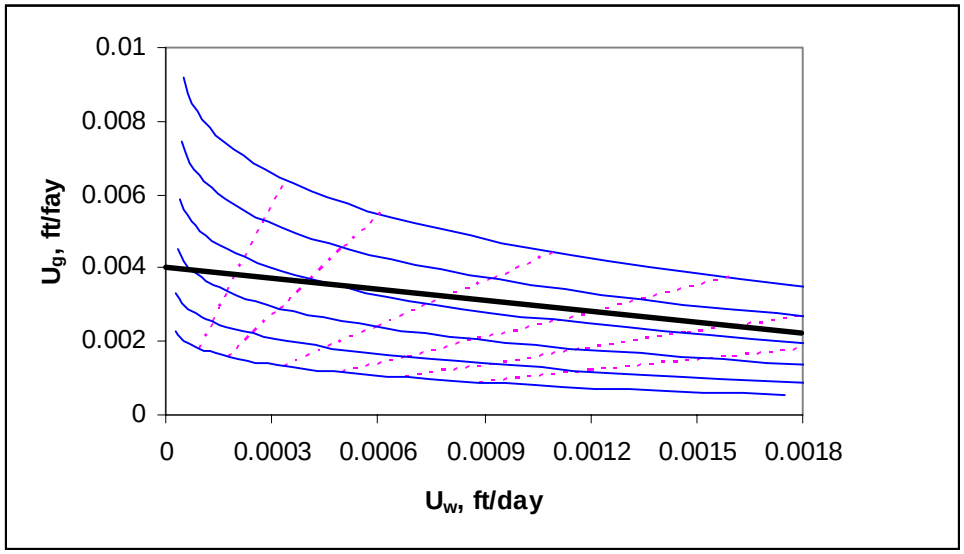

Figure 6.26: Pressure-gradient contours from Figure 6.7, with line of fixed total superficial velocity superimposed. Dashed lines correspond to foam qualities 0.95, 0.9, 0.8, 0.7, 0.6, and 0.5, starting from the left. For these model parameters, pressure gradient hardly changes as foam quality varies at fixed total superficial velocity.

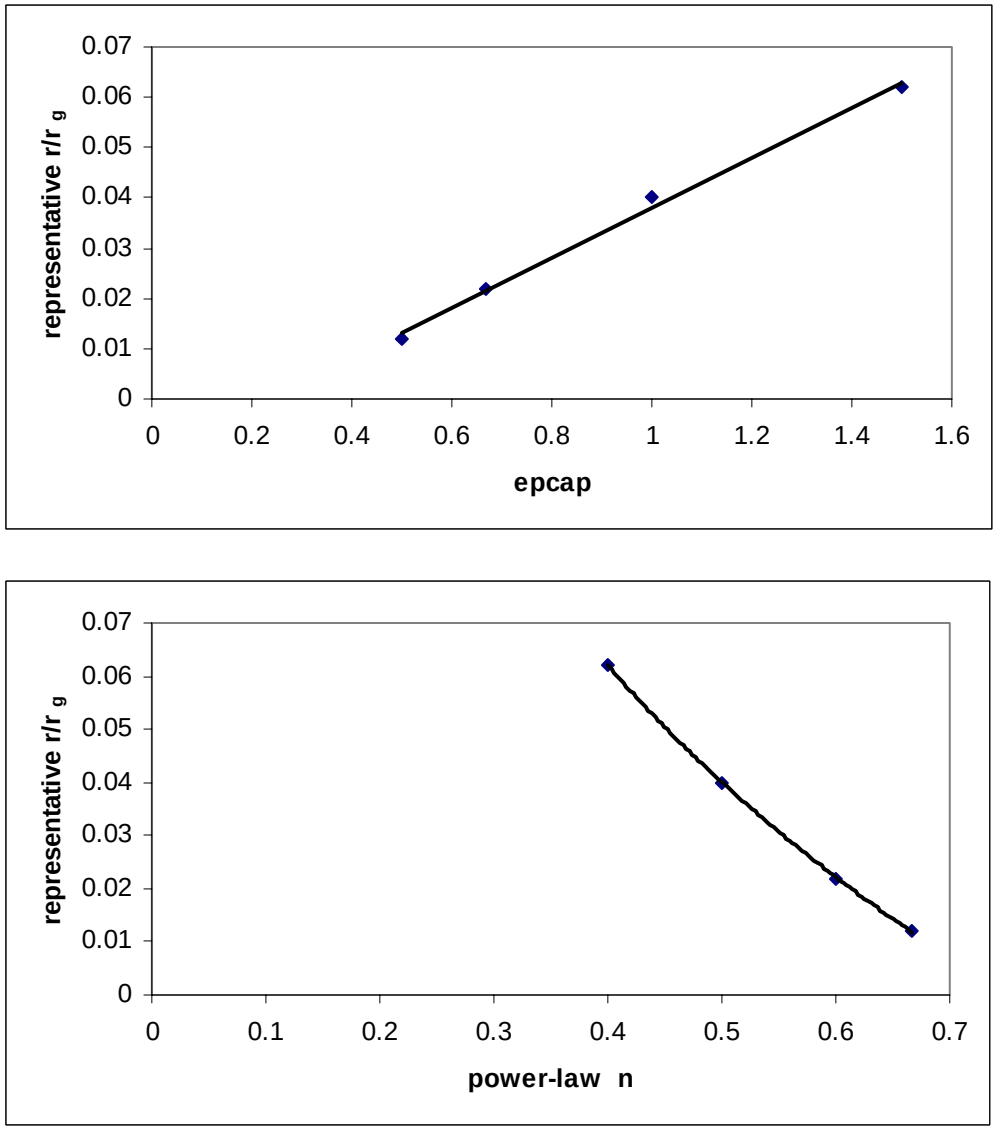

Figure 6.27: Representative value of r/r_g as a function of epcap at fixed $f_g = 70\%$ (fmmob: 3000 ~5000).

CHAPTER 7: SUMMARY, CONCLUSIONS AND RECOMMENDATIONS FOR FUTURE WORK

7.1 SUMMARY AND CONCLUSIONS

This dissertation brings together two studies related to foam and polymers. First, we investigated the effect of the addition of polymer on the stability of foam in porous media, using the two steady-state strong-foam-flow regimes (Figures 2.2 and 2.3) as a window into foam mechanisms. We expected to observe the two foam-flow regimes even with the addition of polymer and oil, and to infer the effects of polymer and oil from their effects on the two regimes. Previous studies have often assumed that drainage from bulk foams in blenders or test tubes reflects stability in porous media, or that pressure gradient in the porous medium is a direct reflection of foam stability. If polymer increases the stability of foam in porous media, however, it should increase pressure gradient more than proportionately to the increase in the viscosity of the aqueous phase. We also expected polymer to increase the prevalence of the low-quality regime and thereby increase the resistance of foam to oil. Instead, in many cases, we did not see the expected two flow regimes. Nevertheless, based on our experimental results, we reached the following conclusions:

- For the polymers (Xanthan and partially hydrolyzed polyacrylamide), oils (decane and 37.5° API crude oil), and surfactant (Bio-Terge AS-40, an alpha-olefin sulfonate) tested here, it appears from coreflood pressure gradient ∇P that polymer *de*stabilized foam somewhat. Any increase in pressure gradient ∇P observed resulted from the increased viscosity of the aqueous phase. In all

cases examined, this increase was less than predicted from the increase in the viscosity of the aqueous phase alone.

- For the same polymers and surfactant, polymer did not stabilize foam in the presence of decane or 37.5°API crude oil.
- The two regimes were observed with and without polymer in Boise sandstone, but not in the sandpacks or in any of the cases with oil present. At the limit of, or in the place of, the high-quality regime, there was sometimes an abrupt jump upwards in ∇P as though from hysteresis and a change of state. In the low-quality regime, ∇P was not independent of liquid superficial velocity, but decreased with increasing liquid superficial velocity.

The second study concerned gravity segregation with shear-thinning foam in a homogeneous reservoir. Foam may be shear-thinning with or without polymer, but it is expected to be more shear-thinning with polymer than without (Huh and Rossen, 2006). Specifically, our work was an extension of the that of Stone (1982), Shi and Rossen (1998) and Cheng *et al*. (2000), who investigated gravity segregation with Newtonian fluids. Based on our simulation study using STARS™, we reached the following conclusions:

- If the injection pressure is limited, a shear-thinning foam rheology offers much deeper foam propagation than is predicted by Stone's model for Newtonian flow. Shear-thinning rheology reduces the pressure gradient near

an injection well and allows higher horizontal pressure gradient away from the well.

- At least over the limited range of conditions tested, one can extend Stone's model to non-Newtonian flow using the estimated mobility at a representative "average" location which depends on the degree of shear-thinning behavior. In the cases examined, the representative location was remarkably close to the injection well.
- A method is proposed for estimating the segregation distance for non-Newtonian foams that requires iterative calculation but not computer simulation. Estimates of segregation length in cylindrical flow were within about 15% of the values obtained by simulation over the limited range of conditions tested.
- The STARS™ foam model can accurately reproduce the two steady-state foam-flow regimes seen in the laboratory.
- The STARS™ model accurately fit the (exact) fractional-flow solution for water saturation and pressure a 1D simulation. Numerical dispersion of the surfactant-concentration front was significant, however.
- In 2D cylindrical flow of foam in the low-quality regime, the STARS™ simulator overestimated the segregation distance for Newtonian foams by as much as 8%. This resulted from dispersion of surfactant into the override zone and failure of foam to collapse promptly by drying out if fmdry (critical water saturation) was set too low. Even though the focus of this study was the low-quality regime, it was important that foam collapse in the override zone.

7.2 RECOMMENDATIONS FOR FUTURE WORK

It is still not clear why the two foam-flow regimes shown in Fig. 2.3 appeared in some cases and not in others. This needs further study over a wider range of injection rates. Our hypothesis is that polymer can increase the stability of foam if polymer can increase Sw in the high-quality regime. We detect the effect of polymer on the stability of foam from increment in pressure gradient generated by foam with and without the addition of polymer. For further study on the effect of polymer on foam, it would be helpful to use CT scanning to image water saturation to observe directly how the addition of the polymer affects Sw. In our work, we inferred the effect on Sw indirectly from krw (i.e., from pressure gradient).

Our experimental study included the two types of polymers most frequently cited for EOR applications, polyacrylamide and Xanthan gum, and the type surfactant most commonly cited for foam (anionic, and specifically AOS). Nevertheless, further study will be needed as other types of polymers and surfactants are proposed for foam EOR. We used two oils that were destabilizing to our foam formulations, but further study with a wider variety of oils would be worthwhile.

In the simulation study on gravity segregation, we encountered numerical issues with STARS™ that forced some compromises: foam parameters with lower resistance (lower value of fmmob (maximum mobility reduction) and less abrupt collapse of foam in the vicinity of fmdry (critical water saturation) (smaller value of epdry) than inferred from laboratory data (Figure 6.6). We did not consider these crucial because our focus was on shear-thinning rheology per se and not matching any particular laboratory data. The dispersion of surfactant into the override zone caused the foam bank to extend further than it should have, for Newtonian foams at least. These problems might be

reduced using the foam simulators UTCHEM and UTCOMP which describe foam behavior in an essentially same way as STARS does (Shi and Rossen, 1998; Cheng et al., 2000; Shan, 2001; Cheng, 2002). Shan (2001), employing UTCOMP, also in effect reduced the magnitude of fmdry (specifically, parameter R in UTCHEM) from the values used to fit laboratory data in their simulations of the low-quality regime. (Her results, with less discussion of the simulation method, appeared in Cheng et al., 2000.) However, she did need to mitigate the abrupt collapse of foam at fmdry (Sw*). Moreover, dispersion of surfactant concentration with UTCHEM was markedly smaller than we found with STARS (cf. Fig. 2.18 of Cheng (2002) to Fig. 6.12 above). As discussed above, surfactant dispersion, we believe, leading to slow accumulation of surfactant in the override zone, was the cause of the foam front appearing to advance further in the STARS simulations than predicted by Stone's equation. Shan does not state the number of pore volumes injection simulated in her study, but it appears to be only a few (cf. Fig. 3.2 of Shan (2001)). It is possible that UTCHEM and UTCOMP would accumulate numerical dispersion of surfactant in the override zone if 150 pore volumes injection was simulated in those studies. Finally, there may be other algorithms within STARS for mitigating dispersion not apparent in the user's manual and therefore not used here. It would be worthwhile to extend this study using a simulator that matches Stone's prediction for Newtonian foams. In addition, the study should be extended over a wider range of reservoir and foam properties, to identify, if possible, a more accurate and reliable method to predict of gravity override with non-Newtonian fluids.

Nomenclature

epcap	=	*foam parameter that controls the dependence of mobility on capillary number*
epdry	=	*foam parameter that regulates the slope of the gas relative-permeability curve near fmdry*
epsurf	=	*foam parameter that controls dependence of gas mobility on surfactant concentration*
f_g	=	*gas volume fraction*
f_g^*	=	*foam quality at transition between foam flow regimes*
fmcap	=	*reference capillary number*
fmdry	=	*critical water saturation*
fmmob	=	*reference (maximum) mobility-reduction factor*
fmsurf	=	*critical surfactant concentration*
f_w	=	*water volume fraction*
FM	=	*dimensionless interpolation factor*
F1	=	*surfactant-concentration-dependent function*
F2	=	*water-saturation-dependent function*
F5	=	*capillary-number-dependent function*
g	=	*gravitational acceleration (m^2/s)*
h_{cr}	=	*critical thickness of lamella (m)*
H	=	*the height of reservoir (m)*
k	=	*absolute permeability of the porous medium (m^2)*

k_x	=	*horizontal permeability of the porous medium (m^2)*
k_{rg}^0	=	*gas relative permeability without foam*
k_{rg}^f	=	*gas relative permeability with foam*
k_{rw}	=	*water relative permeability*
k_z	=	*vertical permeability of the porous medium (m^2)*
L	=	*the length of rectangular reservoir (m)*
L_B	=	*length of thin film portion of bubble (model of Hirasaki and Lawson) (cm)*
L_g	=	*segregation length in rectangular reservoir (m)*
L_s	=	*length of liquid slugs (model of Hirasaki and Lawson, Eq. 5.1) (cm)*
n	=	*power-law index*
n_L	=	*number of equivalent lamellae per unit length (model of Hirasaki and Lawson, Eq. 5.1) (cm^{-1})*
N_{ca}	=	*capillary number*
N_g	=	*gravity number*
N_L	=	*dimensionless length of the thin film portion of bubble (model of Hirasaki and Lawson, Eq. 5.1)*
N_s	=	*dimensionless number for surface tension gradient effect (model of Hirasaki and Lawson, Eq. 5.2)*
P_c	=	*capillary pressure (Pa)*
P_c^*	=	*limiting capillary pressure (Pa)*
Q_{inj}	=	*total injection rate (m^3/s)*

r_c	=	*radius of curvature of gas-liquid interface (model of Hirasaki and Lawson, Eq. 5.1) (cm)*
r_B	=	*equivalent bubble radius (model of Hirasaki and Lawson, Eq. 5.3) (cm)*
r_g	=	*segregation length in cylindrical reservoir (m)*
R	=	*capillary radius (model of Hirasaki and Lawson, Eq. 5.1) (cm)*
R_e	=	*the outer radius of reservoir (m)*
R_L	=	*reservoir aspect ratio*
S_w	=	*water saturation*
S_w^*	=	*critical water saturation*
U	=	*velocity of bubble (model of Hirasaki and Lawson, Eq. 5.1) (cm/s)*
U_g	=	*gas superficial velocity (m/s)*
U_w	=	*water superficial velocity (m/s)*
U_{tr}	=	*lateral total velocity (m/s)*
W	=	*the width of rectangular reservoir (m)*
W_s	=	*injected surfactant concentration*
$\Delta\rho$	=	*difference density between phases (kg/m^3)*
∇P	=	*pressure gradient (Pa/m)*
β	=	*parameter for surface tension gradient effect (model of Hirasaki and Lawson) (cm)*

$(\lambda_{rw}+\lambda_{rg})_m$	=	*the total relative mobility in the mixed zone(Pas^{-1})*
μ	=	*liquid viscosity (model of Hirasaki and Lawson, Eq. 5.1) (Pa s)*
μ_{app}	=	*apparent viscosity of foam (model of Hirasaki and Lawson, Eq. 5.1) (Pa s)*
μ_g^0	=	*gas viscosity (Pa s)*
μ_w	=	*water viscosity (Pa s)*
π	=	*disjoining pressure (Pa)*
σ	=	*surface tension (N/m^{-1})*
Γ	=	*foam quality, gas volume fraction (model of Hirasaki and Lawson, Eq. 5.3)*

References

Aarra, M.G., Ormehaug, P.A., and Skauge, A.: "Foam for GOR Control-Improved Stability by Polymer Additives," paper presented at 9th European IOR Symposium, The Hague, The Netherlands, 20-22 October 1997.

Alvarez, J. M., Rivas, H. J., and Rossen W. R.: "Unified Model for Steady-State Foam Behavior at High and Low Foam Qualities," *SPEJ* (September 2001), 325-333.

Alvarez, J. M.: "Foam-Flow Behavior in Porous Media: Effects of Flow Regime And Porous-Medium Heterogeneity," PhD dissertation, The University of Texas at Austin, 1998.

Apaydin, O. G. and Kovscek, A. R.: "Transient Foam Flow in Homogeneous Porous Media: Surfactant Concentration and Capillary End Effect," SPE 59286 presented at the SPE/DOE Improve Oil Recovery Symposium, Tulsa, OK, 3-5 April 2002.

Austad T., and Taugbøl, J.: "Chemical Flooding of Oil Reservoirs 2. Dissociative Surfactant-polymer Interaction with A Negative Effect on Oil Recovery," *Colloids and Surfaces A* (October 1995), 73-81.

Bernard, G. G., Holm, L. W., and Jacobs, W. L.: "Effective of Foam on Trapped Gas Saturation and on Permeability of Porous Media to Water," *SPEJ* (December 1965), 295-300.

Bikerman, J. J.: *Foams*, Springer-Verlag, New York, 1973.

Bird, R. B., Stewart, W. E., and Lightfoot, E. N.: *Transport Phenomena*, 2nd ed., John Wiley &Sons, New York, 2001.

Burman, J. W., and Hall, B.E.: "Foam Diverting Technique Improved Sandstone Acid Jobs," *World Oil* (November 1987), 31-36.

Calvert, J. R.: "Foams in Motion," in *Foams: Physics, Chemistry, and Structure*, Springer-Verlag, Berlin, 1989.

Chalbaud, C. A., Moreno, R. A., and Alvarez, J. M.: "Simulating Foam Process for a Venezuelan Pilot Test," SPE 77699 presented at the SPE Annual Technical Conference and Exhibition, San Antonio, TX, 29 September-2 October 2002.

Cheng, L.: "Modeling and Simulation Studies of Foam Processes in Improved Oil Recovery and Acid-Diversions," PhD dissertation, The University of Texas at Austin, 2002.

Cheng, L., Reme, A. B., Shan D., Coombe, D. A. and Rossen, W. R.: "Simulating Foam Processes at High and Low Foam Qualities," SPE 59287 presented at the SPE/DOE Improve Oil Recovery Symposium, Tulsa, OK, 3-5 April 2000.

Chukwueke, V.O., Bouts, M.N., and Van Dijkum, C.E.: "Gas Shut-off Foam Treatment," SPE 39650 presented at SPE/DOE Improved Oil Recovery Symposium in Tulsa, OK, 19-22 April 1998.

Dalland, M., and Hanssen, J.E.: "Enhanced Foams for Efficient Gas Influx Control," SPE 37217 presented at SPE International Symposium on Oilfield Chemistry, Houston, TX, 1997.

Dalland, M., and Hanssen, J.E.: "Increased Oil Tolerance of Polymer-Enhanced Foams: Deep Chemistry or Just "Simple" Displacement Effects?" SPE 59282 presented at the SPE/DOE Improved Oil Recovery Symposium, Tulsa, Ok, 3-5 April 2000.

de Vries, A. S. and Wit, K.: "Rheology of Gas/Water Foam in the Quality Range Relevant to Steam Foam," *SPERE* (May 1990) 185-192.

Ettinger, R. A. and Radke, C. J.: "Influence of Texture on Steady Foam Flow in Berea Sandstone," *SPERE* (February 1992), 83-90.

Falls, A. H., Hirasaki, G. J., Patzek, T. W., Gauglitz, P. A., Miller, D. D., and Ratulowski, T.: "Development of A Mechanistic Foam Simulator: The Population Balance and Generation by Snap-off," *SPERE* (August 1988), 884-892.

Falls, A. H., Musters, J. J., and Ratulowski, J.: "The Apparent Viscosity of Foams in Homogeneous Bead Packs," *SPERE* (May 1989), 155-164.

Friedmann, F. and Jensen, J. A.: "Some parameters influencing the formation and propagation of foams in porous media." SPE 15087 presented at SPE California Regional Meeting, Oakland, CA, 2-4 April 1986.

Friedmann, F., Chen, W. H., and Gauglitz, P.A.: "Experimental and Simulation Study of High-Temperature Foam Displacement in Porous Media," *SPERE* (February 1991), 37-45.

Friedmann, F., Hughes, T.L., Smith, M.E., Hild, G.P., Wilson, A., and Davies, S.N.: "Development and Testing of a New Foam-Gel Technology to Improve Conformance of the Rangley CO_2 Flood," SPE 38837 presented at SPE Annual Technical Conference and Exhibition, San Antonio, TX, 5-8 October 1997.

Gauglitz, P.A., Friedmann, A. I., Kam, S. I., and Rossen, W. R.: "Foam Generation in Homogeneous Porous Media." SPE 75177 presented at the SPE/DOE Improved Oil Recovery Symposium, Tulsa, OK, 13-17 April, 2002.

Gdanski, R.D.: "Experience and Research Show Best Designs for Foam-Diverted Acidizing," *Oil Gas J.* (September1993), 85-89.

GeoTrans: "Remediation System Evaluation," GeoTrans. Inc, Report EPA 542-R-02-008q, 10 December 2001.

Gillis, J. V., and Radke, C. J.: "A Dual-Gas Tracer Technique for Determining Trapped Gas Saturation during Steady Foam Flow in Porous Media," SPE 20519 presented at the SPE Annual Technical Conference, New Orleans, LA, 23-26 September 1990.

Hanssen, J.E., and Dalland, M.: "Increased Oil Tolerance of Polymer-Enhanced Foams: Deep Chemistry or Just 'Simple' Displacement Effects?" SPE 59282 presented at SPE/DOE Improved Oil Recovery Symposium, Tulsa, OK, 3-5 April 2000.

Hanssen, J. E., Surguchev, L. M., and Svorstol, I.: "SAG Injection in a North Sea Stratified Reservoir: Flow Experiment and Simulation," SPE 28847 presented at the European Petroleum Conference, London, England, 25-27 October 1994.

Hill, A.D., and Rossen, W.R.: "Fluid Placement and Diversion in Matrix Acidizing," SPE 27982 presented at the SPE Centennial Petroleum Engineering Symposium, Tulsa, Ok, 29-31 August 1994.

Hirasaki, G. J., and Lawson, J. B.: "Mechanisms of Foam Flow in Porous Media: Apparent Viscosity in Smooth Capillaries," *SPEJ* (April 1985), 176-190.

Hirasaki, G.J., Jackson, R.E., Jin, M., Lawson, J.B., Londergan, J., Meinardus, H., Miller, C.A., Pope, G.A., Szafranski, R., and Tanzil, D.: "Field Demonstration of the Surfactant/Foam Process for Remediation of a Heterogeneous Aquifer Contaminated with DNAPL," in NAPL Removal: Surfactants, Foams, and Microemulsions, S. Fiorenza, C.A. Miller, C.L. Oubre, and C.H. Ward, (eds.), Lewis Publishers, Boca Raton, 2000.

Hirasaki, G. J., Miller, C. A., Szafranski, R., and Lawson, J.B.: "Surfactant/Foam Process for Aquifer Remediation," SPE 37257 presented at SPE Annual Technical Conference and Exhibition, Houston, TX, 18-21 February 1997.

Hughes, T.L., Friedmann, F., Johnson, D., Hild, G.P., Wilson, A., and Davies, S.N.: "Large-Volume Foam-Gel Treatments to Improve Conformance of the Rangely CO_2 Flood," SPE 39649 presented at SPE/DOE Improved Oil Recovery Symposium, Tulsa, OK, 19-22 April 1998.

Huh, D. G. and Handy, L. L.: "Comparison of Steady- and Unsteady-State Flow of Gas and Foaming Solution in Porous Media." *SPERE* (February 1989), 77-84.

Huh, C., and Rossen, W. R.: "Approximate Pore-Level Modeling for Apparent Viscosity of Polymer-Enhanced Foam in Porous Media," SPE 99653 presented at the SPE/DOE Symposium on Improved Oil Recovery, Tulsa, OK, 22-26 April 2006.

Jenkins, M. K.: "An Analytical Model for Water/Gas Miscible Displacements," SPE 12632 presented at the SPE/DOE 4th Symposium on Enhanced Oil Recovery, Tulsa, OK, 15-18 April 1984.

Jensen, J. A. and Friedmann, J.: "Physical and Chemical Effects of an Oil phase on the Propagation of Foam in Porous Media," SPE 16375 presented at California Regional Meeting, Ventura, CA, 8-10 April 1987.

Jensen, J. L., Lake, L. W., Goggin, D. J., and Corbett, P. W. M.: *Statistics for Petroleum Engineers and Geoscientists* (2nd edition), Amsterdam, New Yoke, 2000.

Jimenez, A. T. and Radke, C. J.: "Dynamic Stability of Foam Lamellae Flowing Through a Periodically Constricted Pore," presented at the Symposium on Oil Field Chemistry at the National Meeting of the ACS, Toronto, 5-11 June 1989.

Kam, S. I., and Rossen, W. R.: "A Model for Foam Generation in Homogeneous Media," *SPE Journal* **8** (Dec. 2003), 417-425.

Keely, J. F.: "Performance Evaluation of Pump and Treat Remediation," EPA/540/4-89/005, 1989.

Kennedy, D. K., Kitziger, F. W., and Hall, B.E.: 'Case Study on the Effectiveness of Nitrogen Foams and Water-Zone Diverting Agents in Multistage Matrix Acid Treatments." *SPERE* (May 1992) 203-211.

Khatib, Z. I., Hirasaki, G. J., and Falls, A. H.: "Effects of Capillary Pressure on Coalescence and Phase Mobilities in Foams Flowing through Porous Media," *SPERE* (August 1988), 919-926.

Kibodeaux, K. R., Zeilinger, S. C., and Rossen, W. R.: "Sensitivity Study of Foam Diversion Processes for Matrix Acidization," SPE 28550 presented at the SPE Annual Technical Conference and Exhibition, New Orleans, LA, 26-28 September 1994.

Kim, J.S., Dong, Y., and Rossen W.R.: "Steady-State Flow Behavior of CO_2 Foam," SPE 89351 presented at SPE/DOE Fourteenth Symposium on Improved Oil Recovery, Tulsa, OK, 17-24 April 2004.

Kohler, N., and Chauveteau G.: "Xanthan Polysaccharide Plugging Behavior in Porous Media - Preferential Use of Fermentation Broth," *Journal of Petroleum Technology* (February 1981), 349-358.

Kovscek, A. R., and Radke, C. J.: "Fundamentals of Foam Transport in Porous Media," *Foams in Petroleum Industry*, Schramm, L. L., Editor, American Chemical Society, Washington, D. C., 1994.

Lake, L.W.: *Enhanced Oil Recovery*, Prentice Hall, Englewood Cliff, NJ, 1989.

Lake, L. W., Schmidt, R. L., and Venuto, R. B.: "A Niche for Enhanced Oil Recovery in the 1990s," *Oilfield Review* (January 1992), 56-61

Lau, E. C., and Coombe, D. A.: "History Matching the Steam Foam Injection Process in a Thick Athabasca Tar Sand Reservoir," *J. Can. Pet. Tech.* (January 1994), 56-62.

Lau, H. C., and O' Brien, S. M.: "Effects of Spreading and Nonspreading Oils on Foam Propagation through Porous Media," *SPERE* (August 1988), 893-896.

Lee, H. O., Heller, J. P. and Hoeffer, A. M. W.: "Change in Apparent Viscosity of CO_2-Foam with Rock Permeability," *SPERE* (November 1991), 421-428.

Mackay, D. M., and Cherry, J. A.: "Ground-water Contamination: Pump and Treat Remediation," *Environmental Science and Technology* (1989), 630-639.

Mannhardt, K. and Svorstol, I.: "Effect of Oil Saturation on Foam Propagation in Snorre Reservoir Core," *Journal of Petroleum Science and Engineering* (October 1999), 189-200.

Mannhardt, K., Novosad, J. J., and Schramm, L. L.: "Comparative Evaluation of Foam Stability to Oil," *SPEREE* (February 2000), 23-34.

Mamun, C. K., Rong, J. G., Kam, S. I., Liljestrand, H. M., and Rossen, W. R.: "Extending Foam Technology from Improved Oil Recovery to Environmental Remediation," SPE 77557 presented at the SPE Annual Technical Conference and Exhibition, San Antonio, LA, 29 September 2002.

Martinsen, H. A., and Vassenden, F.: "Foam Assisted Water Alternating Gas (FAWAG) Process on Snorre," paper 015 presented at the 10th European Symposium on Improved Oil Recovery, Brighton, England, 18-20 August 1999.

Mohammadi, S. S., and Coombe, D. A.: "Characteristics of Steam Foam Drive Process in Massive Multizone and Thin Single Zone Reservoir, Paper 113 presented at the 5th UNITAE/UNDP Conference on heavy Crude and Tar Sands, Caracas, Venezuela, 4-9 August 1991.

Mohammadi, S. S., Coombe, D. A., and Stevensen, V. M.: "Test of Steam Foam process for Mobility Control in South Casper Creek Reservoir," *J. Can. Pet. Tech.* (December 1993), 49-54.

Nilsson, S., Lohne, A., and Veggelan, K.: "Effect of Polymer on Surfactant Floodings of Oil Reservoirs," *Colloids and Surfaces A* (July 1997), 241-247.

Osterloh, W. T. and Jante, M. J.: "Effects of Gas and Liquid Velocity on Steady-state Foam Flow at High Temperature," SPE 24179 presented at the SPE/DOE Symposium on Enhanced Oil Recovery, Tulsa, OK, 22-24 April 1992.

Persoff, P., Radke, C. J., Pruess, K., Benson, S. M., and Witherspoon, P. A.: "A Laboratory Investigation of Foam Flow in Sandstone at Elevated Pressure," *SPERE* (August 1991), 185-192.

Pope, G.A., Tsaur, K., Schechter, R.S., and Wang, B.: "The Effect of Serveral Polymers on the Phase Behavior of Micellar Fluids," *SPEJ* (December 1982), 816-830.

Reme, A. B.: "Parameter Fitting and Calibration Study with a Commercial Foam Simulator," Thesis, Norwegian university of Science and Technology, 1999.

Robert, J. A., and Rossen, W. R.: "Fluid Placement Diversion and Pumping Strategy," in *Reservoir Stimulation*, Economides, M. J., and Nolte, N. G. (eds.), 3rd ed., Prentice Hall, Englewood Cliffs, NJ, 1997.

Romero, C., Alvarez, J.M., and Muller, A.J.: "Micromodel Studies of Polymer-Enhanced Foam Flow through Porous Media," SPE 75179 presented at the SPE/DOE Improved Oil Recovery Symposium, Tulsa, OK, 13-17 April 2002.

Rong, J. G.: "Experimental Evaluation of Foam in Environmental Remediation," PhD. dissertation, the University of Texas at Austin, 2002.

Rossen, W.R. and Wang, M.W.: "Modeling Foams for Acid Diversion," *SPEJ* (June 1999), 92-100.

Rossen, W.R.: "Foams in Enhanced Oil Recovery," in R. K. Prud'homme and S. Khan, ed., *Foams: Theory, Measurements and Applications*, Marcel Dekker, New York, 1996, pp. 413-464.

Rossen, W.R., and van Duijn, C.J.: "Gravity Segregation in Steady-State Horizontal Flow in Homogeneous Reservoirs," *J. Petr. Sci. Eng.* **43**, 99-111 (2004).

Rossen, W.R., Zeilinger, S.C., Shi, J.-X., and Lim, M.T., "Simplified Mechanistic Simulation of Foam Processes in Porous Media," *SPE Journal* **4**, 279-287 (Sept. 1999).

Rossen, W.R. and Zhou, Z.H., "Modeling Foam Mobility at the Limiting Capillary Pressure," *SPE Adv. Technol*. **3**, 146-152 (1995).

Sanchez, J. M., and Schechter, R. S.: "Surfactant Effects on the Two-Phase Flow of Steam-Water and Nitrogen-Water through Permeable Media," *J. Petr. Sci. Eng.* (October 1989), 185-199.

Seybold, C. A.: "Polyacrylamide Review: Soil Conditioning and Environmental Fate," *Commun. Soil Sci. Plant Analysis* (1994), 2171-2185.

Shan, D.: "Simulation Study of Gravity Override for Foam Processes," MS Thesis, The University of Texas at Austin, 2001

Shi, J. X., and Rossen, W. R.: "Simulation of Gravity Override in Foam Processes in Porous Media," *SPEREE* (April 1998), 148-154.

Smith, C. L., Anderson, J. L., and Roberts, P.G.: "New Diverting Techniques for Acidizing and Fracturing," SPE 2751 presented at the SPE Annual Technical Conference and Exhibition, San Francisco, CA, 6-7 November 1969.

Stone, H. L.: "Vertical Conformance in an Alternating Water-Miscible Gas Flood," SPE 11130 present at the SPE Annual Tech. Conf. And Exhibition of the Society of Petroleum Engineers of AIME in New Orleans, LA, 26-29 September 1982.

Svorstol, I., Blaker, T., Tham, M. J., and Hjellen, A.: "A Production Well Foam Pilot in the North Sea Snorre Field – Application of Foam to Control Gas Breakthrough," paper 001 presented at the 9th European IOR Symposium, the Hague, Netherlands, 20-22 October 1997.

Sydansk, R.D.: "Polymer-Enhanced Foam: Laboratory Development and Evaluation," *SPE Advanced Technology Series* (April 1994a), 150-159.

Sydansk, R.D.: "Polymer-Enhanced Foam Propagation through High-Permeability Sandpacks," *SPE Advanced Technology Series* (April 1994b), 160-166.

Szabo, M. T.: "The Effect of Sulfonate/Polymer Interaction on Mobility Buffer Design," *SPEJ* (February 1979), 4-14.

Thach, S., Miller, K.C., Lai, Q.J., Sanders, G.S., Styler, J.W., and Lane, R.H.: "Matrix Gas Shut-Off in Hydraulically Fractured Wells Using Polymer-Foams," SPE 36616 presented at SPE Annual Tech. Conf., Denver, CO, 6-9 Oct.1996.

Thompson, K., and Gdanski, R. D.: "Laboratory Study Provides Guidelines for Diverting Acid with Foam," *SPEPF* (November 1993), 285-290.

Thomas, R. L., Ali, S. A., Robert, J. A., and Acock, A. M.: "Field Validation of a Foam Diversion Model: A Matrix Stimulation Case Study," SPE 39422 presented at the International Symposium on Formation Damage Control, Lafayette, LA, 18-19 February 1998.

Vassenden F. and Holt, T.: “Experimental Foundation for Relative Permeability Modeling of Foam,” SPE 39660 presented at the SPE/DOE Improved Oil Recovery Symposium, Tulsa, OK, 19-22 April 1998.

Vassenden, F., Holt, T., Ghaderi, A., and Solheim, A.: “Foam Propagation on Semi-Reservoir Scale,” *SPEREE* (October 1999), 436-441.

Yang, S.H., and Reed, R.L.: "Mobility Control Using CO_2 Forms," SPE 19689 presented at the SPE Annual Technical Conference and Exhibition in San Antonio, TX, 8-11 October 1989.

Zerhboub, M., Touboul, E., and Ben Naceur, K.: “Matrix Acidizing: A Novel Approach to Foam Diversion,” *SPERE* (May 1994), 121-126.

Zhou, Z.H. and Rossen, W.R., "Applying Fractional-Flow Theory to Foams for Diversion in Matrix Acidization," *SPE Prod. Fac*. **9**, 29-35 (1994).

Zhou, Z. H.: “Modeling Foam Flow in Porous Media and Applications to EOR and Acidization,” PhD. dissertation, The University of Texas at Austin, 1994.

Zhu, T., Strycker, A., Raible, C.J., and Vineyard, K.: “Foam for Mobility Control and Improved Sweep Efficiency in Gas Flooding,” SPE 39680 presented at SPE/DOE Improved Oil Recovery Symposium, Tulsa, OK, 19-22 April 1998.

Vita

Chun Shen, the daughter of Guoqing Shen and Shuqiong Zhang, was born in Dazhou, China on January 26, 1969. She graduated with a Bachelor of Science degree in Applied Chemistry from Southwest Petroleum Institute, Nanchong, China, in July 1991. Shen received a Master of Science degree in Petroleum Engineering from the same institute in July 1994. Then, she subsequently joined Sichuan Petroleum Exploration and Development Institute, Chengdu, China. In June 2001, she enrolled in the graduate school at the University of Texas at Austin to pursue a PhD in the Department of Petroleum Engineering.

Permanent address: 9 Daoxiang Street, NanChong, Sichuan, China.
This dissertation was typed by the author.